SYNTHESIS AND CHARACTERIZATION OF METALLOPEPTIDE NANOSTRUCTURES

A THESIS SUBMITTED TO
THE MATERIALS SCIENCE AND NANOTECHNOLOGY PROGRAM
OF GRADUATE SCHOOL OF ENGINEERING AND SCIENCE
OF BILKENT UNIVERSITY
IN PARTIAL FULFILLMENT OF THE REQUIREMENTS
FOR THE DEGREE OF
MASTER OF SCIENCE

By
OYA USTAHÜSEYİN
January, 2013

I certify that I have read this thesis and that in my opinion it is fully adequate, in scope and in quality, as a thesis of the degree of Master of Science.

……

Assist. Prof. Dr. Mustafa Özgür Güler (Advisor)

I certify that I have read this thesis and that in my opinion it is fully adequate, in scope and in quality, as a thesis of the degree of Master of Science.

……

Assist. Prof. Dr. Ayşe Begüm Tekinay

I certify that I have read this thesis and that in my opinion it is fully adequate, in scope and in quality, as a thesis of the degree of Master of Science.

……

Assist. Prof. Dr. Tamer Uyar

I certify that I have read this thesis and that in my opinion it is fully adequate, in scope and in quality, as a thesis of the degree of Master of Science.

……

Assist. Prof. Dr. Turgay Tekinay

I certify that I have read this thesis and that in my opinion it is fully adequate, in scope and in quality, as a thesis of the degree of Master of Science.

……

Assist. Prof. Dr. Salih Özçubukçu

Approved for the graduate school of engineering and science:

……

Prof. Dr. Levent Onural

Director of the graduate school of engineering and science

ABSTRACT

SYNTHESIS AND CHARACTERIZATION OF METALLOPEPTIDE NANOSTRUCTURES

Oya USTAHÜSEYİN

M.S. in Materials Science and Nanotechnology

Supervisor: Assoc. Prof. Dr. Mustafa Özgür GÜLER

January, 2013

Organic-inorganic hybrid structures play a number of distinguished roles in the living milieu. For instance, metal ions function as cofactors of enzymes and apatite mineralization in bone is driven by collagen nanofibers serve as both physical and chemical templates. These unique interactions in natural systems are examples for development of synthetic materials for many applications such as catalysts, artificial enzymes or materials for regenerative medicine etc. Manufacturing a catalyst at the nanoscale is important due to increased specific surface area and reduced diffusion path length. In this thesis, we demonstrated peptide based bioinspired nanomaterials. The self-assembled peptide nanofibers were utilized as templates for palladium nanoparticle

formation. Functionalization of insoluble electrospun nanofibers with a heavy metal binding peptide sequence was utilized to remove toxic metal ions from water. In addition, peptide amphiphile nanofibers complexed with Zn^{II} were used as enzyme mimics. The resulting nanostructures resemble natural bone alkaline phosphatase activity, which is a major enzyme for natural bone apatite formation.

Keywords: Peptide amphiphile, self-assembly, nanofibers, palladium catalysis, water cleaning, apatite formation, artificial metalloenzyme

ÖZET

METALLOPEPTİT NANOYAPILARIN SENTEZİ

VE KARAKTERİZASYONU

Oya USTAHÜSEYİN

Malzeme Bilimi ve Nanoteknoloji Programı, Yüksek Lisans

Tez Yöneticisi: Doç. Dr. Mustafa Özgür GÜLER

Ocak, 2013

Organik-inorganik hibrit yapılar canlılar dünyasında çok önemli pek çok göreve sahiptir. Örneğin metal iyonları, enzimlerde kofaktör olarak görev alır, kolajen nanofiberleri kimyasal ve fiziksel bir kalıp oluşturarak kemik dokuda apatit molekülünün biomineralizasyonunu yönlendirirler. Doğal sistemlerdeki bunun gibi eşsiz ve çok değerli etkileşimler, katalizörler, yapay enzimler ya da doku mühendisliği ve rejeneratif tıp için sentetik malzemeler geliştirmek için ilham vermektedir. Nano boyutta yapılan katalizörler düşük difüzyon yol boyu ve genişletilmiş yüzey alanı sayesinde pek çok potensiyel kullanım alanına sahiptir.

Bu tezde doğayı taklit eden/doğadan esinlenmiş malzemeler geliştirdik. Üçüncü bölümde, kendi kendine düzenlenen peptit nanofiberleri

paladyum nanoparçacıkları için kalıp olarak kullanılmıştır. Dördüncü bölümde suda çözülmeyen, elektrikle eğirme yöntemi kullanılarak oluşturulan nanofiberlerin sudaki toksik metal iyonların temizlenmesi için, ağır metallere bağlanabilen, doğadan esinlenerek oluşturulmuş peptit dizini ile fonksiyonel hale getirilmesi anlatılmıştır. Beşinci bölüm Zn^{II} ile kompleks oluşturabilen fonksiyonel peptit amfifil nanofiberlerini kapsamaktadır. Oluşturulan nanoyapı, doğal kemik dokudaki apatit oluşumunda görev alan doğal alkalin fosfataz enzimini taklit etmektedir.

Anahtar Kelimeler: Peptit amfifil, kendiliğinden yapılanma, nano fiber, paladyum katalizörü, su temizleme, apatit oluşumu, yapay metaloenzim

ACKNOWLEDGEMENT

I would like to express my thanks to my supervisor Prof. Mustafa Özgür Güler for his guidance, support and patience during the course of this thesis work.

I would like to thank to Ruslan Garifullin, Aslı Çelebioğlu, Arif Khalily and Prof. Tamer Uyar for their partnership and support in this research.

I would like to express my special gratitude to Prof. Ayşe Begüm Tekinay for her support and leadership for shaping my philosophy towards research.

I want to thank to all members of the Biomimetic Materials and Nanobiotechnology groups but especially to Hakan Ceylan, Melis Şardan, Göksu Çinar, Melis Göktaş, and Handan Acar. They helped me to express and strengthen my knowledge not only in the research but also in life. I could not only appreciate sharing the same research laboratory with them but also the moments enjoying my life. I am very pleased that I am lucky to meet and spend two years with their sincere friendship. Life just consists of coincidences and only the ones who have wisdom or luck to use a chance coloring a life can be happy. I hope that I would be happy with having a chance colliding my life with their lives in future.

Finally, I want to thank my family but especially my sister Özge Ustahüseyin and Ezgi Uluer for their love, support. Özge is not only an

adoring sister but also my support to keep going and making the right decisions. At the times which world seems dark to me, Ezgi has compassed me to go the bright side. I am grateful that she has been patient enough to keep me enlightened in my difficult times.

I would like to thank to UNAM (National Nanotechnology Research Center) and TÜBİTAK (The Scientific and Technological Research Council of Turkey) Grant Numbers 110M353, 109T603 and 112T602 for financial support.

LIST OF ABBREVIATIONS

PA: Peptide Amphiphile

FMOC: 9-Fluorenylmethoxycarbonyl

HBTU: 2-(1H-Benzotriazol-1-yl)-1,1,3,3-tetramethyluronium hexafluorophosphate

DIEA: N, N-Diisopropylethylamine

DMF: Dimethylformamide

TFA: Trifluoroacetic Acid

LC-MS: Liquid Chromatography-Mass Spectrometry

TEM: Transmission Electron Microscopy

FT-IR: Fourier Transform Infrared Spectroscopy

SEM: Scanning Electron Microscopy

CD: Circular Dichroism

ITC: Isothermal Titration Calorimetry

SPSS: Solid Phase Peptide Synthesis

Table of Contents

List of Figures

List of Tables

Chapter 1

Introduction

1. Introduction

Today, materials scientists, chemists, physicists and biologists steadily design novel materials inspired from biological materials of nature, using distinguished properties of natural materials. These novel materials are called bioinspired materials. In the design of bioinspired materials, there are widely accepted strategies.[1] It is not simply application of basic ideas and concepts prevailing in nature. Scientists aim to design “smart materials” with the benefit of what they learn from nature. There are three important steps in the design to follow.[1] Firstly, structure-function association in natural materials should be stated clearly. Secondly, physical/chemical foundation behind this structure-function relation should be expressed with both experimental and theoretical evidences. Finally, the strategies to design and synthesis of bioinspired/biomimetic materials taking into account the engineering sources and economy. In Figure 1.1, paradox in design of biomimetic materials is depicted. A natural material is the solution of an unknown problem with unknown limitations. A scientist conducts a research to find a solution in nature to a problem with known limitations. Therefore, the scientist should have information about the steps and pass the steps to reach the solution, biomaterial.

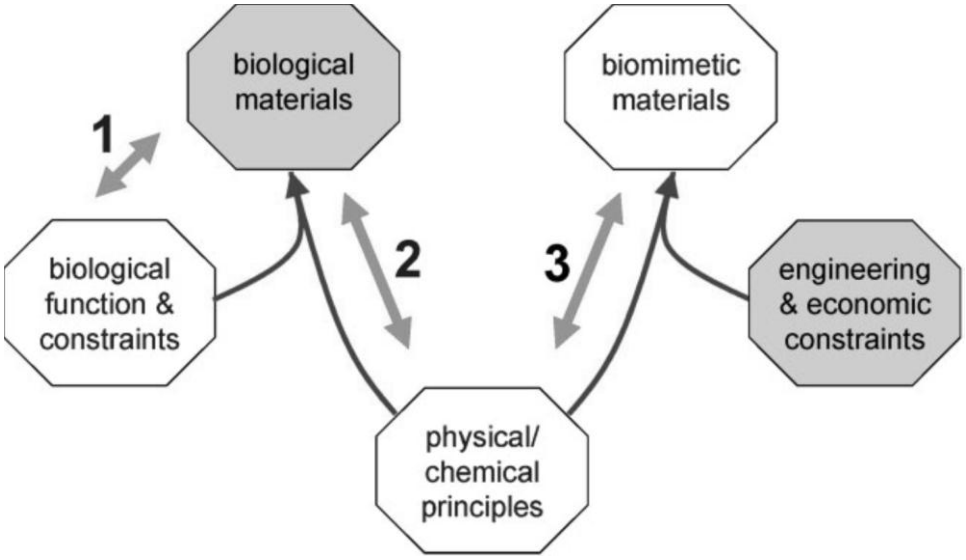

Figure 1.1 Biomimetic materials paradox. (reproduced with permission from[1] 2009 Wiley-VCH)

Natural materials are composites of polymers and minerals with different function and size. Inorganic content of bioinspired materials can be metals in ionic or elemental form, or simply salts. Organic content can be peptide, peptidoglycans, glycolipids, lipoproteins, and carbohydrate polymers such as starch, cellulose, and glycogen. These materials can be used as adhesive surfaces (gecko feet mimetic[2] or tree frog feet mimetic,[3] mussel byssi mimetic[4]), artificial enzymes,[5] composite materials (mollusk shell mimetic[6], bone mimetic[7] materials), or superhydrophobic surfaces (lotus leaves mimetic[8]).

This thesis introduces three different applications of bioinspired peptide molecules. First application covers one dimensional (1-D) palladium nanostructures with peptide amphiphile nanofiber templates. Second application includes functionalization of insoluble electrospun

polymers with a heavy metal binding biomimetic peptide molecule. Finally, last application is peptide based alkaline phosphatase mimetic nanostructures and calcium phosphate production using this artificial system.

Template directed synthesis of metal nanostructures are widely used for shaped controlled synthesis. For this purpose, polymers, carbon structures, dendrimers, mesoporus silica were used as templates. Metal nanostructures with different morphologies were revealed with different templates. For example, metal nanoparticles, nanowires, nanotubes were synthesized. Biological template materials (e.g. peptide, protein, virus, and bacteria) in the synthesis of metal nanostructures as catalysts are of great interest because of their versatile chemical and physical properties.

In removal of xenobiotic heavy metal ions, there are some techniques conventionally used such as ion exchange, chemical precipitation, adsorption, membrane filtration and electrochemical techniques.[9] Here, we used a biomimetic heavy metal binding sequence to scavenge heavy metal ions from water. Then, it was noncovalently bound to an insoluble polymer. The functionalized polymer was used to clean the water from heavy metal ions.

Metalloenzymes are important in biological systems as they control many critical mechanisms.[10-13] Therefore, metalloenzyme design is attractive and widely studied by chemists. In this thesis, an alkaline phosphate mimetic peptide based metalloenzyme was synthesized. In the

catalytic site, imidazole moieties bound to Zn^{II} ions can actively hydrolyzed phosphoester bonds and revealed phosphate ions. Free phosphate ions formed calcium phosphate salt which is important for bone ingredient. Also, *in vitro* studies showed that presence of calcium phosphate promoted the differentiation of Saos-2 cells and formation of bone nodules.

Chapter 2

Background

2. Background

Molecular self-assembly defines organization of molecules with the minimal effect of human or instrument interruption.[14] There are several reasons for scientists to desire self-assembled systems.[15, 16] Firstly, human nature prefers organized structures. Secondly, there are many examples of self-assembly in nature (self-assembly of DNA into double helix,[17] folding of proteins[18] etc.). Therefore, we need to learn self-assembly to learn nature. Thirdly, self-assembly is one the most useful methods to construct a nanostructure. Fourthly, self-assembly is applicable to micro/nanofabrication and robotics. Finally, self-assembly can combine and benefit distinct, complex research areas.

Self-assembly is divided into two in terms of mechanistic differences; static and dynamic.[16] The systems at equilibrium thermodynamically constitute the static self-assembly. This kind of self-assembly is observed for instance at the formation of molecular crystals.[19] Once the structure is formed, dissociation requires energy. In dynamic self-assembly, components of system dissipate energy. System is at nonequilibrium and continually tries to reach equilibrium. This kind of self-assembly is also called as self-organization. In table 1, examples of self-assembly are given.

Table 2.1 Examples of self-assembly (S, static, D, dynamic, T, templated, B, biological). (Reproduced with permission from[16] 2002 AAAS)

System	Type	Applications/Importance
Atomic ionic and molecular crystals	S	Materials, optoelectronics
Phase separated and ionic layer polymers	S	
Self-assembled monolayers	S, T	Microfabrication, sensors, nanoelectronics
Lipid bilayers and black lipid films	S	Biomembranes, emulsions
Liquid crystals	S	Displays
Colloidal crystals	S	Band gap materials, molecular sieves
Bubble rafts	S	Models of crack propagation
Macro and mesoscopic structures	S or D, T	Electronic circuits
Fluidic self-assembly	S, T	Microfabrication

“Light matter”	D, T	
Oscillating and reaction-diffusion reactions	D	Biological oscillations
Bacterial colonies	D, B	
Swarms (ants) and schools (fish)	D, B	New models for optimization/computation
Weather patterns	D	
Solar systems	D	
Galaxies	D	

Self-assembly of peptide amphiphile (PA) molecules is directed with molecular properties, assembly environment (pH, temperature, co-assembling molecules and solvents) and assembly kinetics. [20] Since self-assembly process of peptide amphiphile molecules is dynamic self-assembly, the resulted nanostructure is kinetically-trapped, metastable. However, this thermodynamically nonequilibrium structure can be favorable as its structure is tailorable with environmental factors (pH, temperature etc.). Also, dynamic intrinsic character of the structure

reveals as flexibility which is invaluable as it is absent in static self-assembly.

The PA molecules can self-assemble into nanofibers, nanovesicles, nanobelts, and nanotubes.[21, 22] The leading force in self-assembly can be hydrophobic interactions, H bonding and π- π stacking.[23, 24] These intermolecular forces direct the formation of secondary structures like α-helix and β-sheet.[25] PA molecules possess a hydrophobic tail and hydrophilic amino acid sequence. They aggregate with hydrophobic collapse of acyl tails or hydrophobic amino acid sequence and organization of hydrophilic amino acid sequence with intermolecular interactions (H bonding, π- π stacking etc.). The dislike of hydrophobic tail keeps away the hydrophobic residues from water and buries it inside the core while hydrophilic residues expose to water. This behavior drives the construction of different nanostructures.

Self-assembling PAs are applicable in a variety of areas. They can be used as antimicrobial agent, cell culture scaffold for tissue engineering, template for nanofabrication and mineralization, active compound in skin care and cosmetics, nanocarrier for drug and gene delivery.[14] The difference in functionality arises from the difference in functional amino acid sequence at C terminus of peptide amphiphile as it constructs the surface of PA nanostructures.

Short, cationic peptide amphiphiles are used as antimicrobial agents. Both cationic charges and hydrophobicity of peptide allow PA to

integrate to the membrane and allow them to form pores with “barrel stave”, “carpet” or “worm pore” mechanisms and disturb the bacteria membrane.[26] Commonly used hydrophilic amino acids are K, R, and H and hydrophobic residues are A, V, I, L, F, W, and Y.

Peptide amphiphile gel networks can mimic extracellular matrix in terms of fibrillar nanostructure and biofunctionality.[27] Also, they can be used as biocompatible scaffols in tissue engineering or regenerative medicine.[28] For instance, peptide amphiphiles with heparin binding sequence can create extracellular matrix mimetic environment for cell to enhance angiogenesis.[29]

In cosmetics and personal health care, surfactants are used in several products. Specifically peptide amphiphiles are important not only because they are surfactants but also they can possess biofunctional sequences such as for anti-wrinkling etc.[30]

For drug or gene delivery systems, internalization is most crucial part of the process. The amphiphilic nature of peptide amphiphiles enhances the integration of peptide amphiphile with cell membrane or internalization with vesicles. For instance, peptide amphiphile micelles can encapsulate DNA. Then, encapsulated DNA can internalize to the cell.[31]

Peptide amphiphile nanofibers can also serve as templates for inorganic materials. Nucleated inorganic material can be metal nanoparticles,[32] or inorganic crystals[33].

Chapter 3

Supramolecular Peptide Nanofiber Templated Pd Nanocatalyst

This work was partially published in Chemical Communications, 2012, 48, 11358-11360.

3.1 Introduction

Nanostructures have superior properties since surface atoms are more accessible and they have lower coordination numbers compared to bulk equivalents.[34] Their improved catalytic, optical, electronic and magnetic properties provide wide range of applications to metal nanocrystals. Their assets are determined with size, structure, chemical composition, and shape of nanostructures. Therefore, their shapes are critical in actuation of catalytic activity of nanoparticles. Among nanostructures, 1-D nanostructures are one of the most beneficial structures with their high accessible surface area and aspect ratio. These contributed to nanostructures exclusive catalytic activity.

Nanoparticle growth is composed of three steps; nucleation, formation of seeds from nuclei, and growth of nanoparticle from seeds. (Figure 3.1) [35, 36] In solution phase metal nanostructure synthesis, generally salt of a metal precursor is used as dissolved in a solvent. To reduce metal ions into zero valent metal atoms, a reducing agent is used. As metal ions reduce to zero valent metal atoms, concentration of metal atoms increases and get supersaturated after a definite concentration. After this supersaturation point, atoms start to aggregate and form nuclei. Nucleus has an important role in shape of nanocrystals. However, there is no much information about metal nuclei due to difficulty of their characterization. As a nucleus grown and reached to a critical size, structural fluctuations become less favorable energetically. At this point, it starts to develop a well-defined structure, seed. Once a seed is formed,

it continues on growing until a thermodynamic equilibrium is reached. Thermodynamic equilibrium defines the equilibrium between decrease in bulk energy and increase in surface energy. After this process, evolution of nanocrystals is terminated. At this process, capping agent is also crucial both in determination of size and dominant crystallographic plane of nanocrystal. As capping agents interact with different crystallographic planes with different free energies, growth rates of planes change. It causes to make a specific plane dominant. Thus, capping agent directs the nanocrystal shape with thermodynamic control.

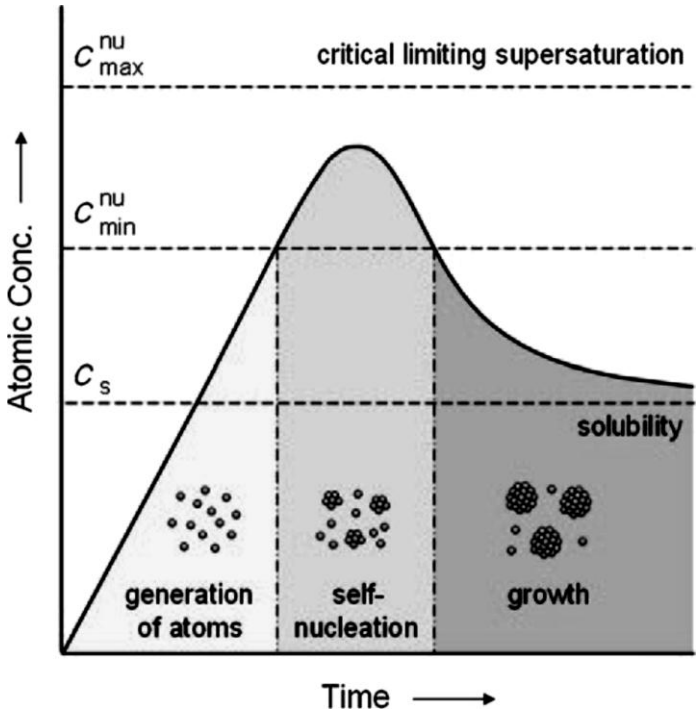

Figure 3.1 Plot of atomic concentration over time course, illustrating the generation of atoms, nucleation, and subsequent growth. (Reproduced with permission from [36] copyright 2009 Wiley-VCH)

Palladium nanostructures are especially important among other metal nanostructures with their enhanced catalytic activity in organic reactions like hydrogenation, C-C coupling and amination reactions. In the literature, carbon based structures,[37] polymers,[38] dendrimers, [39] metal-organic frameworks[40] and mesoporous silica[41] are used as support for nanoparticles. Besides these templates, biological templates such as virus, bacteria, protein and peptide were employed for construction of metal nanostructures because of their taiolorable properties.[42-44] A few studies previously reported heterogeneous palladium catalysts, which were synthesized by a nanoscale and environmentally friendly template for C-C coupling reactions.[45-47] Self-assembled peptide amphiphile (PA) nanofibers are promising candidates as a template and support due to their tailorable surface properties. By employing metal-binding amino acids into PA structure (e.g. lysine, histidine and glutamic acid), peptide nanofibers can specifically bind metal ions for functional materials applications.[48, 49] These bioinspired peptide nanostructures can be further exploited for seeding and nucleation of metal ions for producing nanoscale inorganic nanostructures.[49]

In this thesis, self-assembling peptide amphiphile nanofibers templated palladium nanostructures were synthesized. In addition to template function of peptide amphiphile, they were used as capping agents to stabilize palladium nanoparticles. In this study, we designed and synthesized a *de novo* peptide amphiphile molecule (Lauryl-VVAGHH-

Am) that can coordinate with Pd^{II} ions through lone pair electrons in imidazole moiety of histidine residues.(Scheme 3.1)[50] After addition of reducing agent, palladium ions reduced to zero valent palladium with peptide amphiphile as capping agent to stabilize palladium nanoparticles.

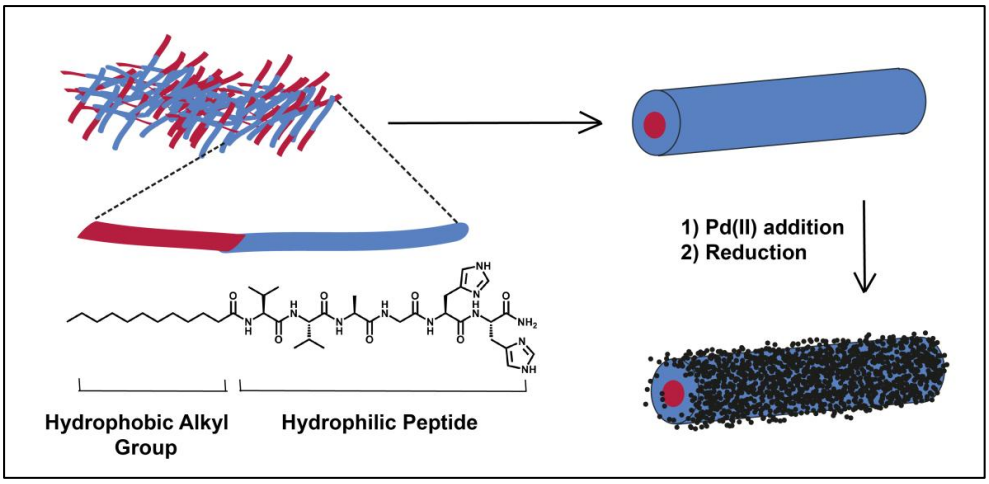

Scheme 3.1 Self-assembly of peptide amphiphile molecules generates nanofibers with 10 nm in diameter. Seeding and reduction of Pd^{II} ions on the surface of peptide nanofibers form hybrid peptide and Pd^{0} nanostructures (Pd@Peptide).

3.2 Experimental

3.2.1 Peptide Synthesis

In the synthesis of peptide amphiphile molecule, solid phase peptide synthesis method was applied with an automated peptide synthesizer (CS Bio. Company model: 136XT). Peptides were constructed on MBHA Rink Amide resin. Amino acid couplings were done with 2 equivalents of fluorenylmethyloxycarbonyl (Fmoc) protected amino acid, 1.95

equivalents O-Benzotriazole-N,N,N',N'-tetramethyl-uronium-hexafluoro-phosphate (HBTU) and 3 equivalents of N,N-diisopropylethylamine (DIEA) for 3 h. Fmoc removals were performed with 20% piperidine /dimethylformamide solution for 10 min. Cleavage of the peptides from the resin was carried out with a mixture of trifluoroacetic acid:triisopropylsilane:water in ratio of 95:2.5:2.5 for 3 h. Excess trifluoroacetic acid was removed by rotary evaporation. The remaining viscous peptide solution was triturated with cold ether and the resulting white product was lyophilized.

3.2.2 Liquid Chromatography-Mass Spectroscopy

For the structural analysis of the peptide Agilent Technologies 6530 Accurate-Mass Q-TOF LC-MS and Zorbax SB-C8 column were used. Concentration of the sample for LC-MS measurement was 0.5 mg/mL. Solvents were water (0.1% formic acid) and acetonitrile (AcN) (0.1% formic acid). LC-MS was run for 25 min for each sample and it started with 2% AcN and 98% H_2O for 5 min. Then, AcN concentration reached to 100% until 20 min. Finally, its concentration was dropped to 2% and it kept running for 5 min. Solvent flow was 0.65 mL/min and injection volume of sample was 5 µL.

3.2.2 Circular Dichroism Spectroscopy

Secondary structure of peptide amphiphile was analyzed with Jasco J-815 circular dichroism spectrometer. 1 wt% peptide solution was

prepared in ddH_2O and gelified with NaOH at pH 7.0. Then, peptide gel was diluted with 1 mM NaOH solution and $5x10^{-4}$ M peptide solution was measured from 300 nm to 190 nm with 0.1 data pitch, 100 nm/min scanning speed, 1 nm band width and 4 s D.I.T. Average of three measurements were used and sensitivity was selected as standard.

3.2.3 Rheology

Anton Paar MCR-301 rheometer was used for mechanical characterization of peptide amphiphile gels. I prepared 1% (w/v) peptide solution in distilled water, and added 0.1 M NaOH solution. After sweep measurements, amplitude kept constant as 0.1% and amplitude frequency as 10 rad/s during 60 min. In frequency sweep measurements, angular frequency varied between 0.1 and 100 rad/s while amplitude was 0.1 %. In strain sweep experiments, amplitude varied between 0.001 and 1000% while angular frequency was constant at 10 rad/s. In all rheometer graphs, x and y axes were in logarithmic scale.

3.2.4 Transmission Electron Microscopy

1% (w/v) peptide solution was prepared and alkalified with 0.1 M NaOH solution. Peptide gel was diluted with 1 mM NaOH solution, a small amount of solution was dropped to carbon covered copper grid. To image organic peptide fibers, 2% (w/v) uranyl acetate solution was used. Finally, carbon grid was dried at atmosphere. FEI Tecnai G2 F30 transmission electron microscope (TEM) was used to display peptide

amphiphile nanofibers. In the characterization of palladium nanoparticles, samples were dropped onto carbon covered copper grids, allowed to dry at atmosphere conditions and imaged with TEM.

3.2.5 Scanning Electron Microscopy/Critical Point Dryer

FEI Quanta 200 FEG environmental scanning electron microscope (SEM) was used to image peptide amphiphile gel after removing solvent with Tousimis Autosamdri-815B, Series C critical point dryer (CPD). 1 wt% solution of peptide in distilled water was prepared and 0.1 M NaOH solution was added to peptide solution on metal mesh to adjust the pH around 7. Since critical point dryer can be used with samples in isopropanol, we washed peptide gels with 20%, 40%, 60%, 80% and 100% (v/v) isopropanol solutions. Then, gels were dried with a critical point dryer. Finally, peptide amphiphile network was imaged with SEM.

3.2.6 Synthesis of Palladium Nanostructures

First, 1 wt% peptide was dissolved in hydrogel was prepared at pH 7. 0.5 eq. of Na_2PdCl_4 at pH 7.0 solution was added for overnight. Then, 0.5 eq. of Na_2PdCl_4 at pH 7.0 solution was added to the sol-gel. After 1 h of incubation for seeding, 0.5 eq. ascorbic acid at pH 7.0 was added. When all of the palladium ions were reduced to Pd^0, sol-gel was divided into two and while one was kept for further characterization, other one was diluted with same amount of palladium by keeping the final palladium concentration constant but decreasing the peptide

concentration to half. After incubation for another 1 h, ascorbic acid solution was added to reduce palladium ions. This cycle was repeated three times. After each addition and reduction of palladium ions, samples were imaged with TEM. In all characterizations, sample after third addition of palladium ions was used.

3.2.7 Characterization of Palladium Nanostructures

To monitor stability of structures, various treatments were applied to nanostructures. Pd nanostructure sample was washed with $3xH_2O$ then 3xEtOH. After evaporation of EtOH, sample was dissolved in EtOH, some amount was poured into Si wafer and heated at 100 °C for 1 h. Finally, SEM images were taken.

3.2.8 X-Ray Diffractometer

In crystallographic analysis of palladium nanostructures, PANanalytical X'Pert X-ray diffractometer was performed by using Cu Kα radiation. Mylar foil of 6 μm thickness was used as the surface to drop peptide/palladium samples. Rotation time was 16 seconds, scan range was from 30° to 90°, and step size was 0.0525°.

3.2.9 Thermogravimetric Analysis

Thermal gravimetric analysis was performed with TA Q500 instrument. Samples were dried under atmosphere conditions and then analysis was performed under high purity nitrogen purge (40.0 mL/min)

with heating the samples from 30 °C to 550 °C with 20 °C/min heating rate.

3.3 Results and Discussion

Peptide molecule was synthesized with SPPS. Chemical structure of peptide molecules was shown in Figure 3.2. After synthesis, purity of peptide was monitored with LC-MS.(Figure 3.3) At pH >6, PA molecules were composed of β-sheet structural motif as figured out in CD spectrum.(Figure 3.4) It can self-assemble into nanofibers with a diameter of *ca.*10 nm (Figure 3.5) and Three-dimensional network of the PA nanofibers formed a self-supporting hydrogel at concentration of 1 wt%.(Figures 3.6-3.8)

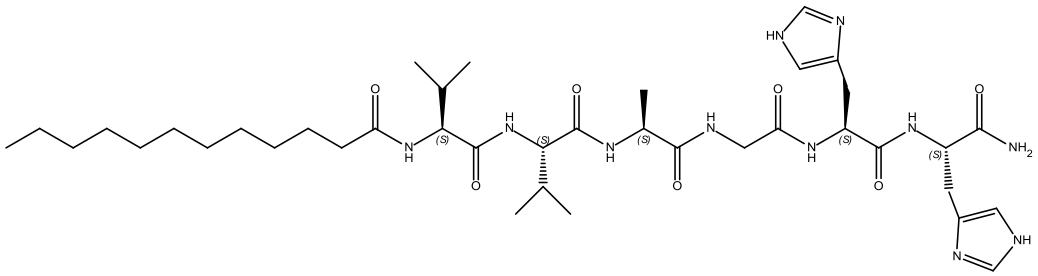

Figure 3.2 Chemical structure of Lauryl-VVAGHH-Am peptide amphiphile molecule.

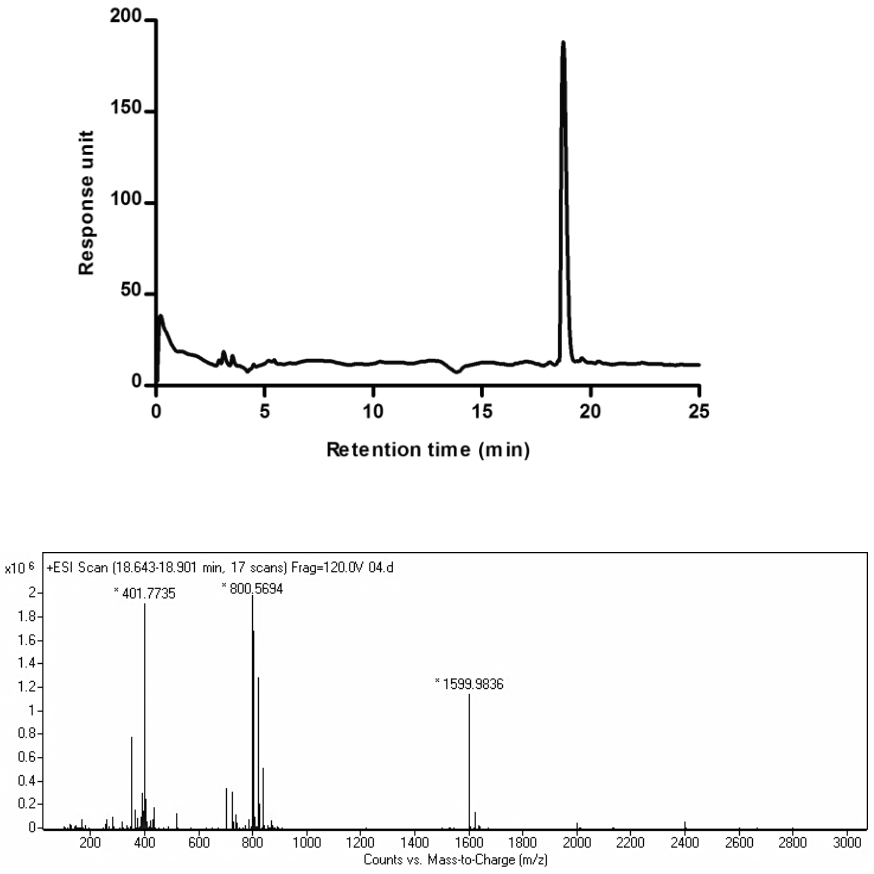

Figure 3.3 HPLC chromatogram of peptide. Absorbance at 220 nm vs retention time graph (top). Mass spectrum of peptide after substracting mass spectrum of water sample at that time interval (bottom). $[M+H]^+$ (calculated)=801.00, $[M+H]^+$ (observed)=800.55, $[M/2+H]^+$ (calculated)=401.00, $[M/2+H]^+$ (observed)=401.77.

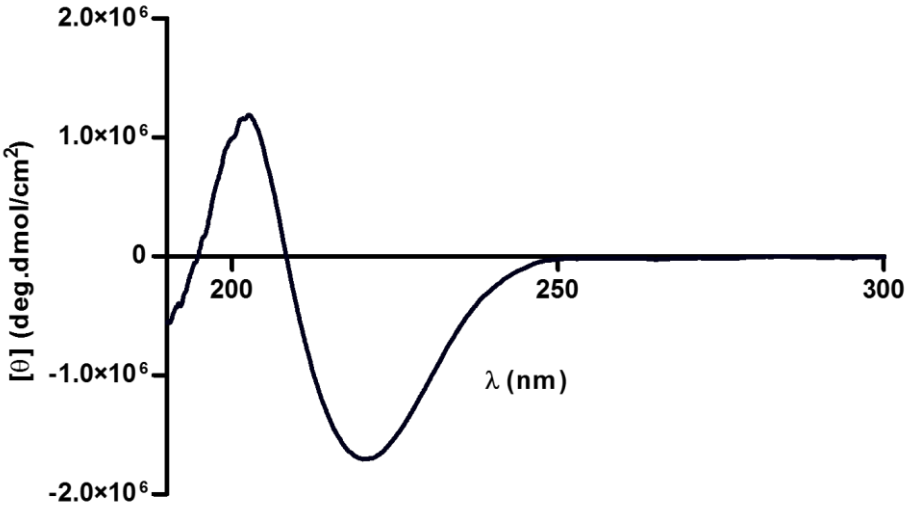

Figure 3.4 CD spectrum of peptide amphiphile at pH 7.

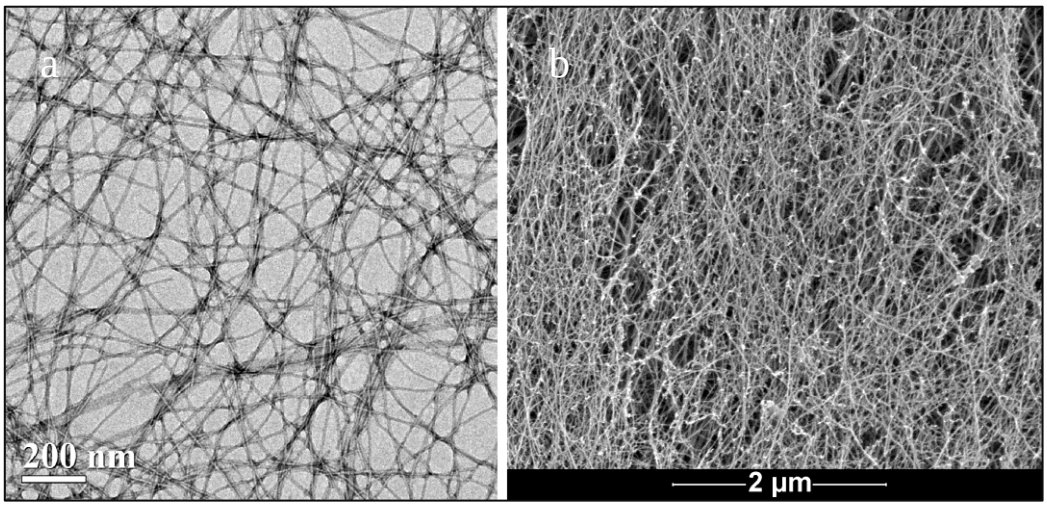

Figure 3.5 a. TEM and b. SEM image of PA at pH 7.0.

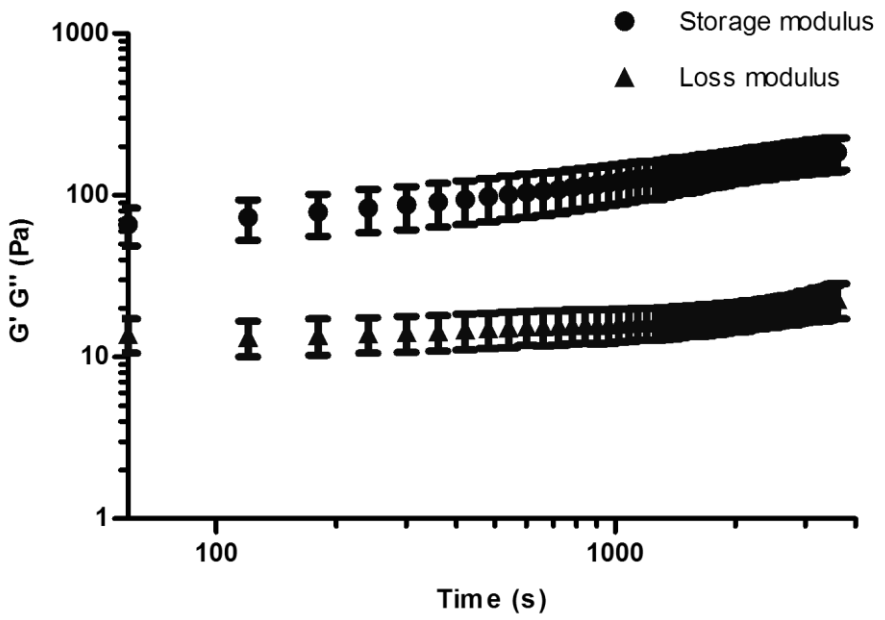

Figure 3.6 Time sweep graph of peptide amphiphile gel.

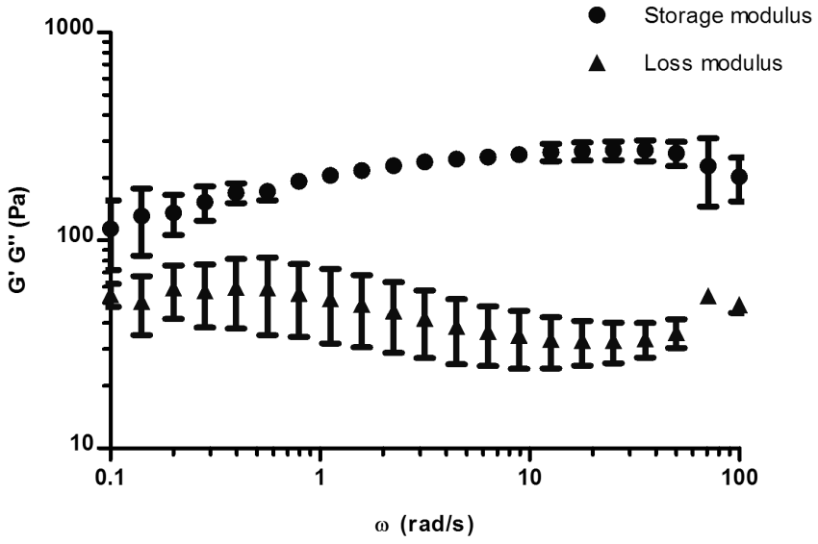

Figure 3.7 Frequency sweep graph of peptide amphiphile gel.

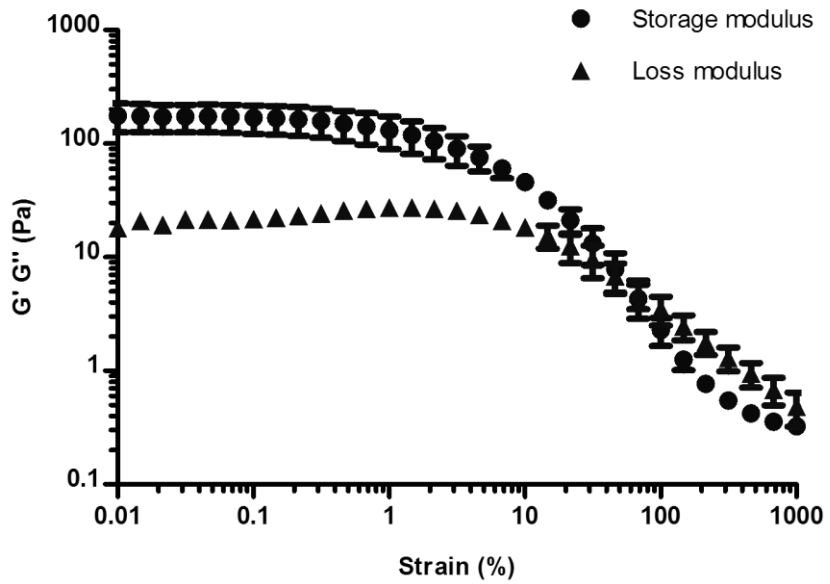

Figure 3.8 Strain sweep graph of peptide amphiphile gel.

In this work, we exploited peptide nanofibers as a nanoscale template for formation of Pd^0 nanoparticles. Resulting hybrid metal-organic architectures mimic metalloenzymes due to palladium nanoparticles grown on peptide nanofibers to catalyze C-C coupling reactions. Following a multi-step reduction methodology, closely-packed one-dimensional palladium nanoparticles were grown on peptide nanofibers. Pd^{II} ions accumulated on the peptide nanofibers due to their affinity to imidazole residues. After peptide nanofiber formation at pH 7, palladium solution was added to peptide nanofiber solution and mixture was left at room temperature overnight to allow interaction of the ions with imidazole moiety of histidine residues. Later, reducing agent (L-(+)-ascorbic acid) was added to the mixture. After the first reduction, the Pd^{II} ion amount was increased for second and third reduction cycle by

increasing Pd/Peptide molar ratio. Nanoparticle formation on peptide template was inadequate in the first reduction cycle. (Figure 3.9) After the third cycle, coating of peptide nanofibers with closely packed palladium nanoparticles was clearly observed. (Figure 3.10)

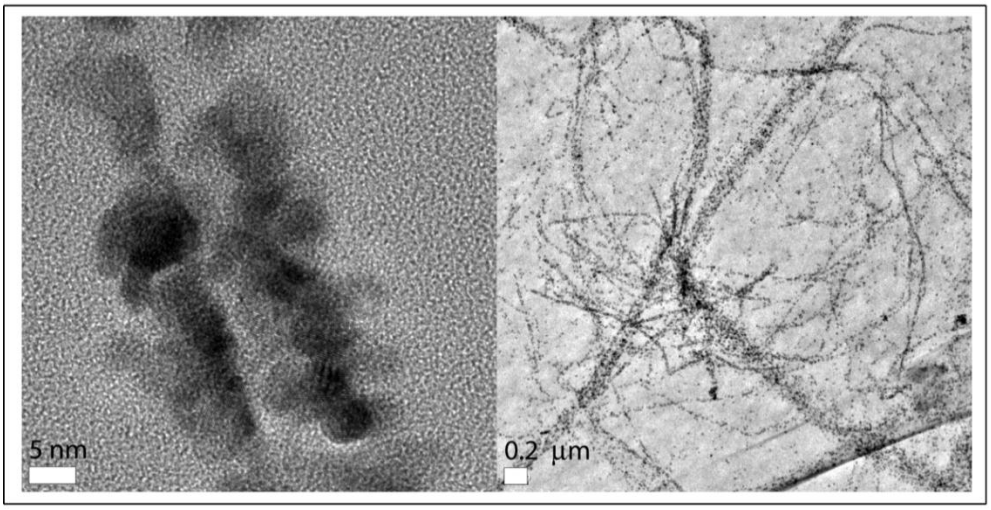

Figure 3.9 TEM images of Pd nanostructures after first reduction cycle.

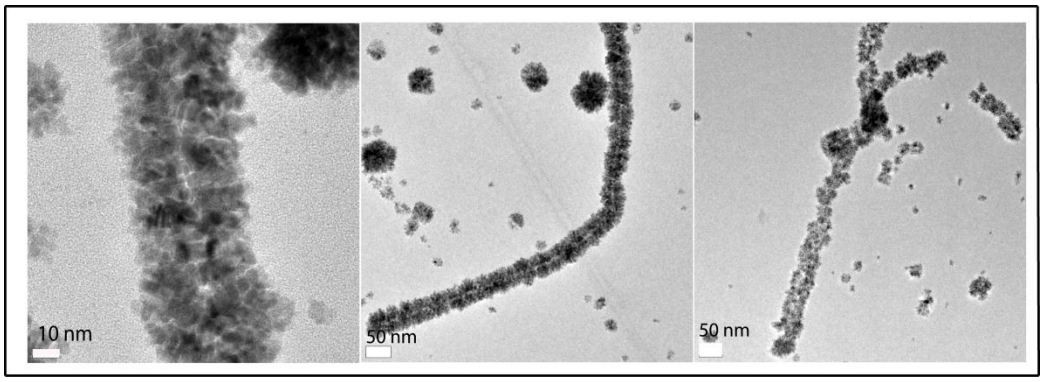

Figure 3.10 TEM images of Pd nanostructures after third reduction cycle.

To remove peptide molecules without Pd, the sample was filtered through cellulose membrane with 0.2 µm cut off. Filtration was found to

be the most effective and easy way of eliminating the excess peptide without disturbing the integrity of the catalyst assembly. To best of our knowledge, this type of highly ordered Pd nanostructures was obtained for the first time by use of peptide nanofiber template methodology.

Metal nanoparticle loading capacity of the peptide nanofiber templates was assessed by thermogravimetric analysis (TGA). The Pd@Peptide sample was dried at 100 °C in an oven, and heated to 550 °C. Inorganic content was found to be 42.5%. (Figure 3.11)

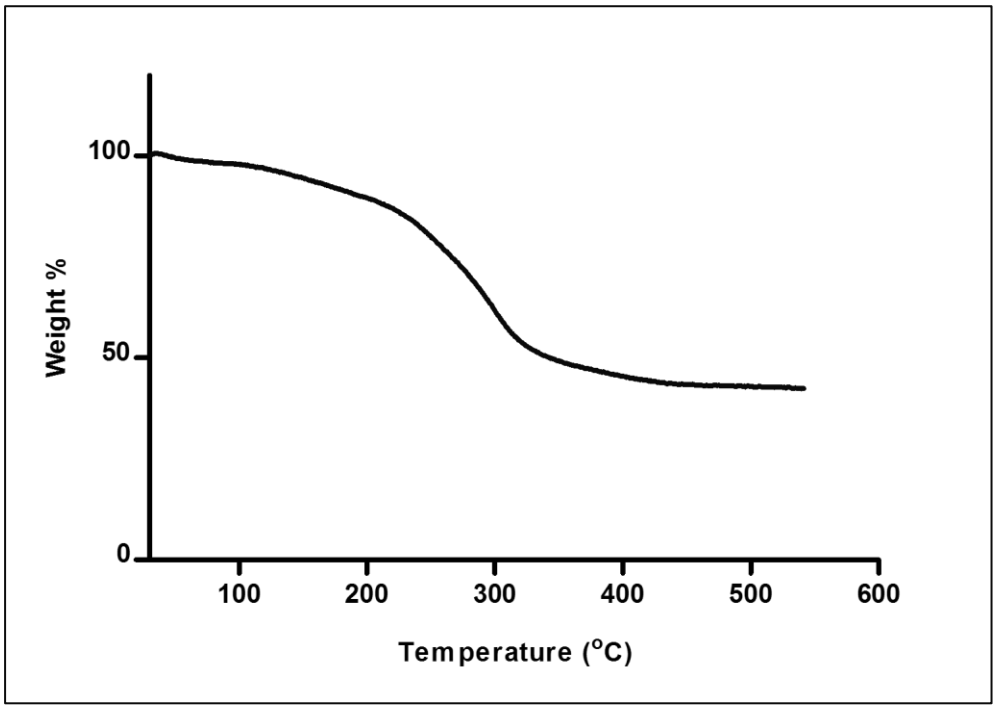

Figure 3.11 TGA of palladium nanostructures filtered with cellulose ester membranes (42.55% palladium content).

Crystalline structure of Pd@Peptide sample was analyzed by X-ray diffractometer (XRD). The dominant surface is (111). Pd (111) is the lowest energy facet and the most stable facet of Pd.[51] Also, the

presence of broad Pd (111) peak expresses low periodic and atomic order of Pd nanoparticles, because as grain size decreases, its XRD peak broadens.(Figure 3.12)

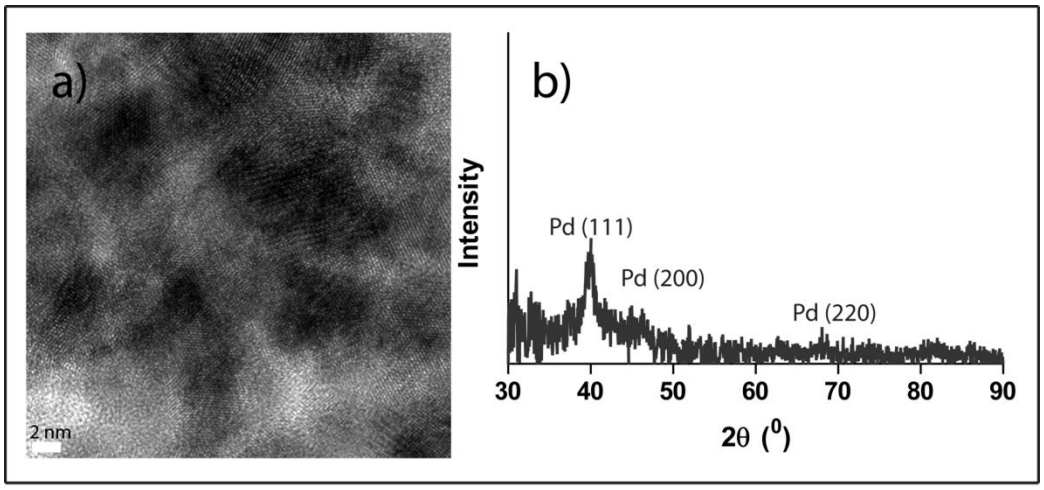

Figure 3.12 a. HRTEM image of Pd nanostructures b. XRD pattern of Pd nanostructures.

To remove unbound peptide amphiphiles or peptide amphiphiles in palladium nanostructures, several procedures were applied. Distilled water was added to mixture and centrifuged at 3000 rpm for 3 minutes. The treatment was repeated for 3 times. Then, ethanol was added to the mixture and centrifuged at 3000 rpm for 3 minutes thrice. Small amount of mixture was dropped to a clean Si wafer and dried under air. SEM image was taken and seen in Figure 3.13.

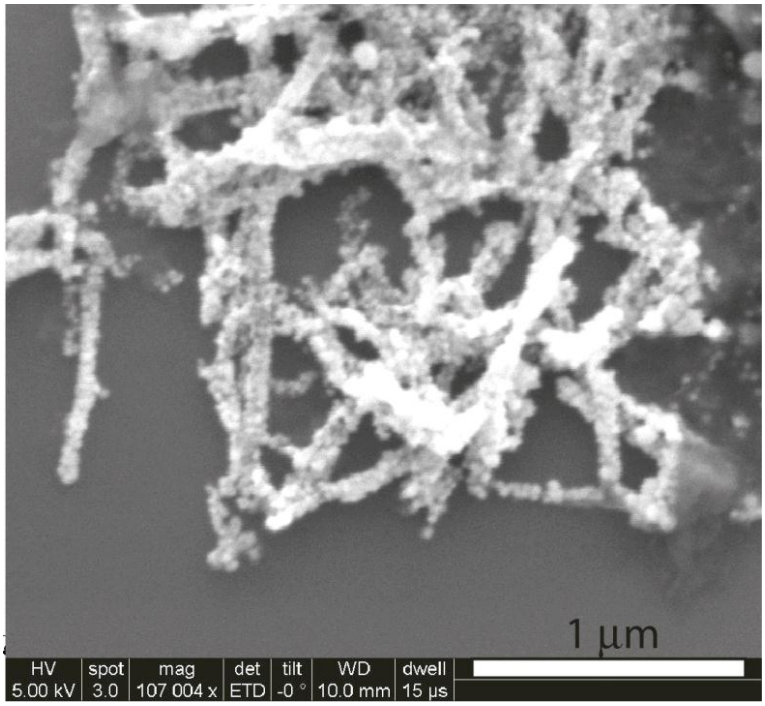

Figure 3.13 SEM image of Pd@Peptide nanostructures

Pd@Peptide was washed with three times with water and then ethanol. After evaporation of ethanol, sample was dissolved in ethanol. Some amount was poured into Si wafer and heated at 100 °C for 1 h. Finally, SEM images were taken.(Figure 3.14)

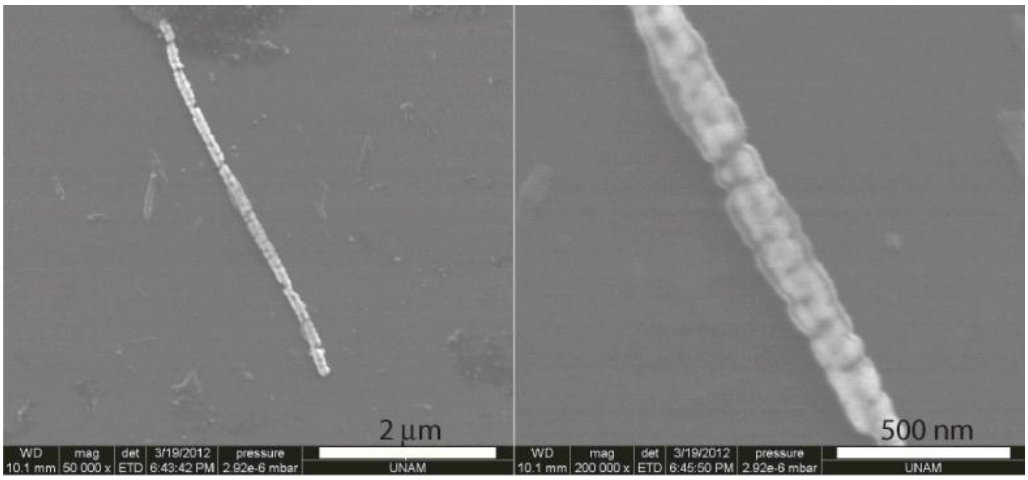

Figure 3.14 SEM images of Pd@Peptide after washing step.

To remove unbound peptide molecules, Pd@Peptide nanostructures were heated to 250 °C for 30 minutes. However, defined structures were damaged and sintered.(Figure 3.15)

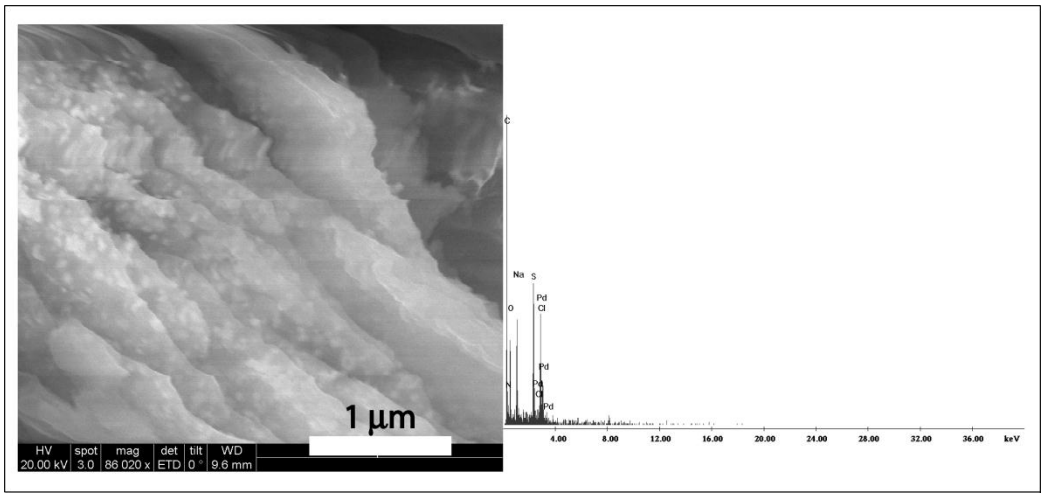

Figure 3.15 SEM image (left) and EDS spectrum (right) of sintered Pd@Peptide nanostructures.

Suzuki coupling reactions were performed as a model reaction to determine catalytic activity of the Pd nanostructures on the peptide nanofibers. Water was used for coupling reactions as an attractive green and cheap solvent.[52] Iodobenzene (0.5 mmol), unsubstituted phenylboronic acid (0.75 mmol) and potassium phosphate tribasic, K_3PO_4, (1 mmol) were used in optimization of the reaction conditions. We optimized suitable reaction conditions in water at room temperature (Table 3.1). The reaction was completed in less than 4 h with 99% biphenyl conversion (Table 3.11, Entry 1). Mixing ethanol, which is another environmentally friendly solvent [53] expedited the reaction rate four folds (Table 3.1, Entry 2). The rate enhancement is potentially due

to improved solubility of the starting materials in water/ethanol mixture.[54]

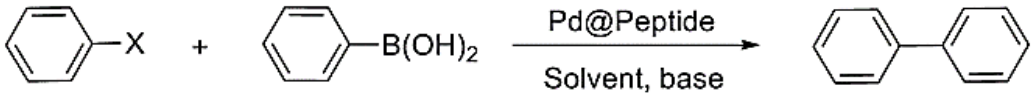

Table 3.1 Suzuki-Miyaura coupling of aryl halides with Pd@Peptide Nanocatalyst.[a]

Entry	X	Base	Solvent	Time (h)	T [°C]	Conversion (%)[b]
1	I	K_3PO_4	H_2O	4	25	99
2	I	K_3PO_4	H_2O:EtOH	1	25	99
3	Br	K_3PO_4	H_2O	10	25	< 3
4	Br	K_3PO_4	H_2O	10	80	< 5
5	Br	K_2CO_3	H_2O	10	25	0
6	Br	K_2CO_3	H_2O	10	80	< 1
7	Br	K_2CO_3	H_2O:EtOH	10	25	< 3
8	Br	K_3PO_4	H_2O:EtOH	10	25	10
9	Br	K_3PO_4	H_2O:EtOH	4	80	99
10	Br	NaOH	H_2O	4	25	99

[a] Reaction conditions: aryl halide (0.5 mmol), arylboronic acid (0.75 mmol), Pd@Peptide (1.5 mol% with respect to aryl halide concentration), K_3PO_4 (2.0 equiv), solvent (4 mL). [b] The reaction yield was determined by GC-MS (Figure S11- S18).

3.4 Conclusion

Developing efficient and green catalysts is important for new technologies to eliminate waste, to avoid use of hazardous solvents and reagents, and to possess high recyclability. Here, we demonstrated a bioinspired peptide amphiphile nanofiber template for formation of one-dimensional Pd^0 nanostructures. The Pd@Peptide nanocatalyst system provided high catalytic activity in Suzuki coupling reactions in environmentally friendly conditions. We believe that this novel approach can find applications in many industrially important catalytic processes in environmentally friendly conditions.

Chapter 4

Noncovalent Functionalization of Polymer Nanofibers with Bioinspired Heavy Metal Binding Peptide

4.1 Introduction

Nature is a source of inspiration for researchers solving a wide range of critical problems of modern age, which delicately culminated in foundation of biomimetic sciences: modelling or imitating natural materials and processes. In nature, metal ions are essential in many processes such as photosynthesis,[55] water oxidation,[55] respiration,[56] and nitrogen fixation[57]. Although metal ions such as Zn^{II}, Cu^{II} are important part of metalloproteins and beneficial at optimum concentration levels, some metal ions such as Hg^{II}, Ni^{II} pose a serious threat for human health even at low concentrations.[58, 59] Moreover, these obnoxious metal ions can contaminate and spread through natural water sources.

In nature, organisms defend themselves against xenobiotic such as heavy metals with glutathione, phytochelatine or metallothionein depending on cell type. For instance glutathione exists at mammalian liver cells at milimolar range concentration to protect cells.[60] The common feature of these proteins is that they all have cysteine residues. Metallothionein is name of cysteine rich protein family.[61] It can exist in prokaryotes, protozoa, plants, yeast, invertebrates and vertebrates. These proteins are rich of cysteine binding heavy metal ions, reactive oxygen species and xenobiotics. Glutathione is a tripeptide (γ-ECG) which has a γ peptide bond between N-terminus of cysteine and carboxyl group at side chain of glutamic acid.[62] Phytochelatin contain polyamino acids consisting of γ-Glu-Cys building blocks.[63] They bind

to metal ions with high affinity and remove them from cytosol with vacuolar membrane vesicles.[64] Carboxylate moiety of glutamic acid coordinates with positively charged metal ions and the sulfhydryl group on cysteine acts as chelating agent. Thus, both of the amino acids in γ-Glu-Cys sequence are required for metal ion binding. However, it was previously observed that Glu-Cys repeating unit possesses similar functionality to γ-Glu-Cys unit.[65]

In this thesis, we synthesized a phytochelatin mimetic peptide (PMP) with Glu-Cys repeating unit conjugated to an adamantyl moiety. Afterwards, we attached it noncovalently on a solid support consisting of cyclodextrin functionalized insoluble electrospun polymer nanofibers. Noncovalent functionalization of nanofibers with PMP was achieved with the help of adamantane-β-CD host-guest inclusion complex. After functionalization, PMP-polymer solid support was used to scavenge of highly toxic metal ions, Cd^{II}, Ni^{II} and Cr^{VI}, from aqueous solutions.(Scheme 4.1) It is known that phytochelatins have high binding ability to Cd^{II}, Ni^{II} ions.[66] Therefore, Cd^{II} and Ni^{II} ions were used as model metal ions that were known to bind phytochelatin mimetic peptides and Cr^{VI} ions were used to demonstrate the binding ability of PMP.

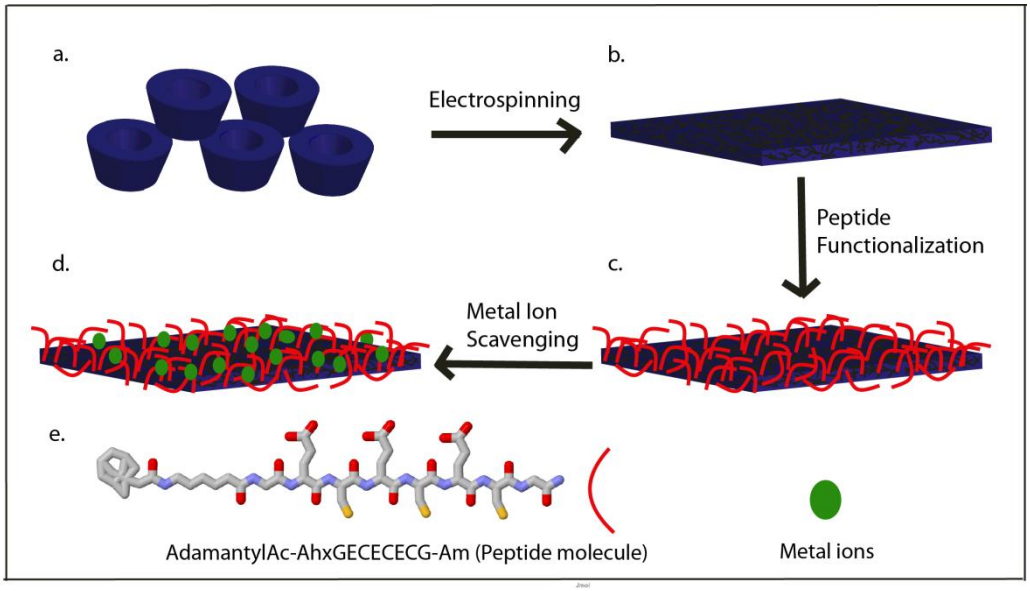

Scheme 4.1 a. Schematic of HPβCD molecules. b. Electrospun HPβCD molecules forms an insoluble polymer support consisting of nanofibers. c. Polymer support was functionalized with PMP via its adamantyl moiety. d. Metal ions were removed from water through scavenging with PMP. e. Chemical structure and representative illustration of the peptide molecule and representative illustration of metal ions.

4.2. Experimental

4.2.1 General Methods

The identity of the peptide amphiphiles were assessed by Agilent 6530-1200 Q-TOF LC/MS equipped with ESI-MS and a Zorbax Extend C18 column (Agilent 4.6 x 100 mm, 3.5 µm). Solvent system was 0.1 % ammonium hydroxide in water and 0.1% ammonium hydroxide in acetonitrile. Amide bond was observed at 220 nm. Peptide was purified with dialysis procedure. For this purpose, Spectra/Por® Biotech

Cellulose Ester dialysis membrane with 100-500D MWCO was used. Secondary structure characterization of peptide was performed with Jasco J 815 CD spectrometer. In isothermal titration calorimetry (ITC) analysis, Microcal ITC 200 was used. Thermo X series II inductively coupled plasma-mass spectrometry (ICP-MS) was to measure heavy metal ion concentration. HPβCD nanofibers were analyzed morphologically with FEI Quanta 200 FEG SEM. Thermal gravimetric analysis was performed with TA Q500 instrument. After peptide immobilization, peptide content in HPβCD nanofibers was analyzed elemental analysis. Thermo Scientific FLASH 2000 series CHNS-O analyzer was used. Bruker, Vertex 70 FT-IR instrument was used to measure absorbance of peptide, HPβCD mesh and peptide-HPβCD mesh.

4.2.2 Materials

Fmoc protected amino acids, 4-(2',4'-Dimethoxyphenyl-Fmoc-aminomethyl)-phenoxyacetamido-norleucyl-(MBHA) resin, and 2-(1H-Benzotriazol-1-yl)-1,1,3,3-tetramethyluronium hexafluorophosphate (HBTU) were purchased from NovaBiochem and ABCR. The other chemicals were purchased from Fisher, Merck, Alfa Aesar or Aldrich and used as received, without any purification.

4.2.3 Synthesis of Peptides

Peptide chain was constructed on MBHA Rink Amide resin. Amino acid coupling reactions were done with 2 equivalents of Fmoc protected

amino acid, 1.95 equivalents HBTU and 2 equivalents of DIEA (N, N-diisopropylethylamine) for 3 h. Fmoc removals were performed with 20% piperidine/dimethylformamide (DMF) solution for 20 min. Potential miscouplings of free N-teminus of peptide were prevented with acetylation, 10% acetic anhydride for 30 minutes. Cleavage of the peptides from the resin was carried out in strong acidic trifluoroacetic acid (TFA) mixture, TFA:TIS(triisopropylsilane):H_2O:EDT (ethane dithiol) in ratio of 92.5:2.5:2.5:2.5 for 2 h. Excess TFA was removed by rotary evaporation. The remaining viscous peptide solution was triturated with cold ether at -20 ^{o}C for overnight. The resulting white product was collected at 8000 rpm for 20 min in centrifuge. Supernatant was dissolved in deionzed water and lyophilized.

4.2.4 Electrospinning of insoluble HPβCD nanofibers

The preparation of CDNF was started by adding epichlorohydrin (ECH) as cross-linking agent to the HPβCD solution. This solution was stirred at 50 °C for the sufficient viscosity just before the fully solidification (gelation) of sample. The electrospinning of solution was carried at 15kV with 10 cm tip-to-collector distance and the 1mL/h flow rate. The cross-linking of CD chains in the uniform nanofibers was completed by the curing treatment that applied in oven for 5 h. Thus, the soluble, partially cross-linked nanofibers became insoluble showing the increment in crosslinking density. Finally, the excess amount of unreacted CDs and epicholorohydrin were removed by washing the

ultimate CDNFs with water and ethanol, before the filtration experiments.

4.2.5 Characterization of Peptide Amphiphile

4.2.5.1 Liquid Chromatography-Mass Spectrometry

Concentration of the sample for LC-MS measurement was 0.5 mg/mL. Solvents were H_2O (0.1% NH_4OH) and acetonitrile (AcN) (0.1% NH_4OH). LC-MS was run for 20 min for each sample and it started with 2% can and 98% H_2O for 2 minutes. Then, AcN concentration reached to 80% until 14 min. Finally, its concentration was dropped to 2% in one minute. Total analysis lasted for 20 min.

4.2.6 Characterization of Interaction Between Peptide and β-Cyclodextrin

4.2.6.1 Isothermal Titration Calorimetry (ITC) Analysis

Binding of metal ions to PMP-HPβCD complex and HPβCD molecules were quantified with ITC. In PMP-HPβCD measurements, PMP was dissolved in 36 mM TCEP-HCl at TRIS buffer at pH 8.0.

In metal binding experiments, PMP solution was mixed with HPβCD in equivalent mol with peptide. Cell temperature was 25 °C, reference power was 5 µcal/s, and stirring speed was 1200 rpm.

4.2.7 Peptide-HPβCD Conjugation

PMP was dissolved in 36 mM TCEP.HCl at 50 mM TRIS buffer at pH8.0. Then, peptide was diluted with 50 mM TRIS buffer at pH 8.0. CDNF was added to this solution in 1:1 mol ratio and stirred for 24 h for complete conjugation. Afterwards, PMP-CDNF was analyzed and used for metal removal.

4.2.7.1 Elemental Analysis

PMP amount in PMP-CDNF was analyzed with CHNS-O elemental analysis instrument. To calculate PMP content precisely, only PMP, only CDNF, PMP-CDNF and nanofiber treated with only buffer (TRIS) and TCEP were analyzed. 1-1.5 mg samples was analyzed, while standard was 2,5-(bis(5-tert-butyl-2-benzo-oxazol-2-yl) thiophene and additive for complete combustion of molecule vanadium (V) oxide. Elemental analysis of PMP was not only used in determination of immobilized PMP amount but also pointed out that PMP molecule was synthesized and purified with dialysis successfully.

4.2.7.2 Thermogravimetric Analysis

Thermal behavior of host-guest inclusion complex (adamantyl-HPβCD) was analyzed thermogravimetric analysis. Only PMP, only CDNF and PMP-CDNF were combusted to 550 °C to determine decomposition points and whether there was a shift due to the host-guest inclusion complex. Samples were dried under atmosphere conditions and then

analysis was performed under high purity nitrogen purge (40.0 mL/min) with heating the samples from 30 °C to 450-500 °C with 20 °C/min heating rate.

4.2.7.3 FT-IR Spectroscopy

FT-IR spectra of PMP, CDNF and PMP-CDNF were taken to investigate adamantyl-HPβCD complex. Samples were mixed with 100 mg KBr to obtain homogenous mixtures and crushed to form transparent pellets. Then, absorbance of samples was measured with FTIR instrument and shifts due to the host-guest inclusion complex were investigated.

4.2.7.4 X-Ray Photoelectron Spectroscopy

The X-ray photoelectron spectrums of samples were recorded by using Thermo κ-alpha monochromated high performance X-ray photoelectron spectrometer. PMP-CDNF and CDNF were analyzed before and after metal ion incubation. The survey analysis was performed at 5 scans and for detailed information, the high resolution spectra were recorded for the spectral regions relating to interested metal type at pass energy of 50 eV and 15 scans.

4.2.7.5 Scanning Electron Microscopy

CDNF were analyzed morphologically with FEI Quanta 200 FEG scanning electron microscope. EDX was performed without any coating

procedure. After 3 nm Au-Pt coating of nanofibers, SEM images were taken. For element mapping, NW was not coated with anything and element mappings were taken at 5 kV.

4.2.8 Metal Ion Scavenging from Water

4.2.8.1. Inductively Coupled Plasma-Mass Spectrometry

Thermo X series II inductively coupled plasma-mass spectrometry (ICP-MS) was used to measure heavy metal ion concentration. All ICP samples were prepared in 2% nitric acid solution. ICP-MS using parameters were as follows; dwell time was 10000 ms, channel per mass was 1, acquisition duration was 7380, channel spacing was 0.02, carrier gas was argon.

4.3 Results and Discussion

HPβCD was electrospun to obtain cyclodextrin functionalized polymer nanofiber solid support system. Since adamantane is known to form a host-guest inclusion complex with β-CD,[67] for immobilization of PMP on HPβCD nanofibers, an adamantyl group was conjugated to N-terminus of the peptide sequence by solid phase peptide synthesis method. 6-amino-hexanoic acid was used as a spacer to enhance the coupling efficiency of 1-adamantaneacetic acid to the peptide backbone. Thereafter, a glycine residue was added both to C and N termini of $(Glu\text{-}Cys)_3$ peptide sequence. (Figure4.1) Purity of PMP was confirmed with

liquid chromatography and dialyzed for further purification.(Figures 4.2-4.3)

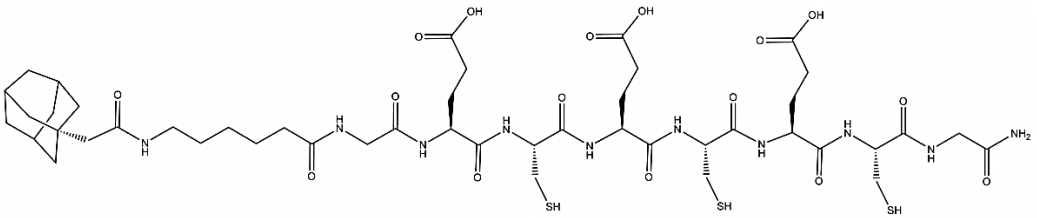

Figure 4.1 Chemical structure of PMP.

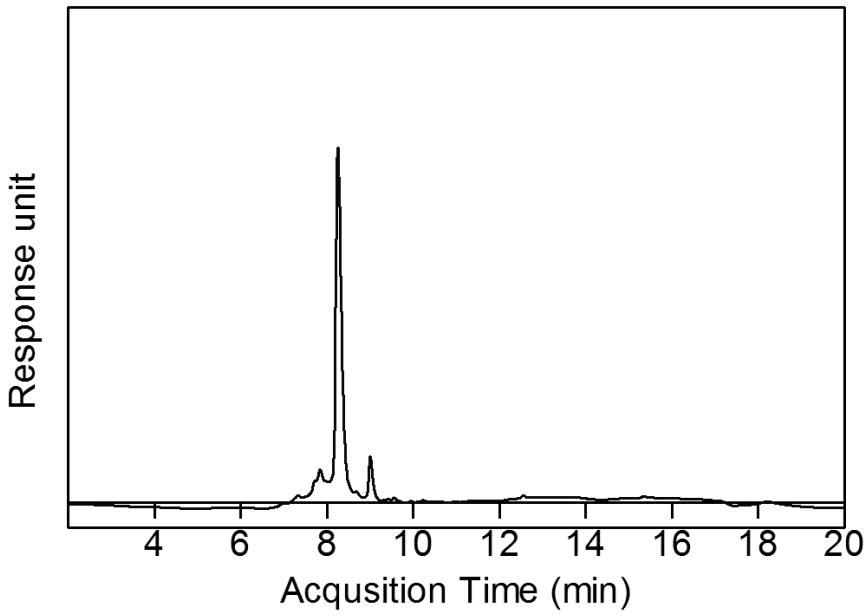

Figure 4.2 Liquid chromatogram of PMP after dialysis.

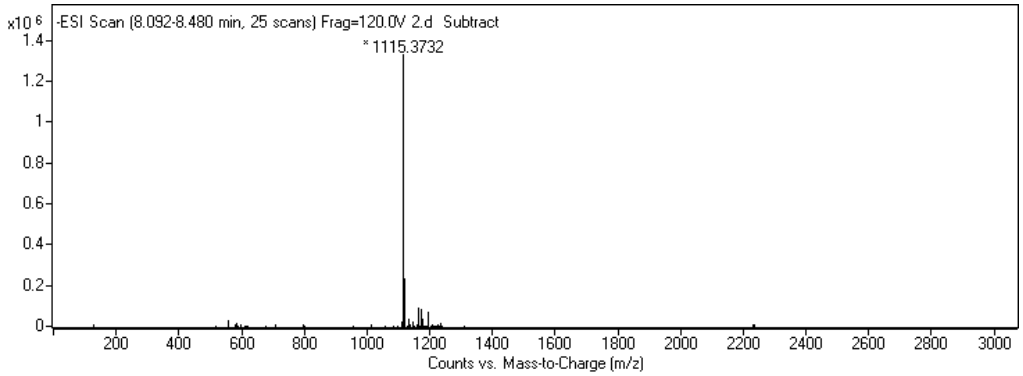

Figure 4.3 Mass spectrum of PMP after substracting mass spectrum of water sample at that time interval. Mass data $[M-H]^-$ (calculated) =1116.43; $[M-H]^-$ (observed) = 1115.3732.

Interaction between metal ions, Cd^{II}, Ni^{II} and Cr^{VI}, and PMP, was monitored through the change in absorbance in the UV spectra. In $CdCl_2$ titration, an additional peak at 240 nm appeared with the addition of PMP indicating $S \rightarrow Cd^{II}$ charge transition.(Figures 4.4-4.5)[68] Additionally, titration of Ni^{II} revealed another peak centered around 270 nm was attributable to $S \rightarrow Ni^{II}$ charge transition.(Figure 4.6)[69] Titration of Cr^{VI} with PMP, an absorption band at 245 nm was raised after PMP addition. (Figure 4.7)

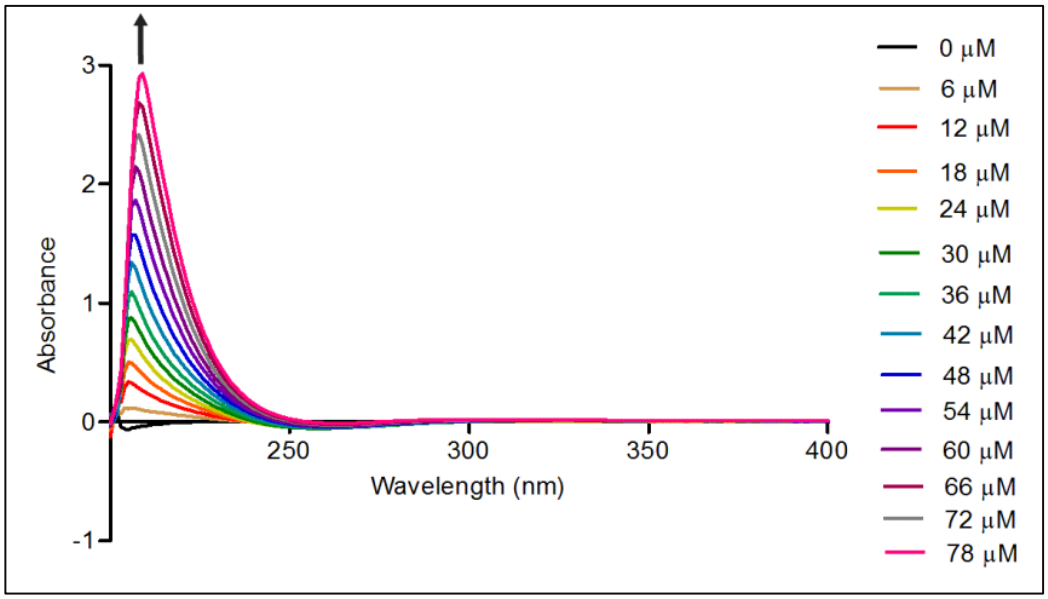

Figure 4.4 Absorbance of PMP solution in 50 mM TRIS buffer at pH 8.0.

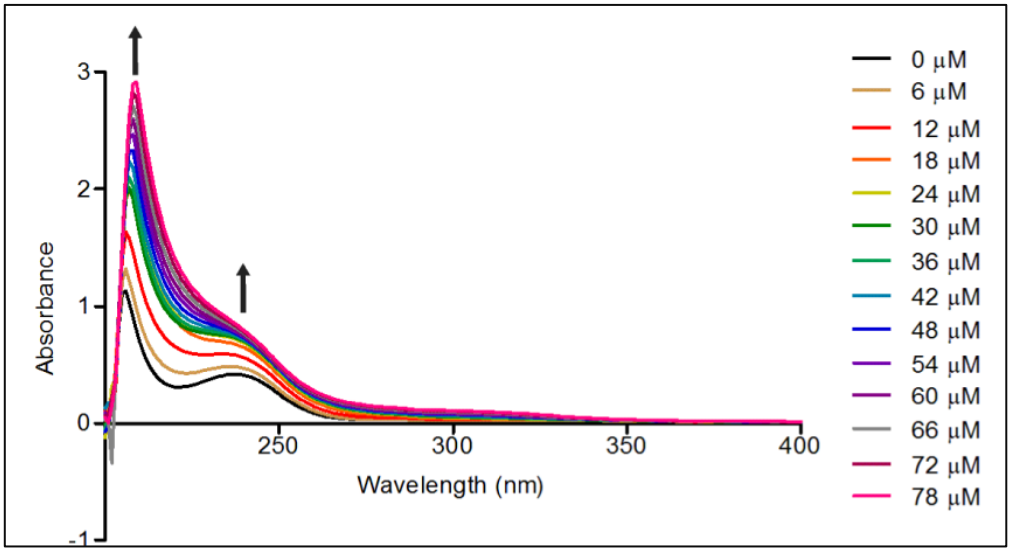

Figure 4.5 Absorption change within 20 μM $CdCl_2$ titration with PMP solution in 50 mM TRIS buffer at pH 8.0.

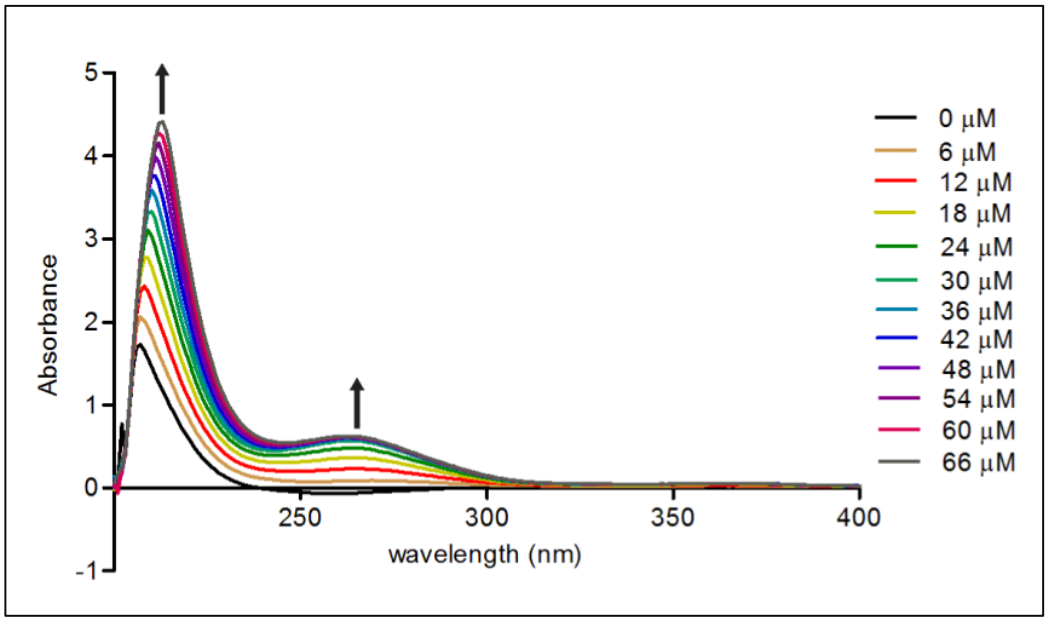

Figure 4.6 Absorption change in 20 µM $Ni(NO_3)_2$ titration with PMP solution in 50 mM TRIS buffer at pH 8.0.

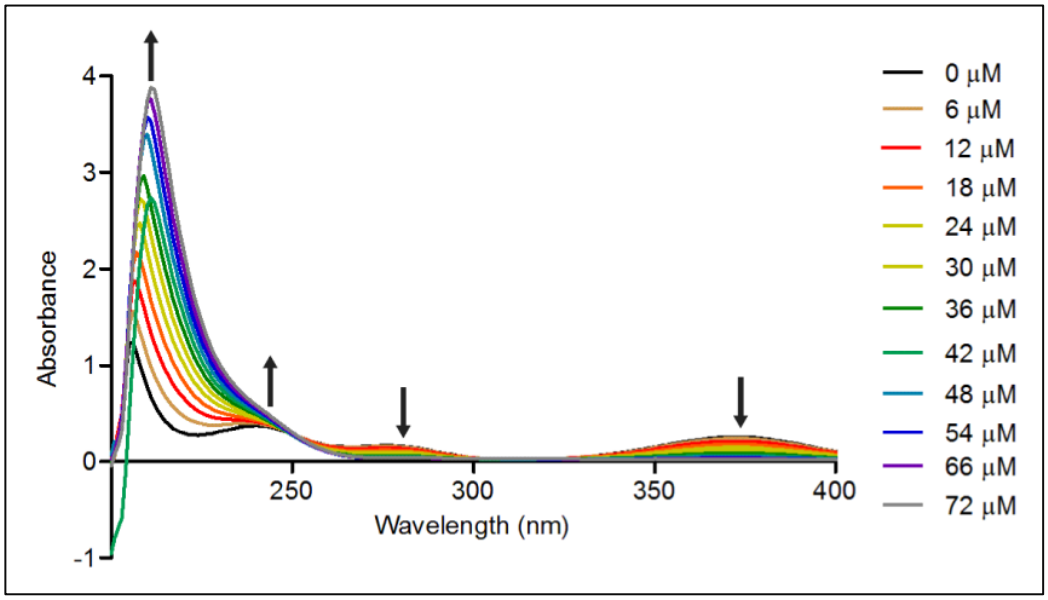

Figure 4.7 Absorption change in 20 µM $K_2Cr_2O_7$ titration with PMP solution in 50 mM TRIS buffer at pH 8.0.

To confirm interaction between metal ions and PMP, ITC was employed. Solutions of Cd^{II}, Ni^{II} and Cr^{VI} were titrated with PMP solution at pH 8. The interaction between HPβCD molecule and metal ions was at negligible level.(Figures 4.8-4.10)

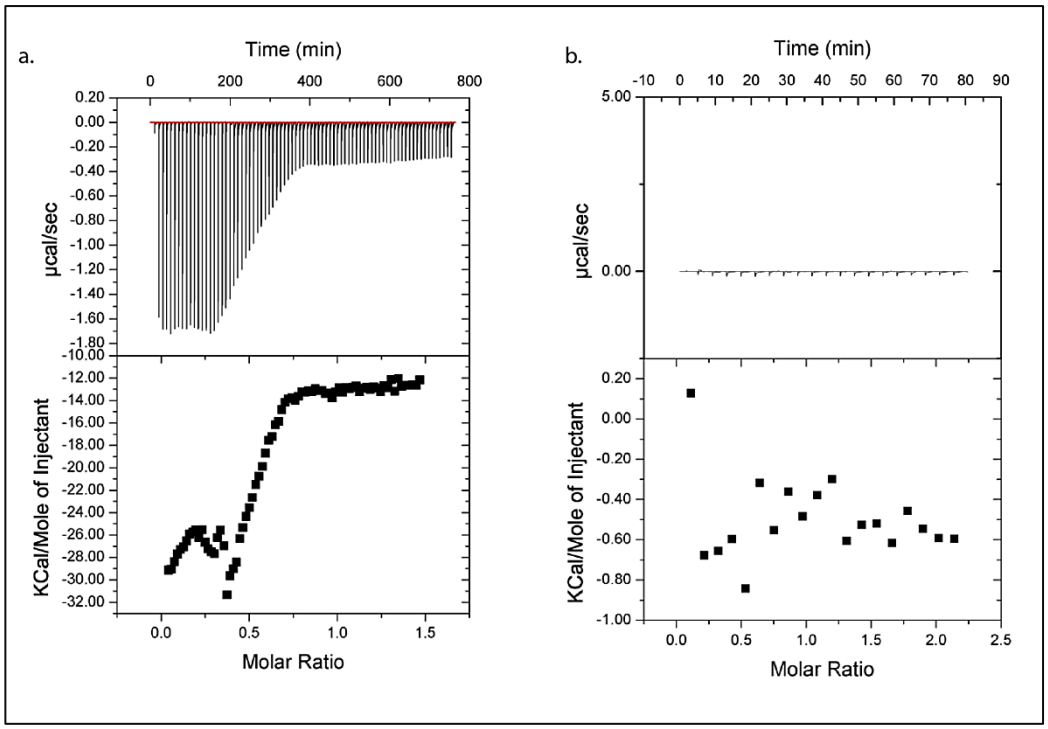

Figure 4.8 Isothermal titration curve of (**a**) PMP, (**b**) HPβCD molecule with $CdCl_2$ solution.

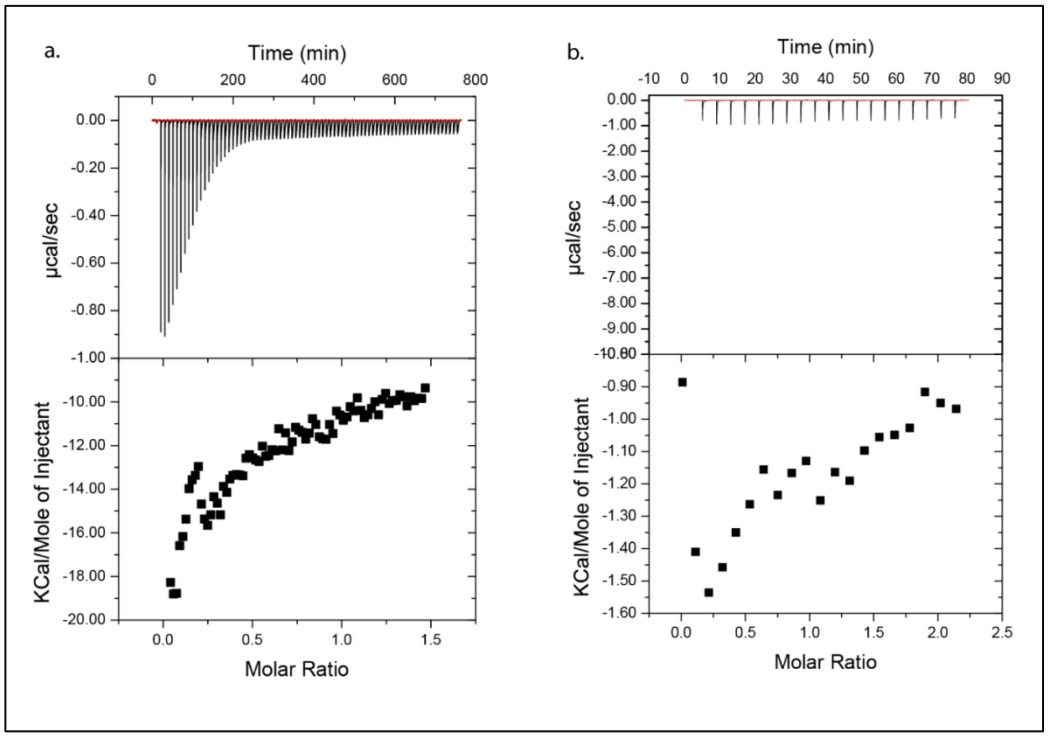

Figure 4.9 Isothermal titration curve of (a) PMP, (b) HPβCD molecule with $Ni(NO_3)_2$ solution.

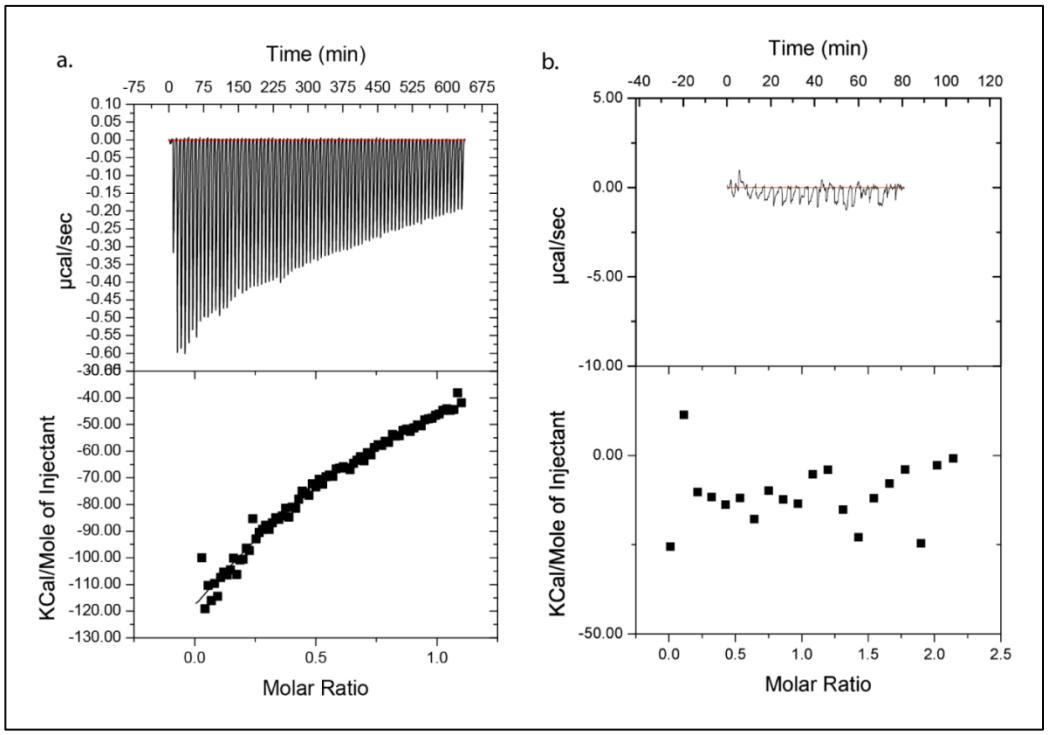

Figure 4.10 Isothermal titration curve of (a) PMP, (b) HPβCD molecule with $K_2Cr_2O_7$ solution.

Interaction between adamantyl moiety of PMP to β-CD was quantified with ITC. In ITC measurements, titration of β-CD with PMP revealed a moderate binding affinity (N=1.17, K_d=3.85x10^4 M^{-1}). (Figure 4.11)

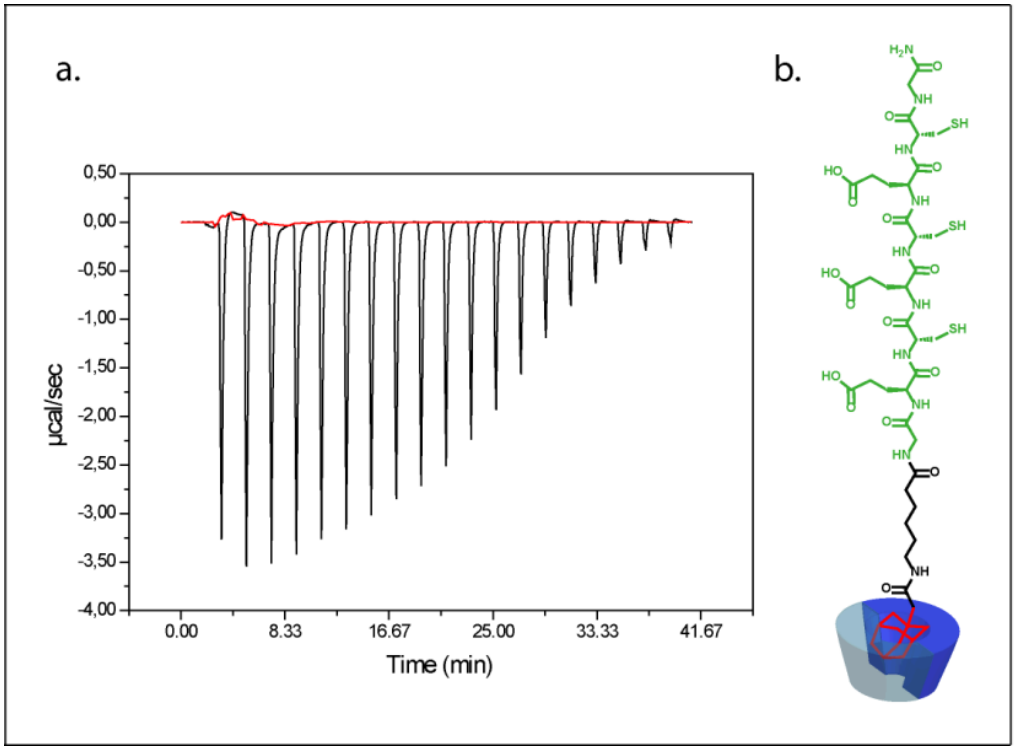

Figure 4.11 a. ITC curve obtained from titration of β-CD with adamantane conjugated PMP. b. Schematic presentation of interaction between β-CD and PMP. Adamantyl moiety of peptide formed an inclusion complex with β-CD so that peptide was noncovalently bound to β-CD of CDNF.

Binding constant of PMP and β-CD was correlated with the binding constant of adamantane acetate and β-CD.[67] After quantification of interaction between PMP and β-CD, CDNF were functionalized with PMP molecule. CDNF is a polymer solid support consisting of insoluble crosslinked HPβCD nanofibers with approximately 1µm diameter. Element maps of C and O in CDNF matched with back scattered electron image of uncoated CDNF. (Figures 4.12-4.13)

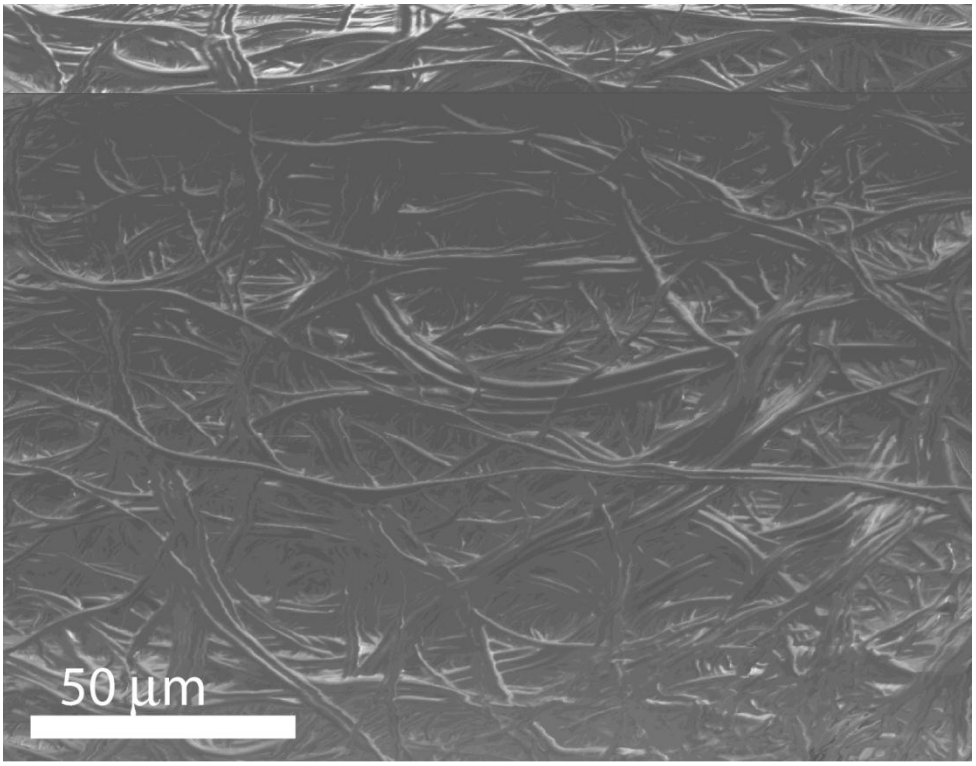

Figure 4.12 Back scattered electron image of uncoated CDNF.

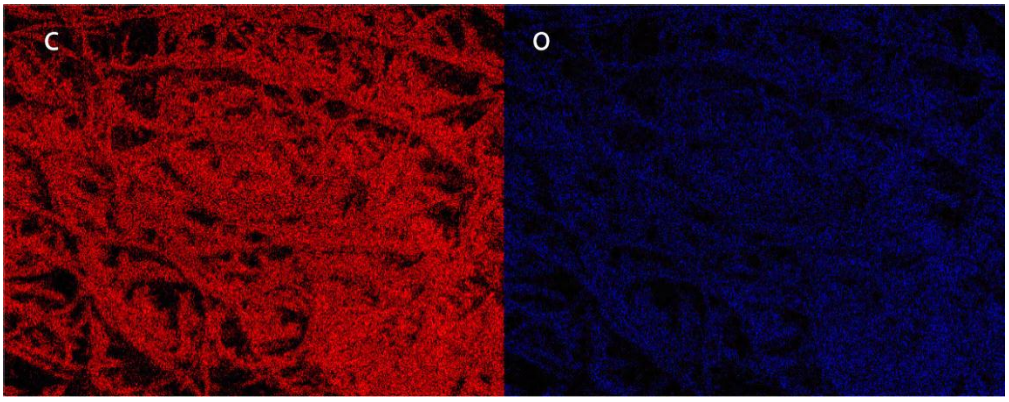

Figure 4.13 Element map of C and O in CDNF.

Noncovalent functionalization of CDNF with PMP was achieved by incubation of CDNF in PMP solution. CDNF was saturated with PMP solution at pH 8.0 for over 20 h for equilibration. PMP-CDNF was characterized by scanning electron microscopy and no substantial change

was observed on CDNF after addition of the PMP molecules. Moreover, CDNF could withstand water (pH ~5-8).(Figure S14)

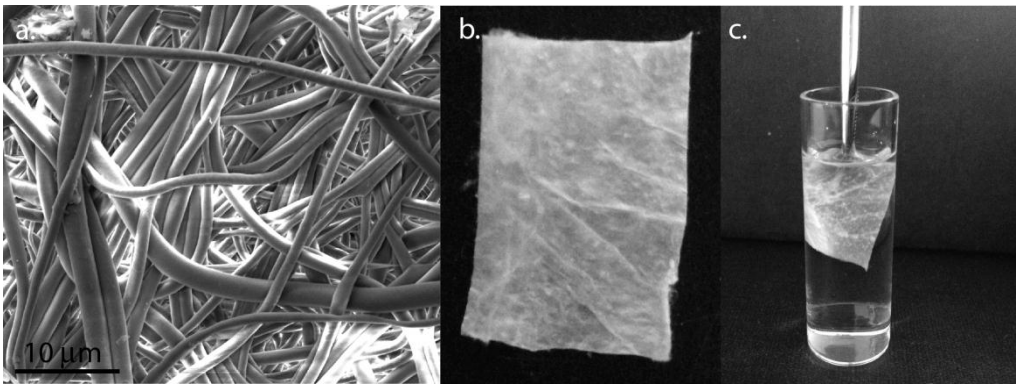

Figure 4.14 a.SEM image of electrospun PMP-HPβCD nanofibers. b.A macro-scale photographic image of PMP-CDNF. c. PMP-CDNF can withstand water.

The nature of interaction between PMP and CDNF was further investigated by using XPS, FT-IR spectroscopy, TGA and Raman spectroscopy. Surface characterization of CDNF by XPS revealed that CDNF contains only C, and O atoms.(Figure 4.15a) However, PMP-CDNF has additional N and S atoms indicating the presence of PMP within the structure.(Figures 4.15b-4.16) On the surface of PMP- CDNF, atom percentages of N and S were 5.90% and 2.04% respectively.(Table 4.1)

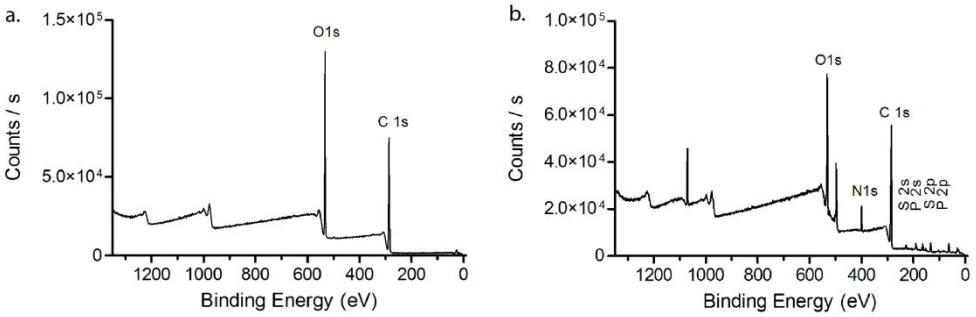

Figure 4.15 XPS spectra of (a) CDNF and (b) PMP-CDNF.

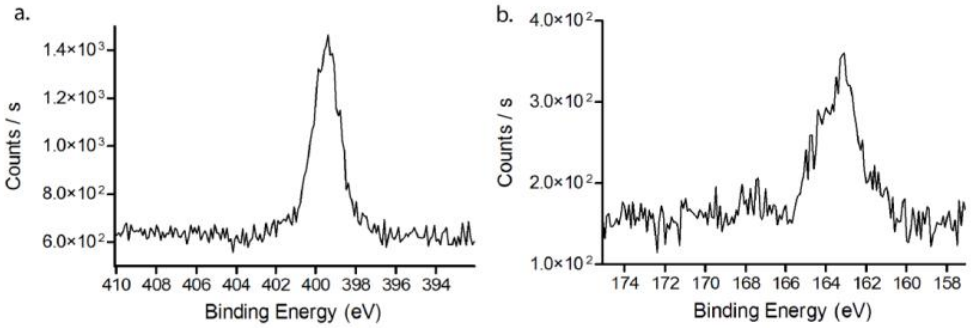

Figure 4.16 a. N1s and b. S2p XPS spectrums of PMP-CDNF.

Table 4.1 Atom percentages of PMP-CDNF in terms of XPS spectrum of PMP-CDNF.

O1s	C1s	N1s	P2p	S2p
26.97	61.72	5.9	3.38	2.04

FT-IR spectra of CDNF and PMP-CDNF were obtained to investigate adamantane-HPβCD complexation. Amide II band of lyophilized PMP shifted from 1533 cm^{-1} to 1581 cm^{-1} upon complexation of PMP with CDNF. (Figure 4.16) Observed shift is indicative of increased in-plane N-H bending, which appears when peptide interactions significantly

reduce PMP interactions. Complexation of PMP with CDNF disrupts interactions of individual PMP molecules (mainly H-bonds).

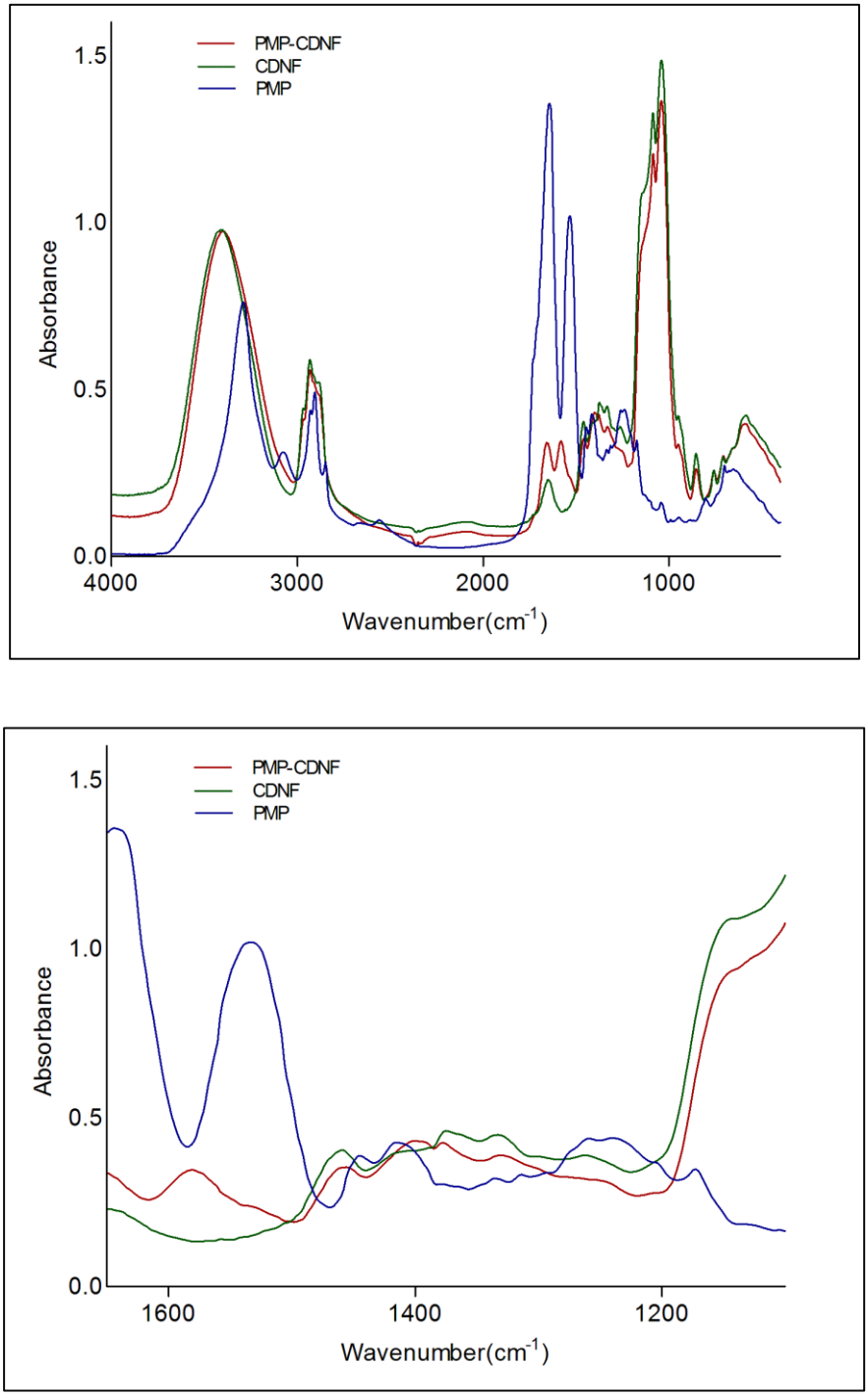

Figure 4.17 FTIR spectra of PMP, CDNF and PMP-CDNF.

Also, TGA of PMP-CDNF was performed to learn additional information about interaction between PMP and CDNF. TGA of only CDNF indicated main degradation at about 300 °C and 370 °C.(Figure 4.18) On the other hand, the crosslinked CDNF showed enhanced degradation temperature of sample due to more energy required for their decomposition so the main degradation of insoluble CDNF shifts to higher temperature (350–400 °C) compared to CDNF. Figure 4.19 indicates the thermograms of pure PMP and adamantane. While TGA of PMP had one main decomposition point at around 265 °C, the adamantane had a main decomposition at around 195 °C. There was a main decomposition point around 370 °C for decomposition of glycopyranose units in HPβCD molecules.(Figure 4.20) The immobilization of the PMP was achieved by the adamantane site with complexation with CD cavity. Thermal degradation of immobilized PMP occurred at two stages with two decomposition points, 210 °C, 265 °C.

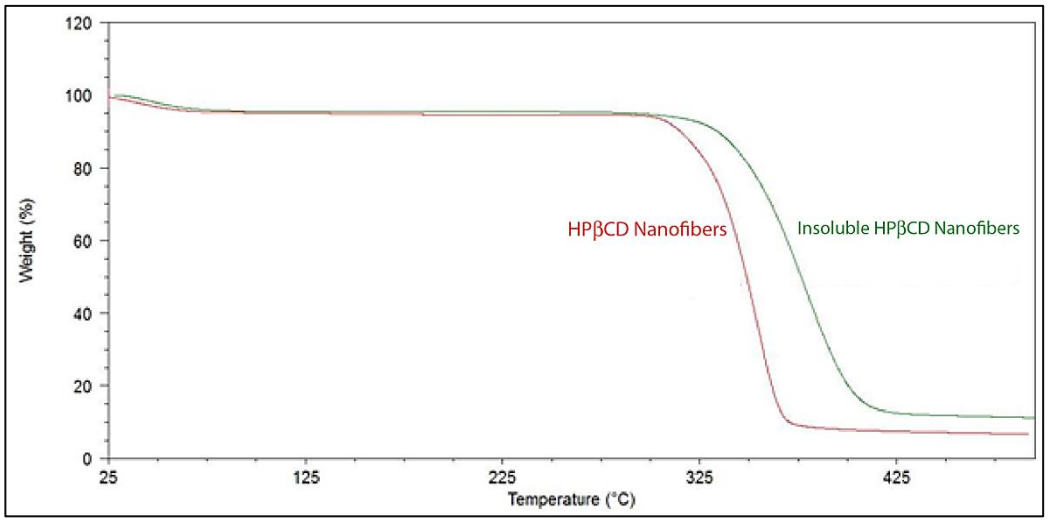

Figure 4.18 TGA thermogram of HPβCD nanofibers and insoluble nanofibers.

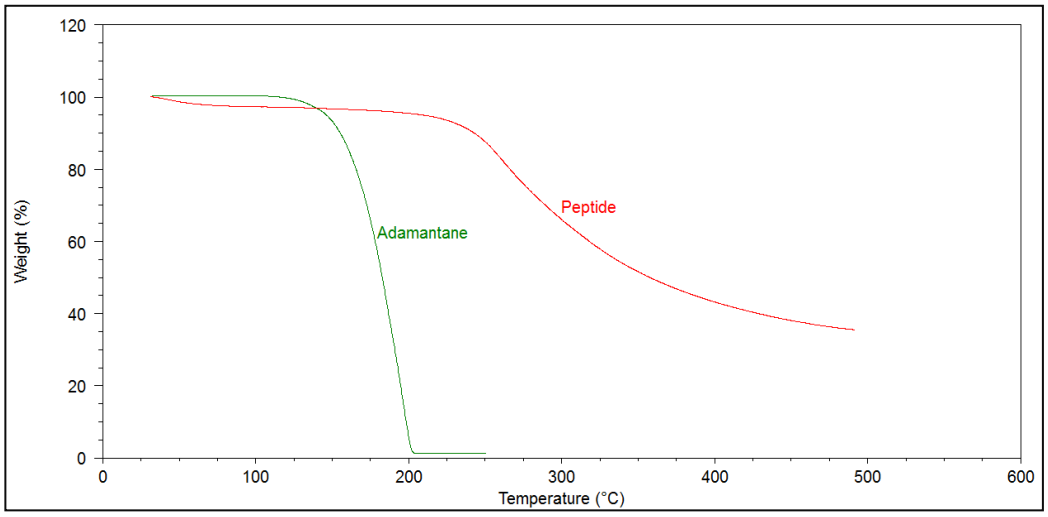

Figure 4.19 TGA thermograms of peptide and adamantane.

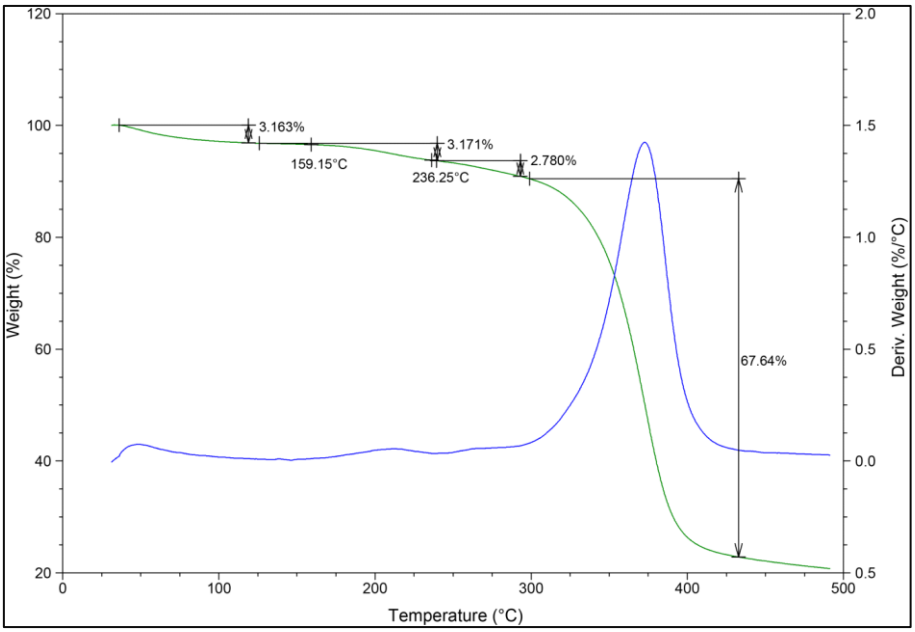

Figure 4.20 TGA thermogram of PMP-CDNF.

Raman spectrum of bare CDNF showed significant β-CD Raman bands such as symmetric stretching of C–O–C at 938 cm^{-1}, stretching vibration of CH_2 at 2934 cm^{-1}, scissoring vibration of CH_2 and CH at 1344 cm^{-1}, and scissoring vibration of O-H at 1409 cm^{-1}. At Raman spectrum of PMP-CDNF revealed additional bands at 2450 cm^{-1} and 1650 cm^{-1} corresponding to stretching vibration of S-H and amide I vibration.(Figure 4.21) Also, confocal Raman image of CDNF at 2750 cm^{-1} demonstrated HPβCD nanofibers.(Figure 4.22)

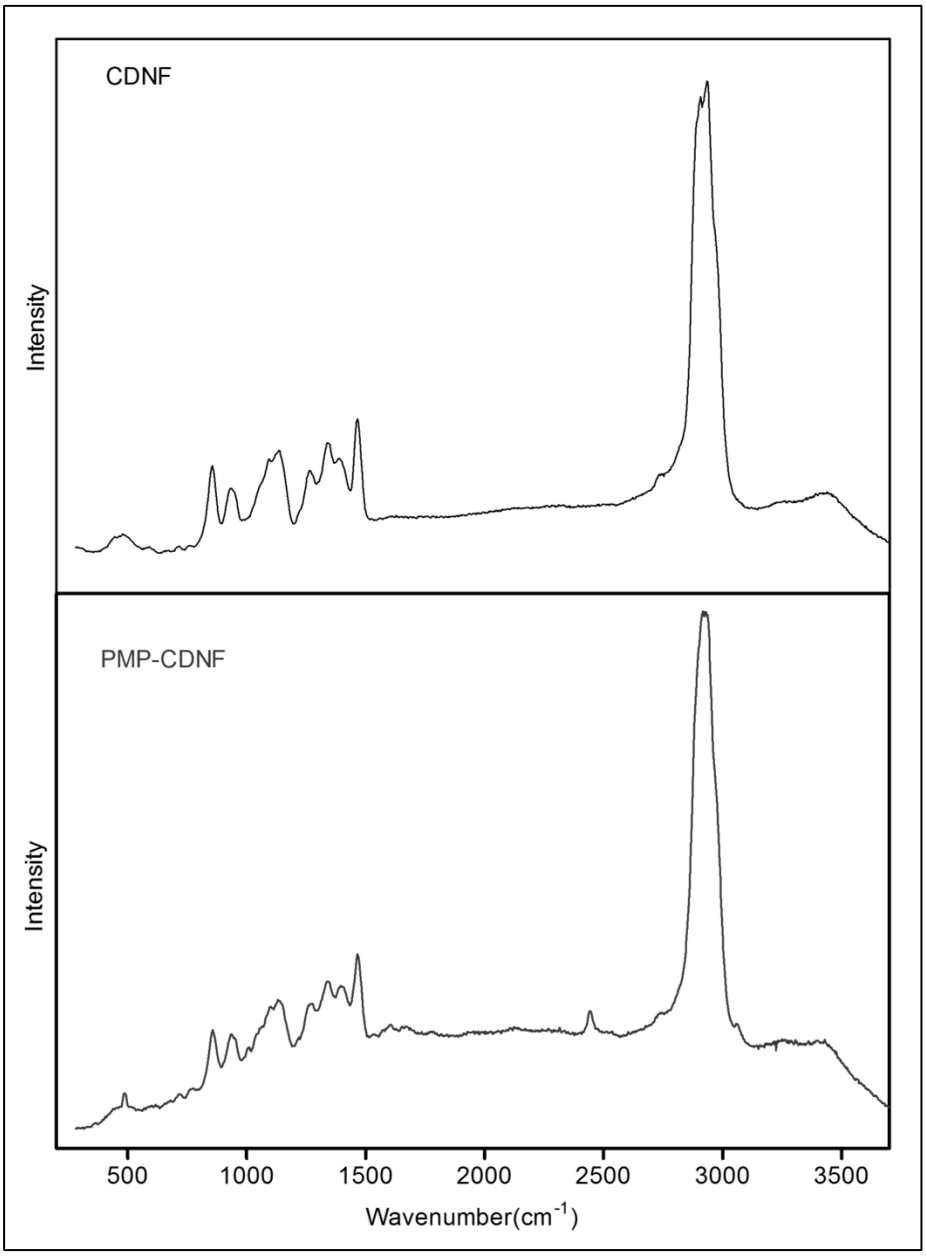

Figure 4.21 Raman spectra of CDNF and PMP-CDNF.

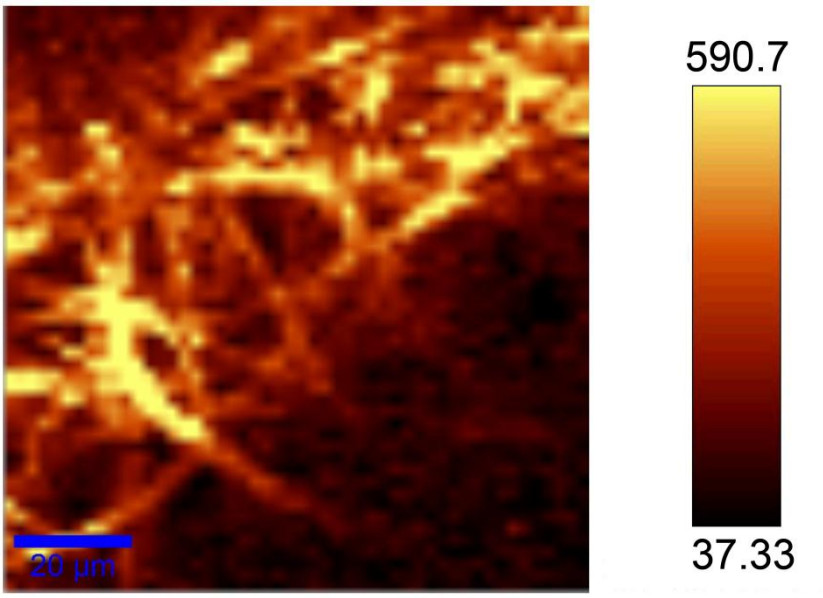

Figure 4.22 Raman spectroscopy image at 2750 cm^{-1} of 100 µm x100 µm CDNF. Color bar shows the corresponding intensity values.

PMP content in CDNF was determined quantitatively with elemental analysis. Only PMP, CDNF, CDNF treated with buffer and TCEP and PMP- CDNF samples were analyzed with CHNS-O analyzer after drying under ambient conditions.(Table 4.2) Mass difference in C, H, N, and S of PMP between experimental and theoretical values was only 1%.(Table 4.3) Moreover, there was negligible amount of N and no S atom in HPβCD nanofibers treated with buffer although there was no N and S in CDNF. N content could be caused by nonspecific binding of buffer. For consistency, PMP content in PMP-CDNF was calculated by using S amount.(Table 4.4)

Table 4.2 Atom weight percentages of PMP, CDNF, CDNF treated with TCEP and TRIS and PMP-CDNF in terms of CHNS-O analyzer.

Compound	**wt % C**	**wt % H**	**wt % N**	**wt % S**
PMP	46.119± 0.5075	5.8676± 0.2769	11.156± 0.1063	7.9138± 0.0842
CDNF	46.888± 0.6483	6.7914± 0.1449	0	0
PMP-CDNF	43.572± 0.2839	6.4800± 0.0123	1.2238± 0.0546	0.4751± 0.0349
CDNF treated with TCEP&TRIS	44.670± 1.0894	6.8153± 0.0326	0.8670± 0.2824	0

Table 4.3 Comparison of experimental and theoretical [C]/[S], [N]/[S], [H]/[S], and [C]/[N] of PMP.

Compound	**[C]/[S]**	**[N]/[S]**	**[H]/[S]**	**[C]/[N]**
Experimental -PMP	15.540	3.2222	23.726	4.823
Theoretical -PMP	15.333	3.3333	23.000	4.6000
% Difference	1.0135	0.9667	1.0315	1.0484

Table 4.4 PMP and CDNF amount in 100 g PMP-CDNF.

PMP[a,b,c] (g)	**CDNF[c] (g)**	**PMP[a,c] (mol)**	**CDNF[c] (mol)**
5.5080	94.492	0.0049	0.0647

[a] Calculated in terms of S amount in PMP-CDNF and experimental S content in PMP elemental analysis. [b]Calculated based on deprotonated PMP molecular weight. [c] Amount of molecules in 100 g PMP-CDNF.

PMP functionalized and bare CDNFs were immersed into metal ion solutions (Ni^{II}, Cd^{II}, Cr^{VI} and mixture of all of these metal ions). Since metal ions can bind to PMP molecules, metal ions can be removed from water solution with immersion of PMP functionalized CDNFs into solution. Metal ion concentration in solution was monitored with ICP-MS. PMP- CDNF and CDNF were incubated with different metal ion solutions. Fabricated PMP-CDNF captured 0.041±0.004 μmol/mg Cd^{II}, 0.010±0.001 μmol/mg Ni^{II} and 0.008±0.005 μmol/mg Cr^{VI} after 24 h of incubation.(Figure 4.23a) However, CDNF had less than 0.005 μmol Cd^{II}, Ni^{II} and Cr^{VI}.(Figure 4.23a) Moreover, PMP-CDNF and CDNF were incubated in mixture of Ni^{II}, Cd^{II}, Cr^{VI} to understand the selectivity of PMP-CDNF and CDNF.(Figure 4.24b) PMP-CDNF had the highest binding affinity towards Cd^{II} and the lowest towards Cr^{VI}. In the same conditions, CDNF itself scavenged almost no metal ion from the water. Also, amount of metal ions bound to per mg of PMP-CDNF within time increased linearly both from different metal ion solutions and from mixture of metal solutions.(Figure 4.24) Within time metal ions bound to

bare CDNF did not increase and no nonspecific binding was observed.(Figure 4.25)

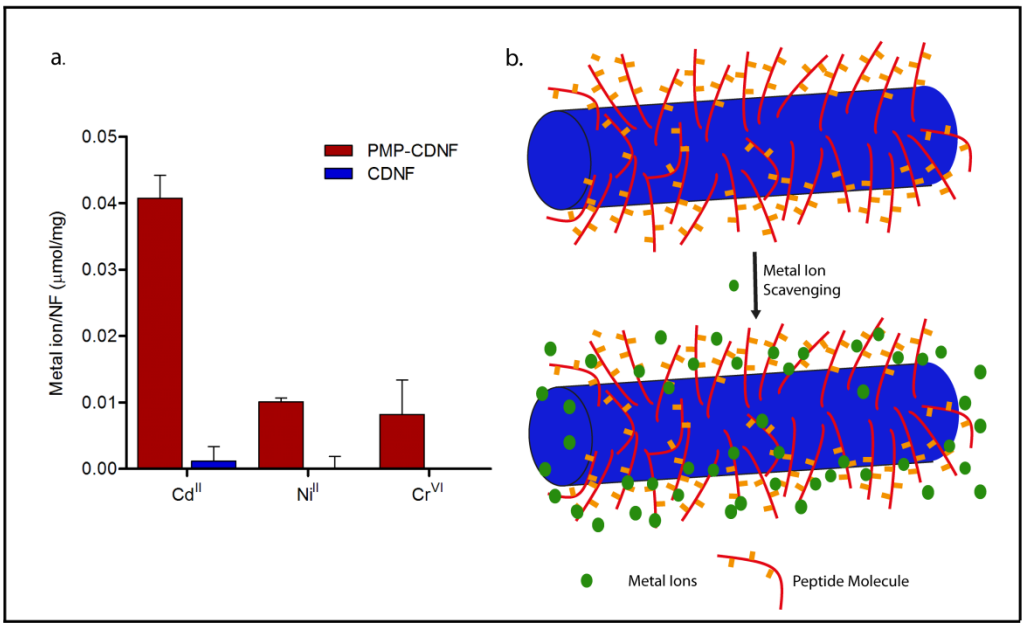

Figure 4.23 a. The graph shows the amount of metal ions in µmol bound to per mg of PMP-CDNF and CDNF in 24 h. b. Schematic presentation of metal ions binding.

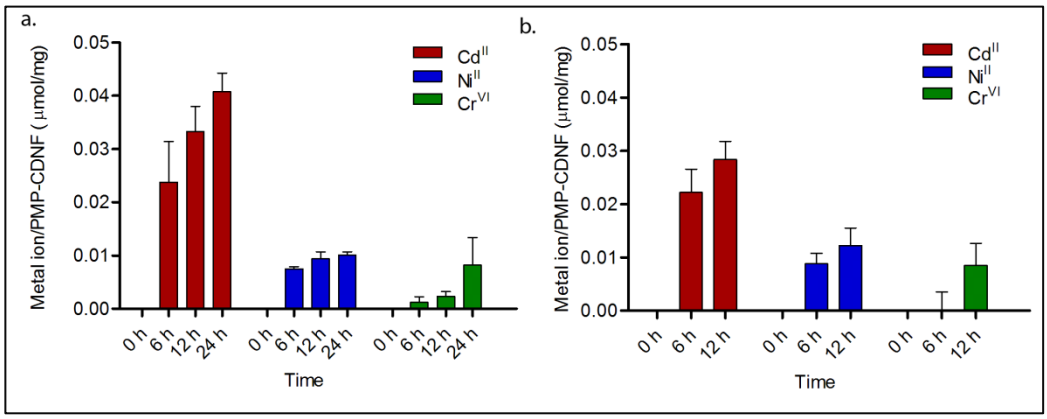

Figure 4.24 Amount of metal ions in µmol bound to per mg of PMP-CDNFa. from different solutions b. from a mixture of metal ions within time.

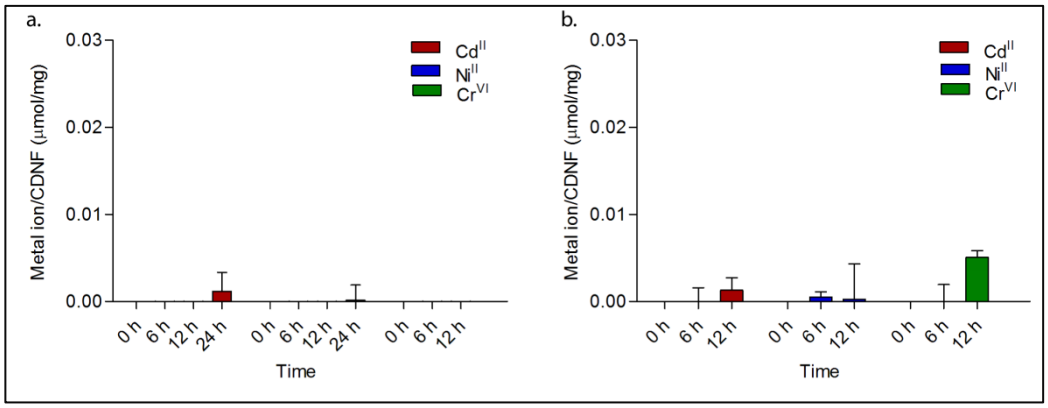

Figure 4.25 Amount of metal ions in µmol bound to per mg of CDNF from metal ions a. from different solutions b. from mixture of metal ions within time.

No significant difference in morphology of PMP functionalized CDNF was observed upon binding to metal ions.(Figure 4.26) The XPS analysis showed that number of metal ions were significantly higher on the surface of PMP-CDNFs than CDNFs.(Figures 4.27-4.37) Surfaces of bare and PMP functionalized CDNFs were analyzed with Raman spectroscopy after metal immersion. As vibration of S-H decreased, vibration of amide I remained constant at PMP-CDNF.(Figure 4.38) Bare CDNF demonstrated none of the amide I and S-H bands.(Figure 4.39)

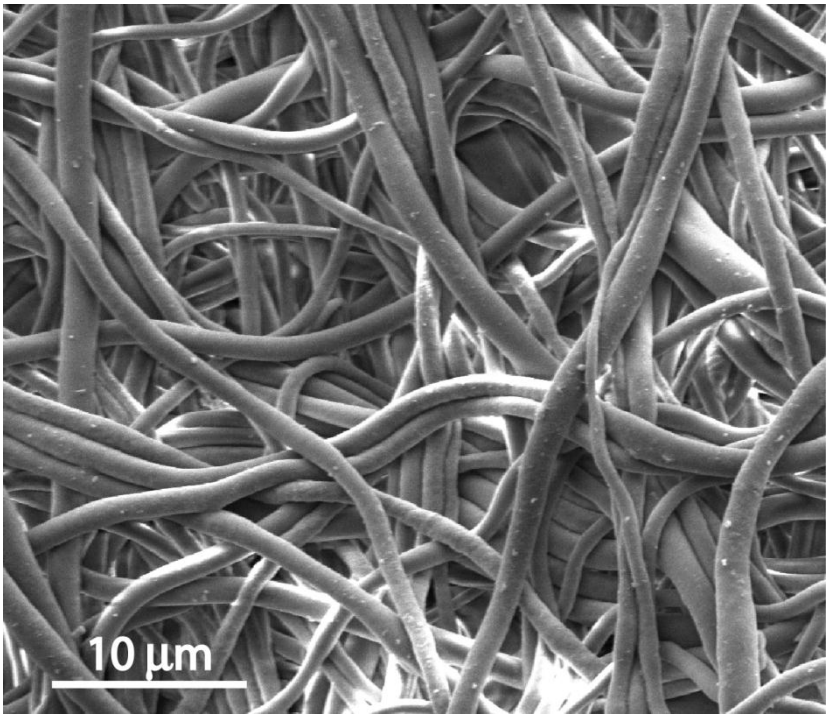

Figure 4.26 SEM image of PMP-CDNF after metal incubation.

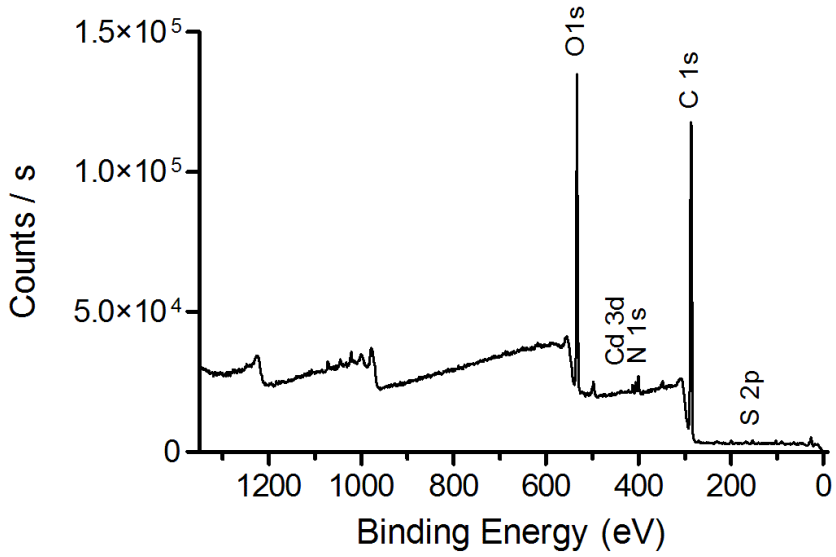

Figure 4.27 XPS spectrum of PMP-CDNF after 24 h incubation in Cd^{II} solution.

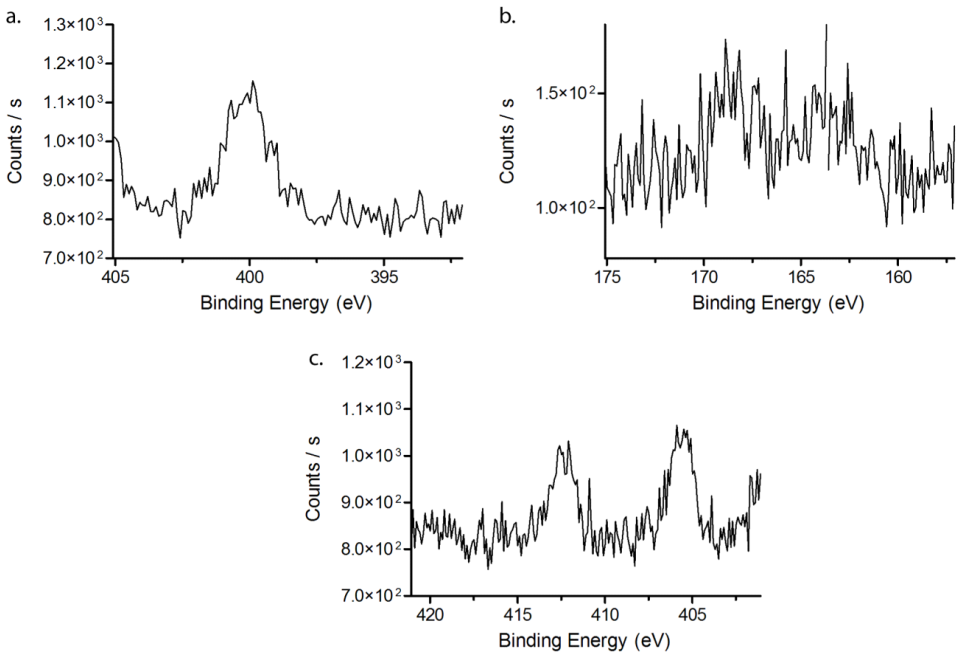

Figure 4.28 a. N1s and b. S2p c. Cd3d XPS spectra of PMP-CDNF after 24 h incubation in Cd^{II} solution.

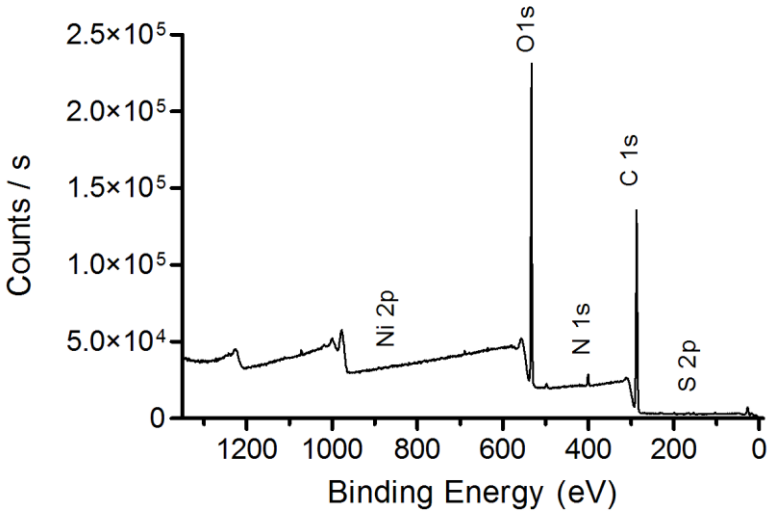

Figure 4.29 XPS spectrum of PMP-CDNF after 24 h incubation in Ni^{II} solution.

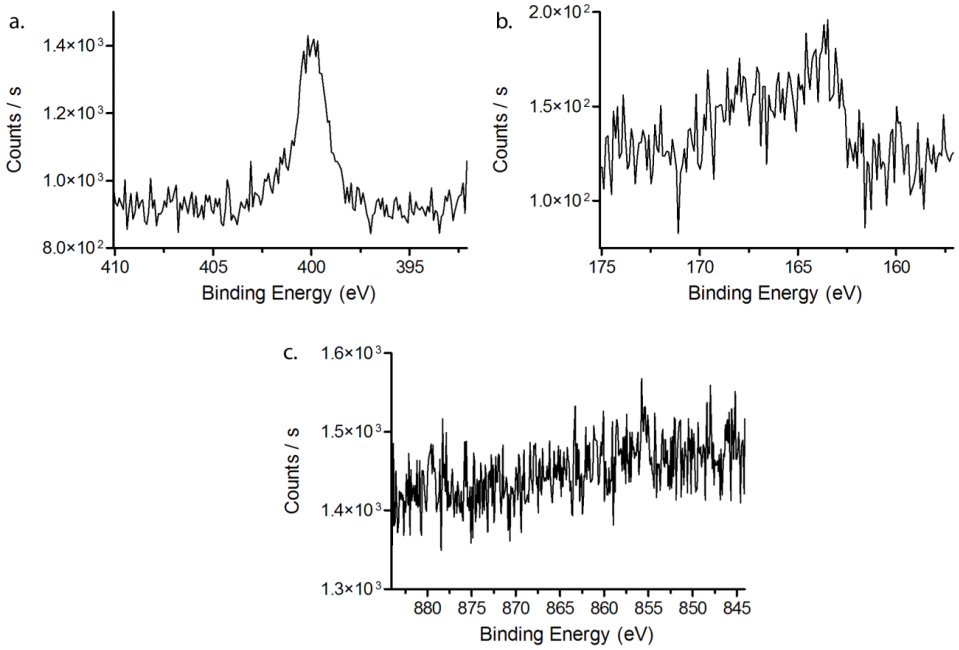

Figure 4.30 a. N1s and b. S2p c. Ni2p XPS spectra of PMP-CDNF after 24 h incubation in Ni^{II} solution.

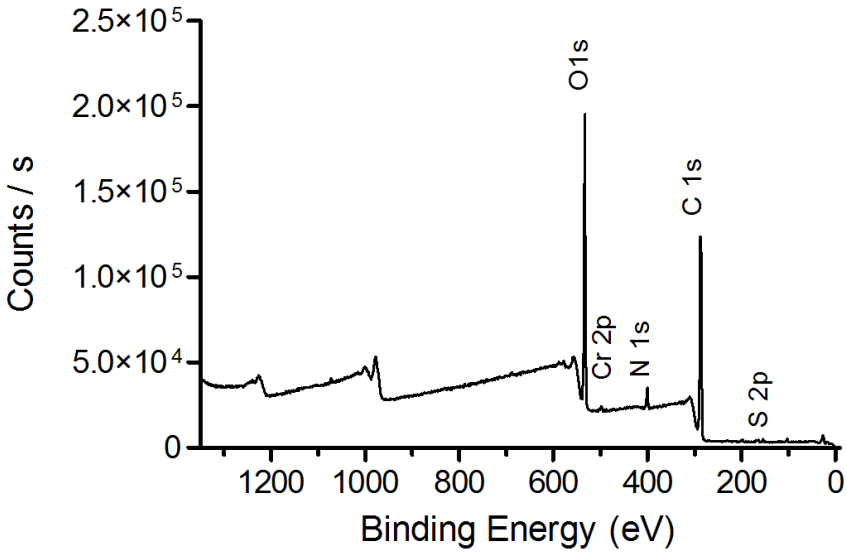

Figure 4.31 XPS spectrum of PMP-CDNF after 24 h incubation in Cr^{VI} solution.

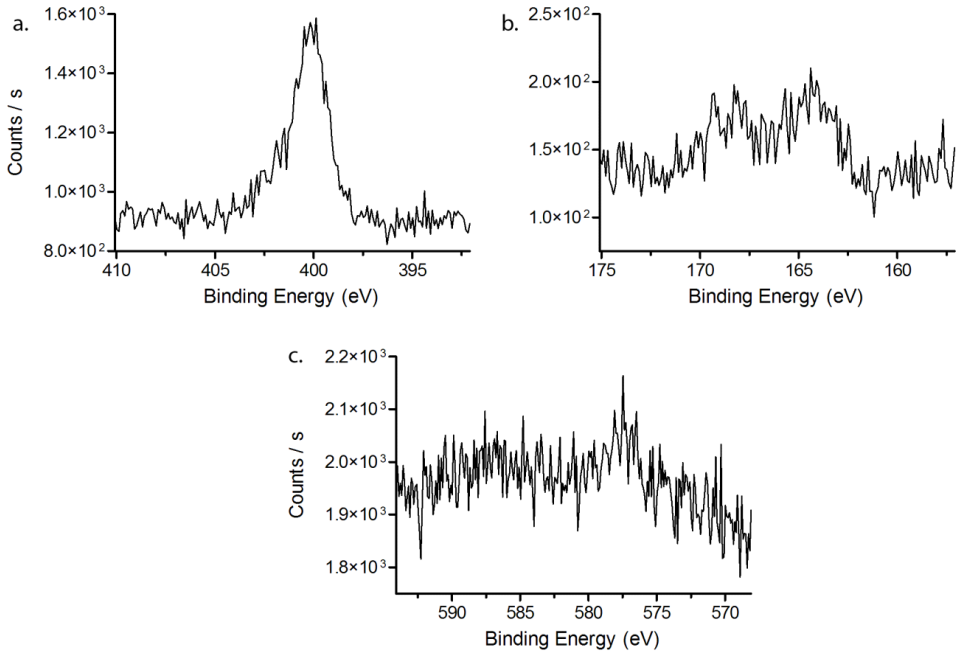

Figure 4.32 a. N 1s and b. S 2p c. Cr 2p XPS spectra of PMP-CDNF after 24 h incubation in Cr^{VI} solution.

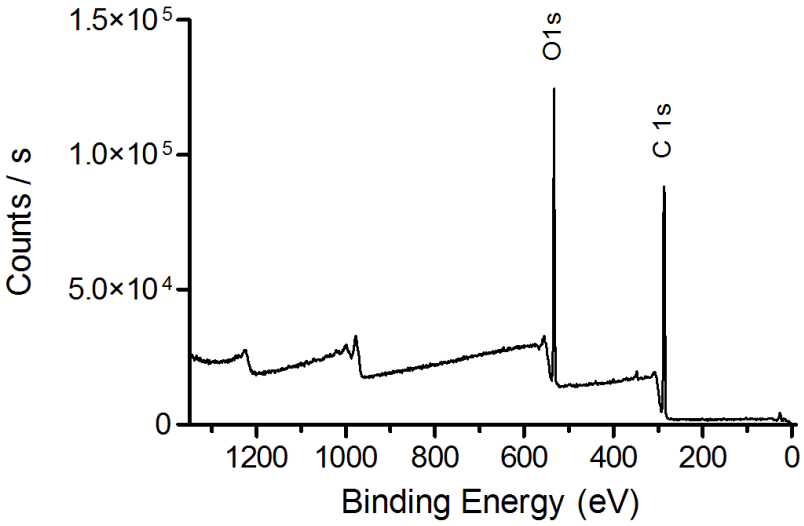

Figure 4.33 XPS spectrum of CDNF after 24 h Cd^{II} incubation.

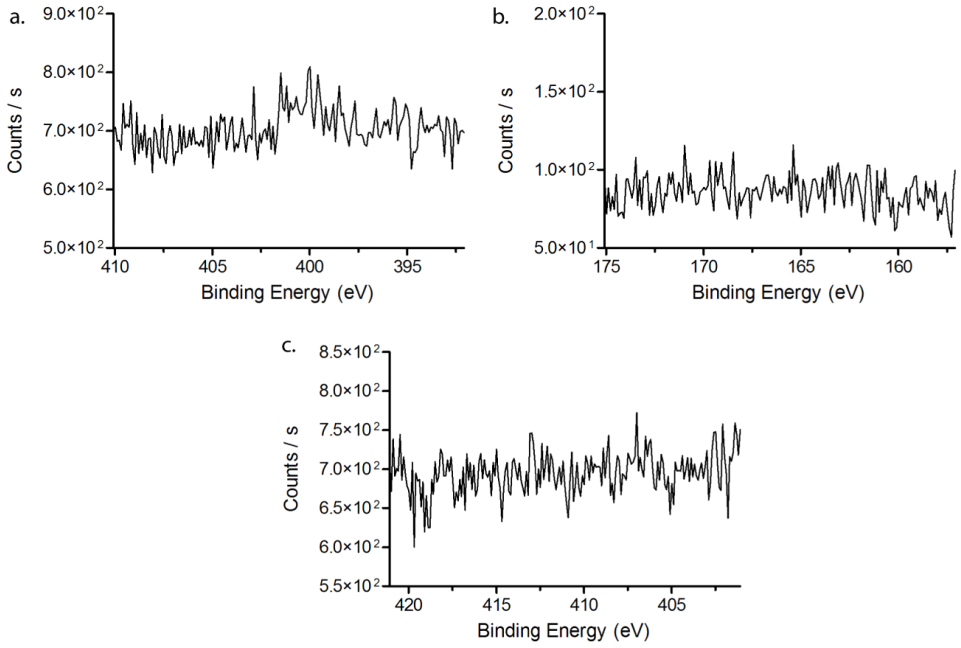

Figure 4.34 a. N 1s and b. S2p c. Cd3d XPS spectra of CDNF after 24 h Cd^{II} incubation.

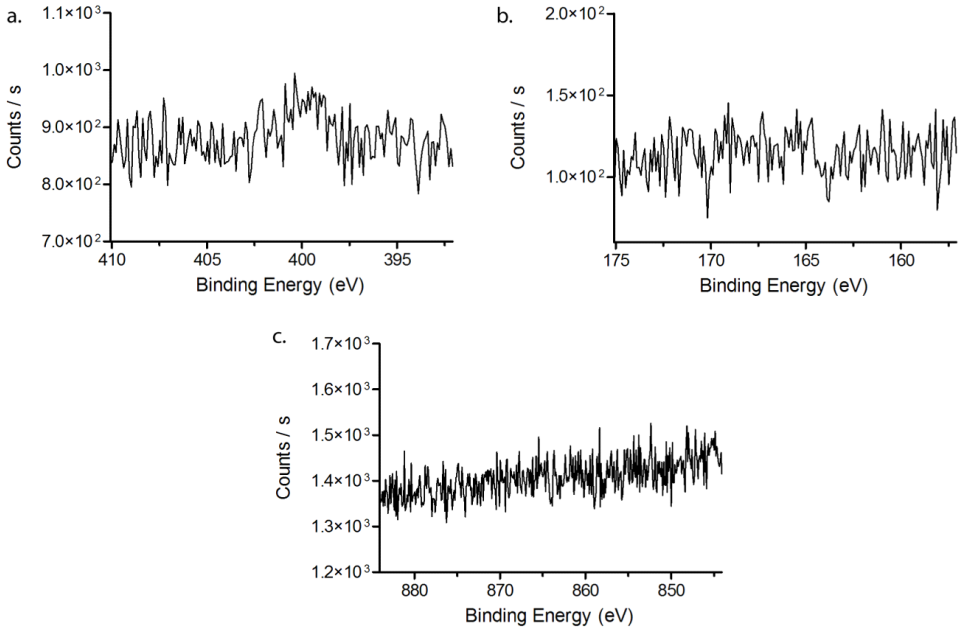

Figure 4.35 a. N 1s and b. S 2p c. Ni2p XPS spectra of CDNF after 24 h Ni^{II} incubation.

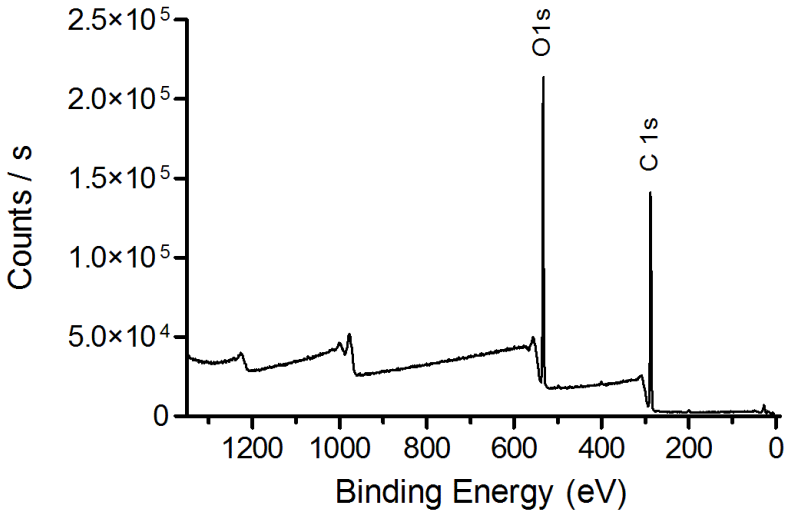

Figure 4.36 XPS spectrum of HPβCD NW after 24 h Cr^{VI} incubation.

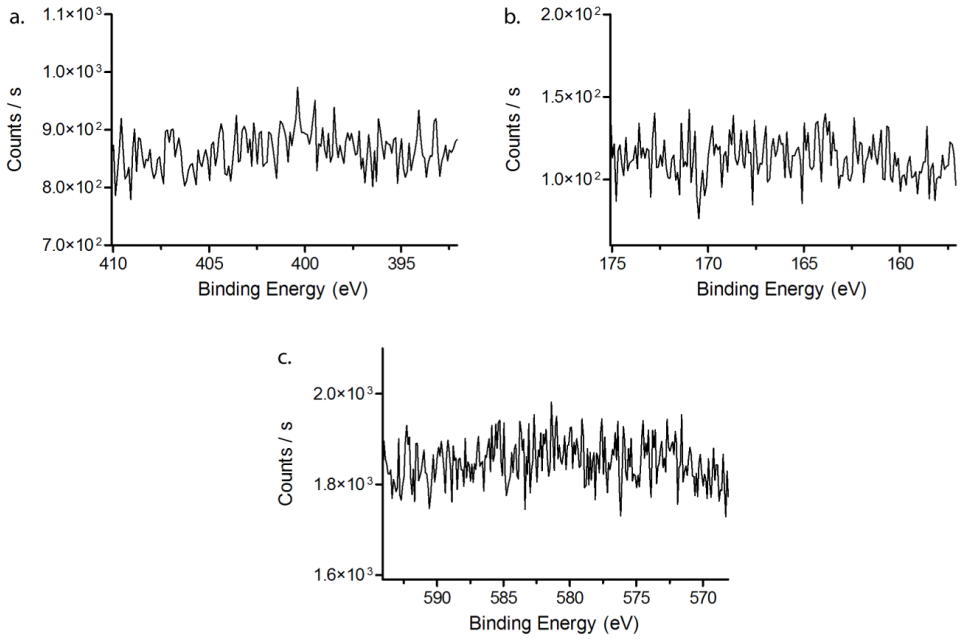

Figure 4.37 a. N 1s and b. S 2p c. Cr 2p XPS spectra of CDNF after 24 h Cr^{VI} incubation.

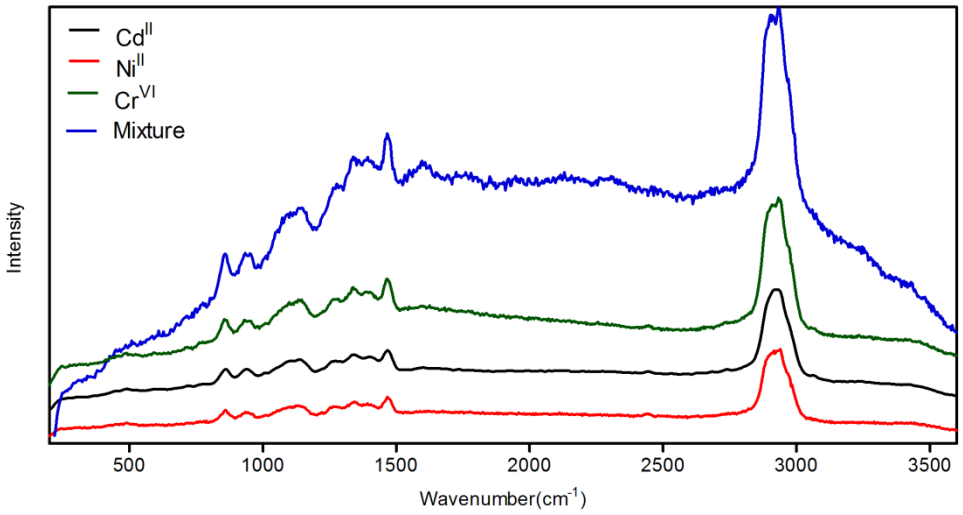

Figure 4.38 Raman spectra of PMP-CDNF after 24 h incubation with different metal solutions and mixture of the metal solutions. As amide I band at around 1650 cm^{-1} stayed almost constant, peak height at 2450 cm^{-1} decreased after metal incubation.

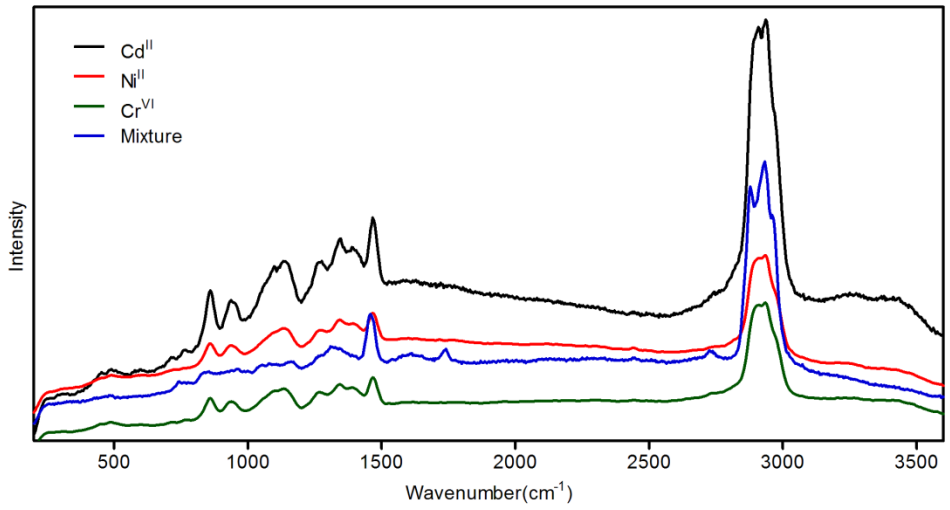

Figure 4.39 Raman spectra of CDNF after 24 h incubation with different metal solutions and mixture of the metal solutions.

4.4 Conclusion

In conclusion, we demonstrated design and synthesis of a heavy metal binding peptide sequence, which can functionalize electrospun β-cyclodextrin nanofibers through adamantane-HPβCD host-guest inclusion complex. Metal ion binding ability of PMP molecule was certified with Cd^{II}, Ni^{II}, and Cr^{VI} ions in aqueous conditions. ITC measurements and titrations of metal ions with PMP molecule confirmed the binding of PMP molecules to corresponding metal ions. ITC measurement of PMP and β-CD showed that there was moderately binding affinity between the engineered PMP and HPβCD. Furthermore, PMP conjugated CDNF was characterized quantitatively and qualitatively with XPS, FT-IR spectroscopy, TGA, Raman spectroscopy and elemental analysis. After employment of PMP-CDNF for metal ion solutions to scavenge, the amount of metal ions bound to CDNFs was quantified with ICP-MS. Surface and physical characterization of CDNFs was accomplished with XPS, Raman spectroscopy and SEM analysis. Hence, we successfully acquainted design, synthesis, application and characterization of a peptide based water scavenging system. Our peptide based water scavenging system is utile for development of further water scavenging systems with variant peptide sequences or host-guest inclusion complexes.

Chapter 5

Metalloenzyme Mimetic Peptide Supramolecular Nanostructures for Bone Tissue Regeneration

5.1 Introduction

Metalloenzymes comprise nearly half of the known enzymes controlling critical aspects of biological systems like photosynthesis,[70] water oxidation,[11] respiration,[12] and nitrogen fixation[13] etc. Therefore, *de novo* metalloenzyme design is attractive for many scientists since it is not only a challenging exercise in terms of complexity of metalloenzyme structure but also can reveal the unsolved structural and functional secrets of metalloenzymes.[71] In metalloenzymes, geometry of metal ions is crucial because it determines the enzymatic capacity of the metalloenzyme besides 3-D structure of proteins. Hence, insertion of a metal ion to the protein environment requires an ordered but flexible structure of proteins to function properly. Here, we presented alkaline phosphatase mimicking nanostructures consisting of Zn^{II} coordinating catalytically active sites.

Among various metal ions, zinc is especially important because it takes part in many critical functions involving metalloenzymes.[72] It is known that there are 300 zinc containing metalloenzymes having strong interactions between zinc ion and nitrogen, sulfur, and oxygen. Also, zinc ion is resistive to reduction and oxidation.[73] Moreover, the flexibility in coordination geometry makes ligand exchange facile and enhances the ability of zinc to effect a catalytic cycle.

Alkaline phosphatase, ALP, is a zinc containing metalloenzyme functioning in formation of inorganic phosphate from phosphate monoesters.[74] Promoting the formation of hydroxyapatite (HA),

$Ca_5(PO_4)_3(OH)$, it exists especially in extracellular matrix vesicles in bone tissue.[75] It is known that HA enhances biomineralization and has osteoconductive and osteoinductive effects.[76] Therefore, ALP has a crucial role in regeneration of bone tissue. In stabilization of zinc ions, histidine residues have an important role with respect to coordination with zinc ions through its Lewis basic nitrogen atom of histidine's side chain. The water molecule bound to zinc ion is deprotonated and becomes facile to make a nucleophilic attack to break ester bond.

A histidine tagged peptide amphiphile (PA) is one of the most suitable structures for being an ALP mimetic structure because of the following features: i. PA molecules can self-assemble into nanofibers concentrating functional groups (His) in the surface of the structures, ii. histidine residues can coordinate with divalent zinc ions as it is in natural AP, iii. PA is neutral at physiological pH values, while it possesses acidic and basic nitrogen atoms in histidine side chain, iv. Zinc ions can interact with each other in an order as in natural, dinuclear, ALP, v. PA molecules are biocompatible.

In the present study, ALP mimetic nanostructures were designed. We designed two self-assembling PA molecules having histidine residues in different positions.(Figure 5.1) In bottom-up synthesis approach, we constructed coordination spheres through branched peptide amphiphile structures. The branched geometry enables proper cavity for metal ions to interact with imidazole moieties efficiently. As a result of self-assembling of PA molecules into nanofibers, zinc coordinating sites will

concentrate over the surface of nanofibers. Also, cooperativity between Zn^{II} coordinating sites will enhance the catalytic activity of nanofibers. In the linear sequence, imidazole moieties in peptide become less facile because of the steric hinderance although there is cooperative effect between imidazole moieties in peptide amphiphile nanofiber.

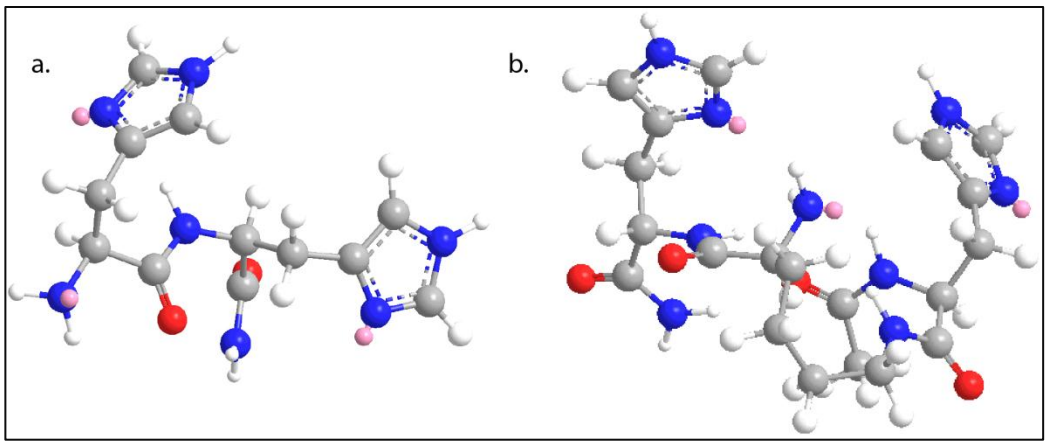

Figure 5.1 Zn^{II} binding site of **a.** linear and **b.** branched peptide amphiphiles.

Peptide amphiphiles were synthesized with solid phase peptide synthesis method. Thereafter, peptide amphiphiles were characterized with liquid chromatography-mass spectrometry, circular dichroism spectroscopy and transmission electron microscopy. Interaction between peptide amphiphiles and Zn^{II} was characterized with CD spectroscopy, isothermal titration calorimetry, and dynamic light scattering (DLS). For the determination of catalytic activity of nanostructures, *p*-nitrophenyl acetate (*p*NPA) was used as a model substrate because of its higher hydrolysis rate compar.ng to *p*-nitrophenyl phosphate hydrolysis. Moreover, they were used in inorganic calcium phosphate formation as a

supplier of inorganic phosphate ion from organic phosphate molecules. The resulting calcium phosphate was characterized with scanning electron microscopy, electron diffraction X-ray spectroscopy and Raman spectroscopy. Also, osteogenic activities and effects of calcium phosphate formation of ALP mimetic nanostructures will be tested in *in vitro* studies with Saos-2.

5.2. Materials and Methods

5.2.1 Materials

Fmoc protected amino acids, Fmoc-N'-methyltrityl-L-lysine (Fmoc-Lys(mtt)-OH), MBHA Rink Amide Resin, HBTU (O-Benzotriazole-N,N,N’,N’-tetramethyl-uronium-hexafluoro-phosphate) were purchased from Novabiochem, lauric acid was purchased from Merck.

5.2.2 Synthesis and Purification of Peptide Amphiphile Molecules

Peptide amphiphile (PA) molecules were synthesized by using Fmoc chemistry. Synthesis was performed manually on a 0.25 mmole scale using a 50 mL peptide synthesis vessel on a wrist action shaker. Rink amide MBHA resin was used for peptide synthesis. For each coupling reaction, Fmoc groups were removed by shaking resins in 20% piperidine in DMF for 20 min. After each reaction, resins were washed three times with DMF, DCM and DMF respectively. All amino acids were activated by adding 2 molar equivalents of amino acid to 1.95 equivalents of HBTU and dissolved in 10 mL of DMF. After complete

dissolution of amino acid and HBTU in DMF, 3 molar equivalents of DIEA were added into the solution. The solution was mixed thoroughly and kept for 3 min before adding to the resin. Each coupling reaction was performed for 3 h. Lauric acid was coupled to the peptides N-terminal. Ninhydrin test was performed after addition of each amino acid and after addition of the lauric acid. When ninhydrin test yielded positive results, coupling reaction was repeated; otherwise 10 mL of 10% acetic anhydride in DMF was added and resins were shaken for 30 min. Peptide cleavage and removal of the protecting groups were performed with 95:2.5:2.5 TFA:TIS:water for 2.5 h at room temperature. After cleavage reaction, PA molecules were collected in a clean round bottom flask and DCM wash was performed for several times. Collected solution was rotary-evaporated. After evaporation, ice-cold diethyl ether was added and was left at -20 °C overnight. PA-diethyl ether mixture was collected in 50 mL falcon tubes and centrifuged at 8000 rpm for 25 min. Supernatant was decanted and the remaining diethyl ether was evaporated. The pellet was dissolved in deionized H_2O and was freeze-dried.

For the synthesis of branched peptide amphiphile, PA1, synthesis route was different. After addition of lauric acid to resin, the peptide backbone bound to resin, Lauryl-VVAGK(mtt)H was treated with 5 mL 5% TFA solution (95:2.5:2.5 TFA:TIS:water) in DCM for three times. This step was required for cleavage of protecting group in side chain of lysine (methyltrityl). After treatment, resin was washed with DCM. Coupling of

histidine to lysine's side chain was performed with traditional HBTU-DIEA coupling. Then, peptide was acetylated. Finally, peptide was removed from resin as described above.

5.2.3 Liquid Chromatography

For the structural analysis of the peptide Agilent Technologies 6530 Accurate-Mass Q-TOF LC-MS and Zorbax SB-C8 column were used. Concentration of the sample for LC-MS measurement was 0.5 mg/mL. Solvents were water (0.1% formic acid) and acetonitrile (AcN) (0.1% formic acid). LC-MS was run for 25 min for each sample and it started with 2% ACN and 98% H_2O for 5 min. Then, AcN concentration reached to 100% until 20 min. Finally, its concentration was dropped to 2% and it kept running for 5 minutes. Solvent flow 0.65 mL/min and 5 µL sample was injected.

5.2.4 Circular Dichroism

Secondary structure of peptide amphiphile was analyzed with Jasco J-815 circular dichroism spectrometer. 1 wt % peptide solution was prepared in ddH_2O and gelified with 0.1 M NaOH. Then, peptide gel was diluted with 1 mM NaOH solution and $5x10^{-4}$ M peptide solution was measured from 300 nm to 190 nm with 0.1 data pitch, 100 nm/min scanning speed, 1 nm band width and 4 s D.I.T. Average of three measurements were used and sensitivity was selected as standard.

5.2.5 Isothermal Titration Calorimetry

Peptide solutions were titrated with $ZnCl_2$ solution NaOH solution at pH 7.4. Cell temperature was 25 °C, reference power was 5 µcal/s, and stirring speed was 500 rpm.

5.2.6 Hydrolysis Experiments

Hydrolysis experiments were performed at 50 mM TRIS buffer at pH 7.4. 0.028-1.2 mM *p*-nitrophenyl phosphate solutions were prepared in distilled water from a stock solution prepared in acetonitrile. The reactions were catalyzed with 10 µM $ZnCl_2$ and 15 µM PA solutions.

5.2.7 CaP Mineralization

For biomineralization studies, glass coverslips were coated with 600 µM PA with and without 400 µM $ZnCl_2$ and placed in each well of 24 well-plates (HC surfaces). As control, $ZnCl_2$ coated and bare coverslips were used. Then, 50 mM TRIS buffer at pH 7.4 with 24 mM $CaCl_2$, 14.4 mM β-glycerophosphate was added to each well. In *in vitro* control experiments, coverslips were coated with 1 mM PA and 25 µM $ZnCl_2$ (LC surfaces). 10 mM β-glycerophosphate and 1.8 mM $CaCl_2$ were added to 50 mM TRIS buffer at pH 7.4. At day 1 and 3, solution was removed from surface and coverslips were dried at ambient conditions.

5.2.8 Raman Spectroscopy

WITec Alpha300S Scanning Near-field Optical Microscope with Raman module was used to characterize NWs. Nd:YAG 532 nm laser source was used in the experiments. Integration time was 0.53492 s. Number of accumulation was 50. For Raman spectral image, 150 μm x150 μm was scanned with 50 points per line and 50 lines per image. Scan speed was 10.610 s/line and integration time was 0.2122 s.

5.2.9 Scanning Electron Microscopy

FEI Quanta 200 FEG environmental scanning electron microscope was used. Coverslips were coated with 3 nm Au-Pd. Images were taken with 10-15 kV.

5.2.10 X-Ray Diffractometer

In crystallographic analysis of calcium phosphate crystals, PANanalytical X'Pert X-ray diffractometer was performed by using Cu Kα radiation. Peptide coated glass surfaces were measured. Rotation time was 16 seconds, scan range was from 20° to 70°, and step size was 0.0525°.

5.3 Results and Discussion

Chemical structures of peptide molecules were shown in Figure 5.2. After synthesis of PA1 and PA2 with solid phase peptide synthesis

method, purity of peptide molecules were analyzed with LC-MS.(Figures 5.3-5.4)

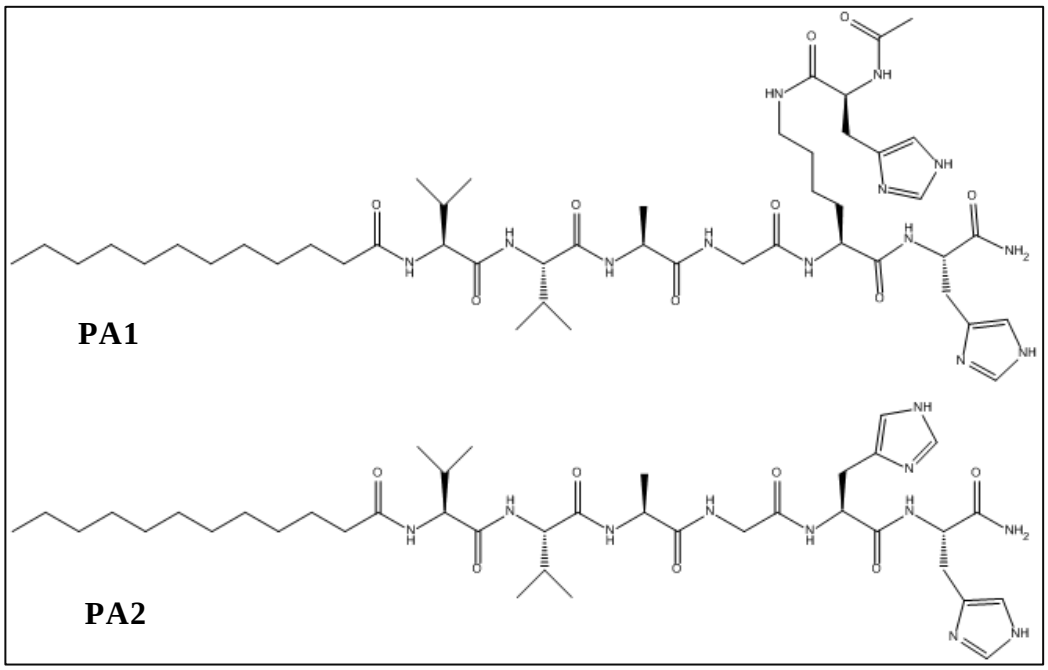

Figure 5.2 Chemical structure of peptide amphiphiles.

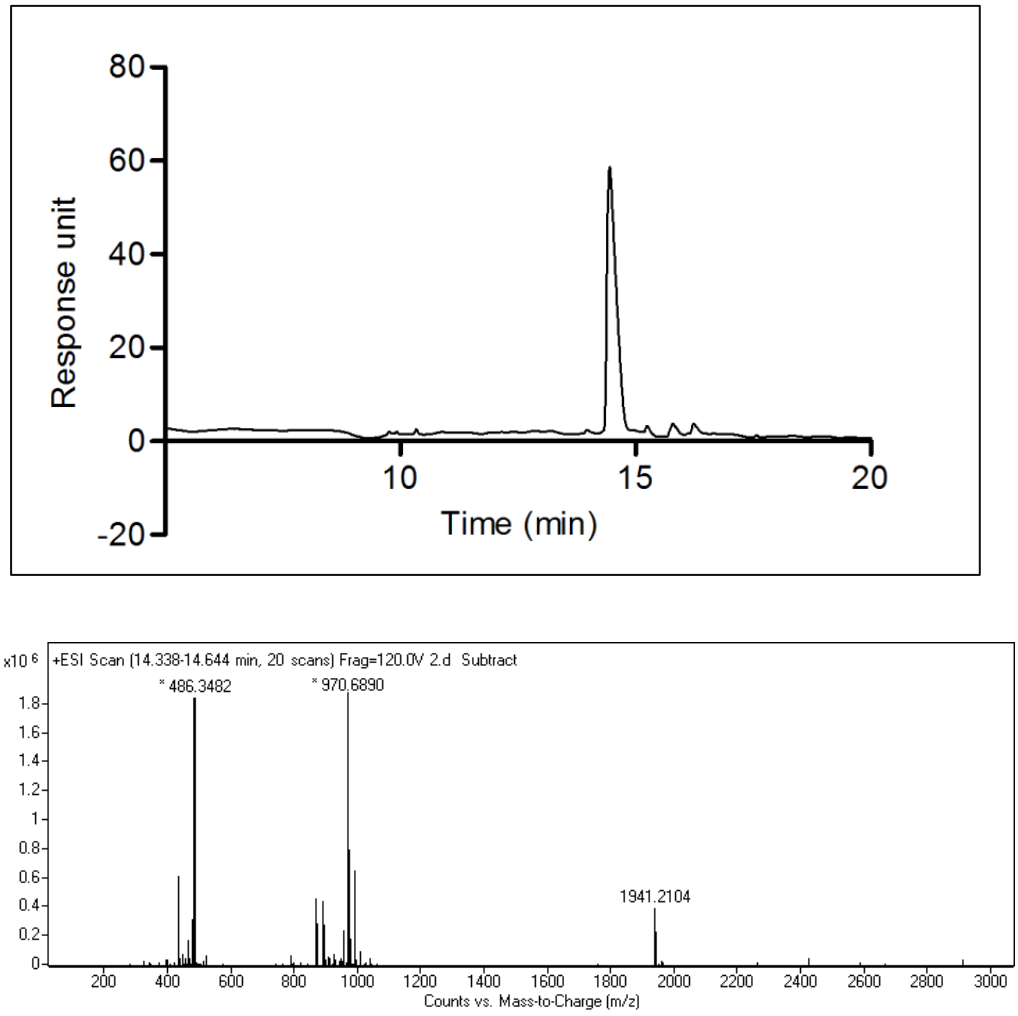

Figure 5.3 HPLC chromatogram of peptide. Absorbance at 220 nm vs. retention time graph (top). Mass spectrum of peptide after subtracting mass spectrum of water sample at that time interval (bottom). $[M+H]^+$ (calculated)=971.21, $[M+H]^+$(observed)=970.6890, $[M/2+H]^+$ (calculated)=486.105, $[M/2+H]^+$ (observed)=486.3482.

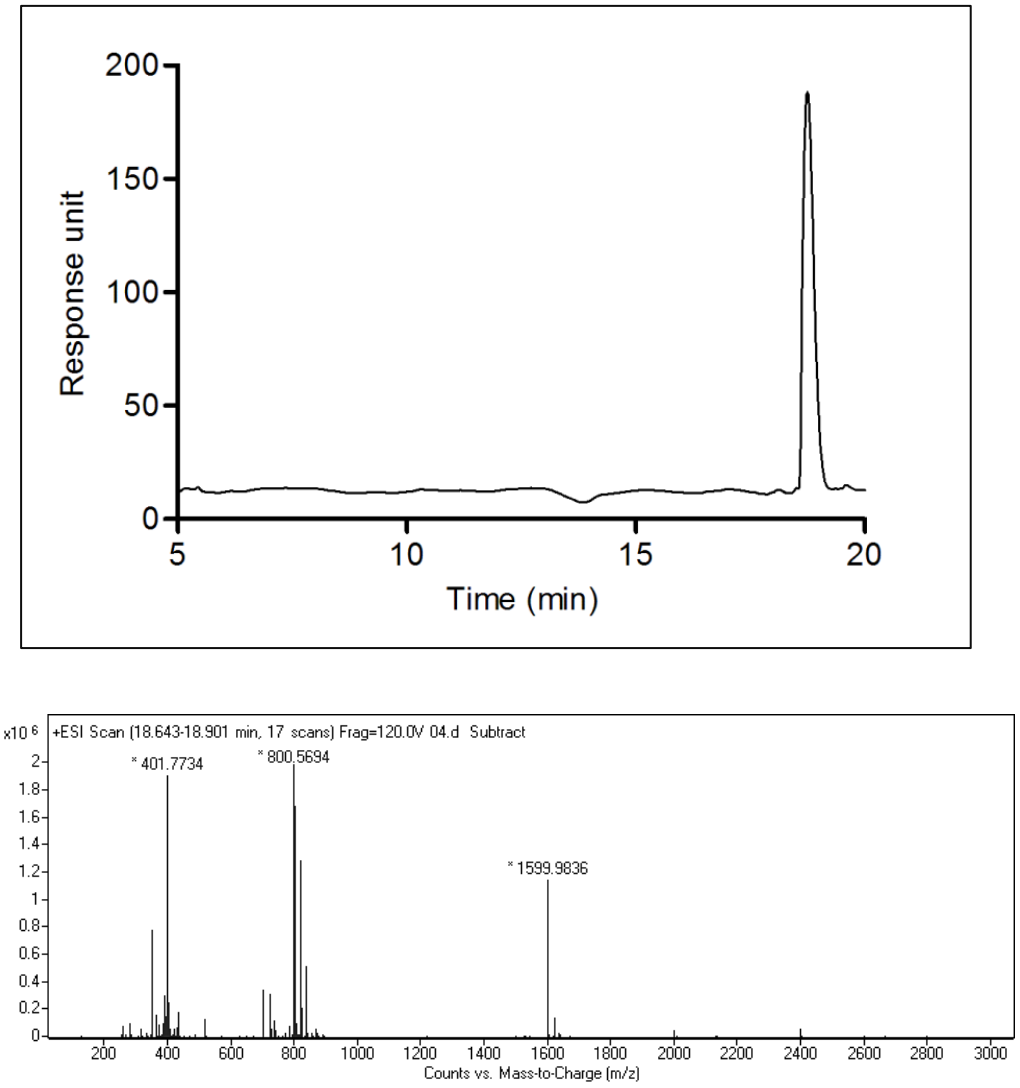

Figure 5.4 HPLC chromatogram of peptide. Absorbance at 220 nm vs. retention time graph (top). Mass spectrum of peptide after substracting mass spectrum of water sample at that time interval (bottom). $[M+H]^+$ (calculated)=801.00 $[M+H]^+$ (observed)=800.5694, $[M/2+H]^+$ (calculated)=401.00 $[M/2+H]^+$ (observed)=401.7734.

At pH values above 6.5, PA1 and PA2 can self-assemble and form β-sheet. Secondary structures of PA1 and PA2 were characterized with CD.(Figure 5.5-5.6) Also, $ZnCl_2$ solution was added to dilute PA hydrogel solutions to learn the effect of $ZnCl_2$ to secondary structure of PA molecules. A slight decrease on positive and minimum peaks indicating β-sheet presence was observed.

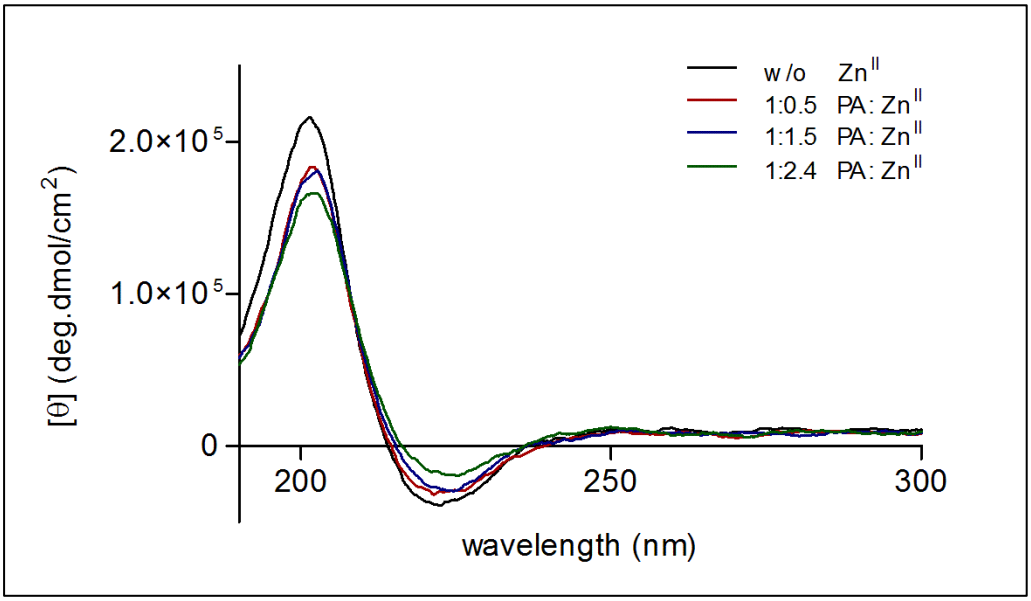

Figure 5.5 Titration of PA1 with Zn^{II} solution at 37 °C.

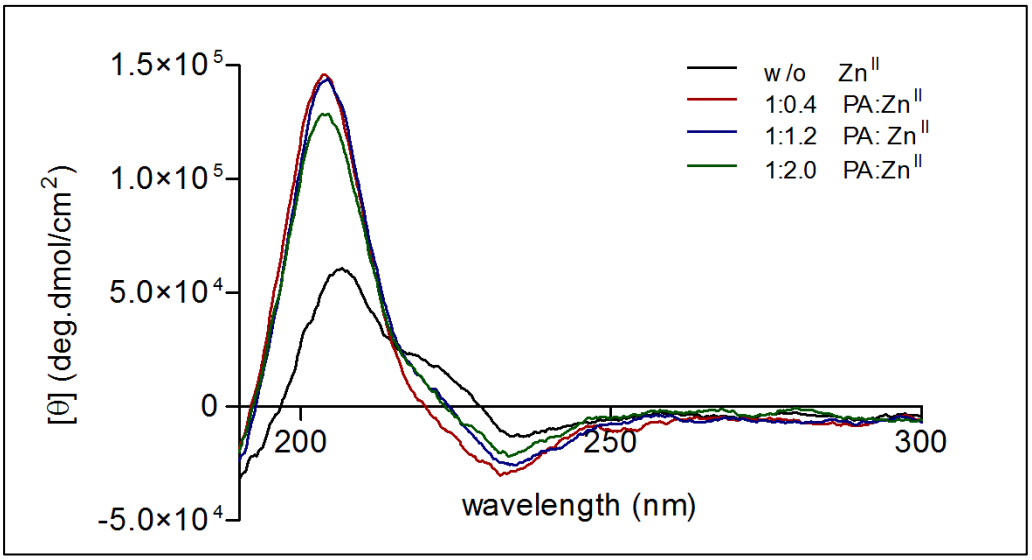

Figure 5.6 Titration of PA2 with Zn^{II} solution at 37 °C.

Binding efficiency between Zn^{II} and PA molecules was revealed with isothermal titration calorimetry analyses. In Figures 5.7 and 5.8, titrations of PA1 and PA2 at pH 8.0 with $ZnCl_2$ solution were demonstrated, respectively. It was found that binding efficiency of PA1 to Zn^{II} was higher than binding efficiency of PA2 to Zn^{II}. Also, TEM images of self-assembled PAs proved the nanofiber formation. (Figure 5.9)

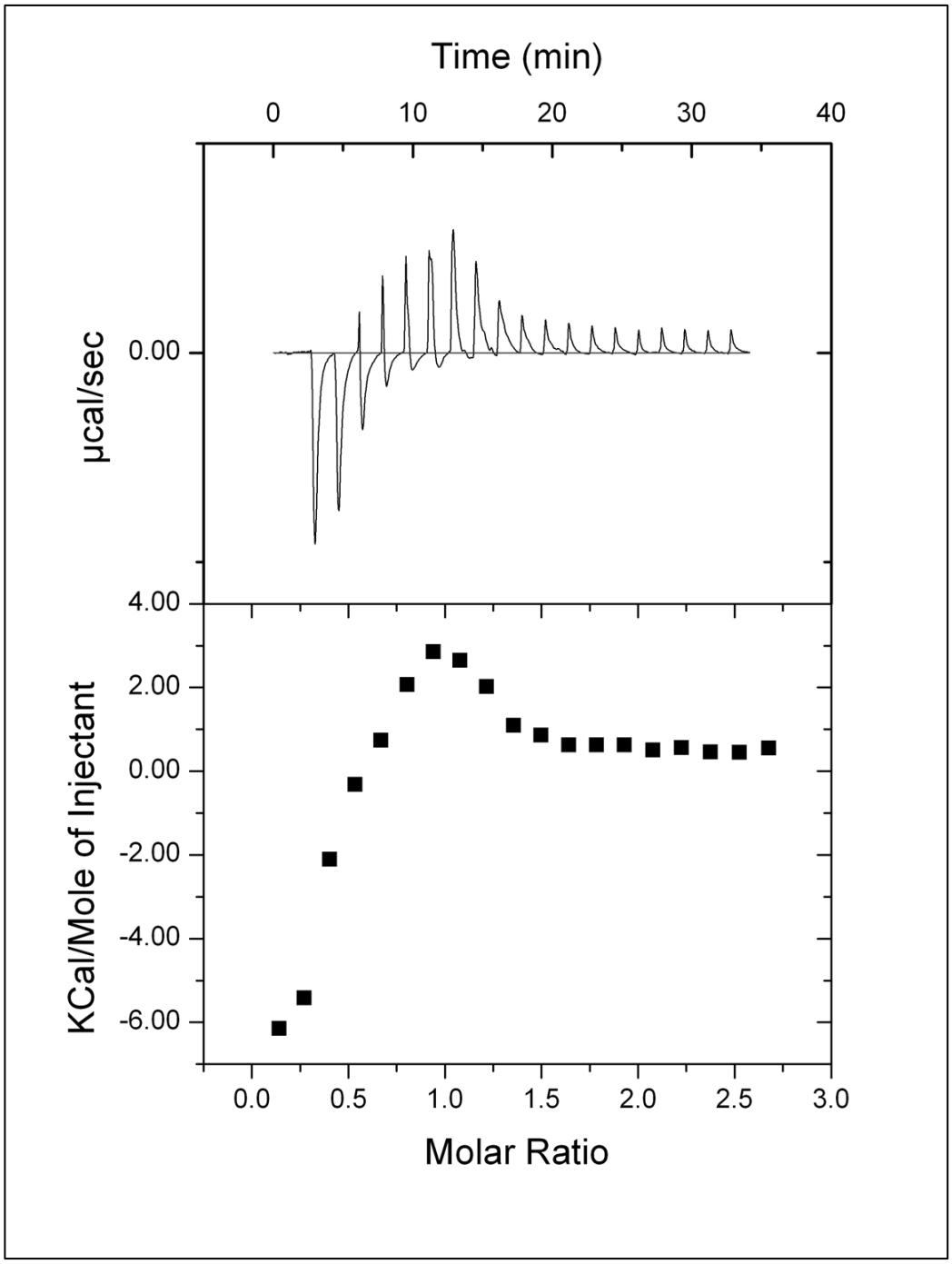

Figure 5.7 Isothermal titration curve of PA1 with $ZnCl_2$.

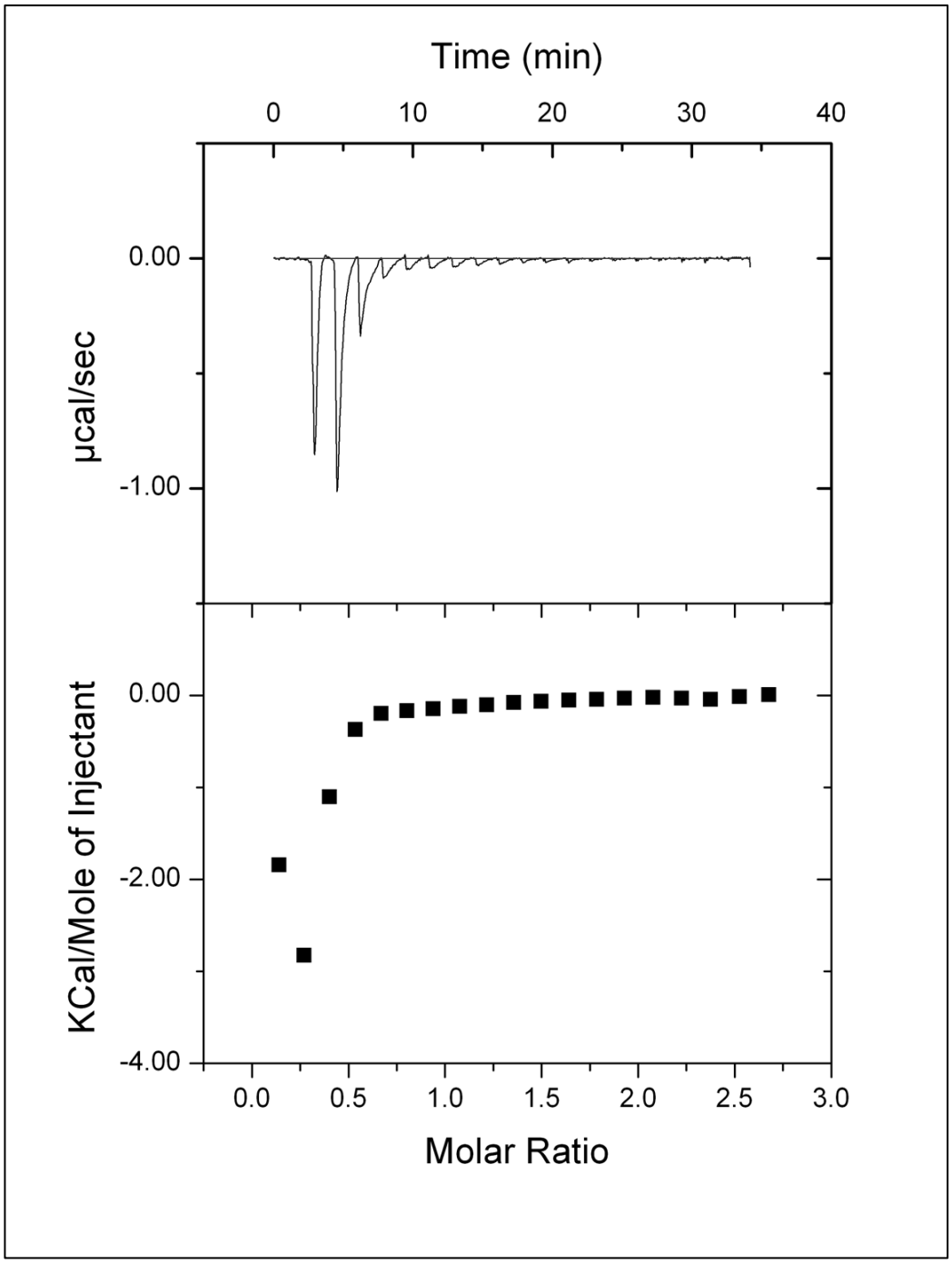

Figure 5.8 Isothermal titration curve of PA2 with $ZnCl_2$.

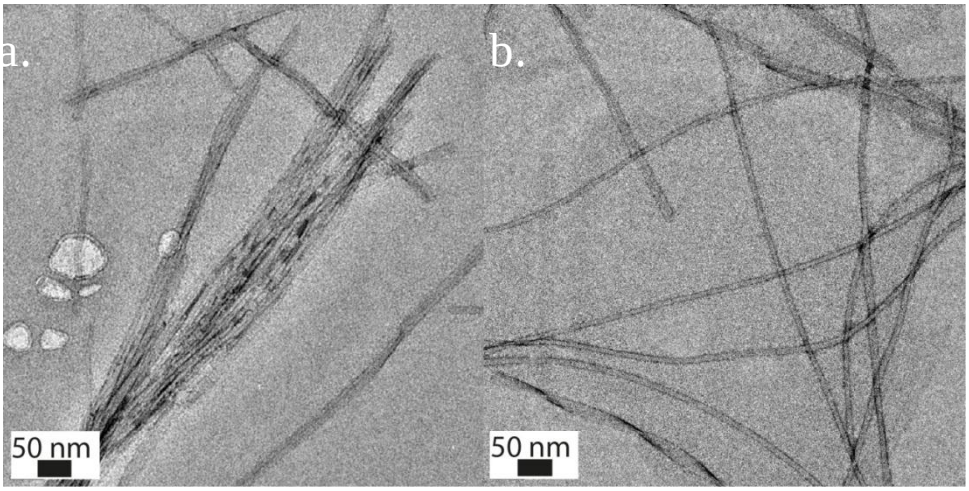

Figure 5.9 TEM images of self-assembled a. PA1 and b. PA2.

In the hydrolysis experiments, it was found that kinetics of hydrolysis performed with PA and PA+Zn^{II} fitted to Michealis-Menten equation.(Figures 5.10-5.13) It proved the catalytic activity of peptide amphiphile molecule. However, addition of Zn^{II} did not affect the hydrolysis dramatically although it was found that there was an interaction between Zn^{II} and PA molecules.(Figures 5.11, 5.13 and 5.14) Hydrolysis of *p*-nitrophenyl acetate fitted to linear regression as expected.(Figure 5.15) The experiment set up can be revised for further investigation of Zn^{II} and PA interaction effect to hydrolysis of *p*-nitrophenyl acetate.

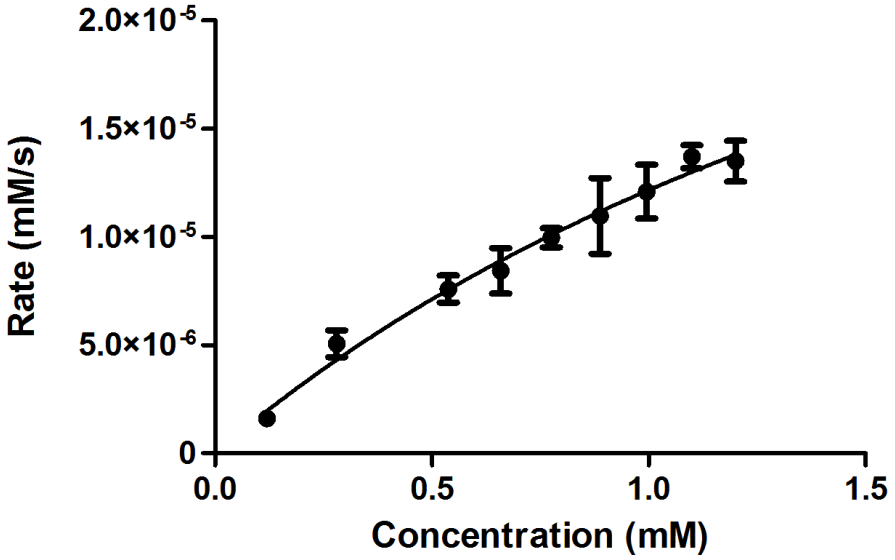

Figure 5.10 Hydrolysis kinetics of *p*-nitrophenyl acetate in the presence of PA1.

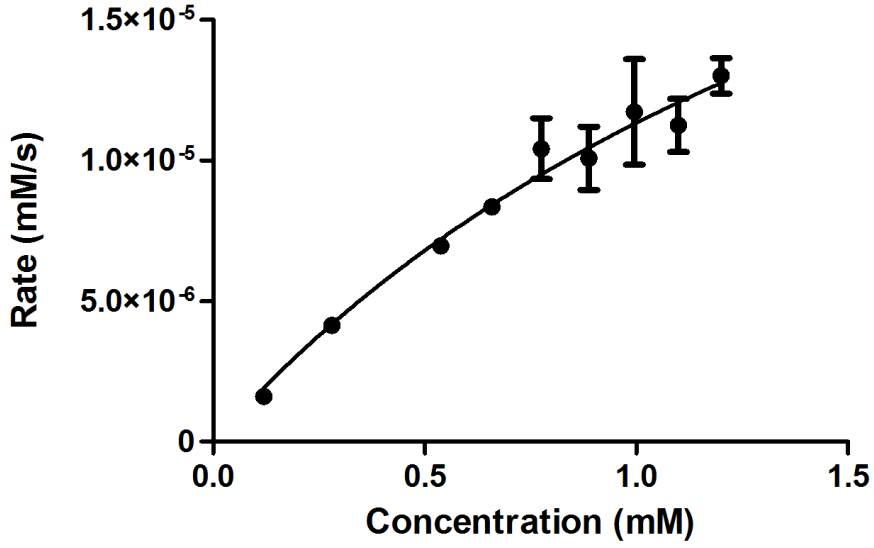

Figure 5.11 Hydrolysis kinetics of *p*-nitrophenyl acetate in the presence of PA1+Zn^{II}.

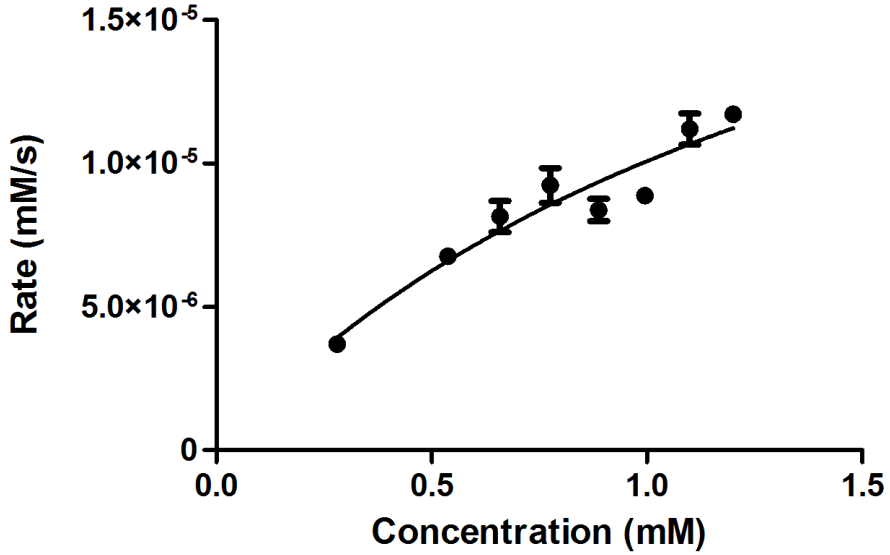

Figure 5.12 Hydrolysis kinetics of *p*-nitrophenyl acetate in the presence of PA2.

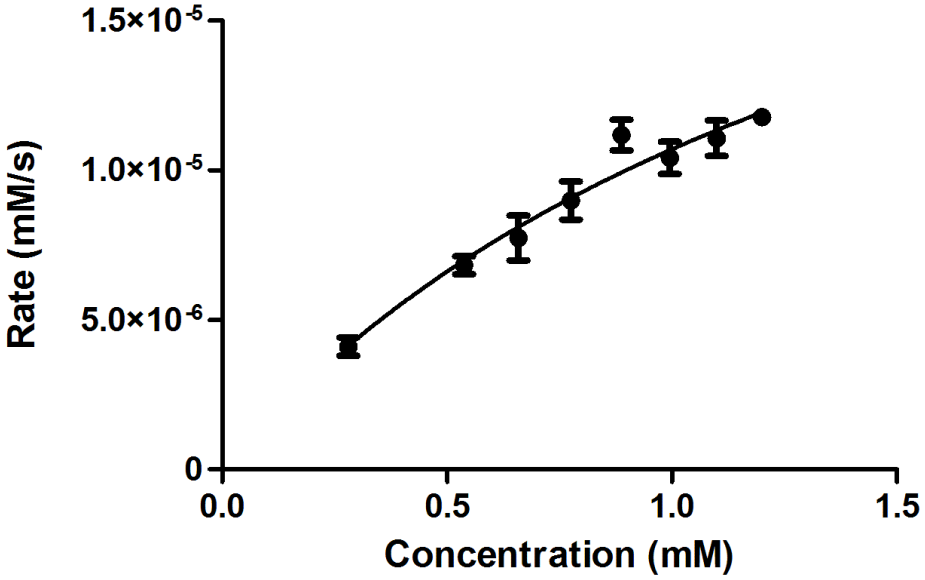

Figure 5.13 Hydrolysis kinetics of *p*-nitrophenyl acetate in the presence of PA2+Zn^{II}.

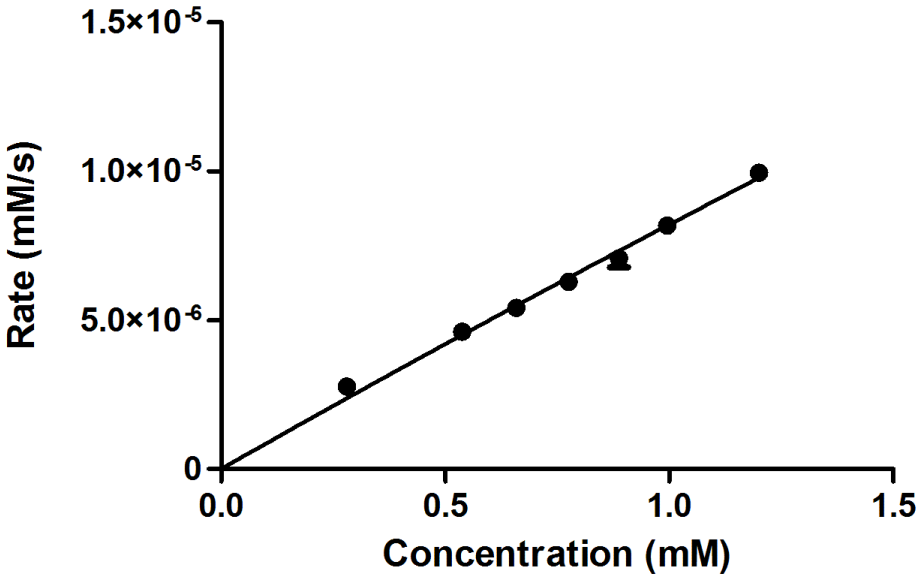

Figure 5.14 Hydrolysis kinetics of *p*-nitrophenyl acetate in the presence of Zn^{II}.

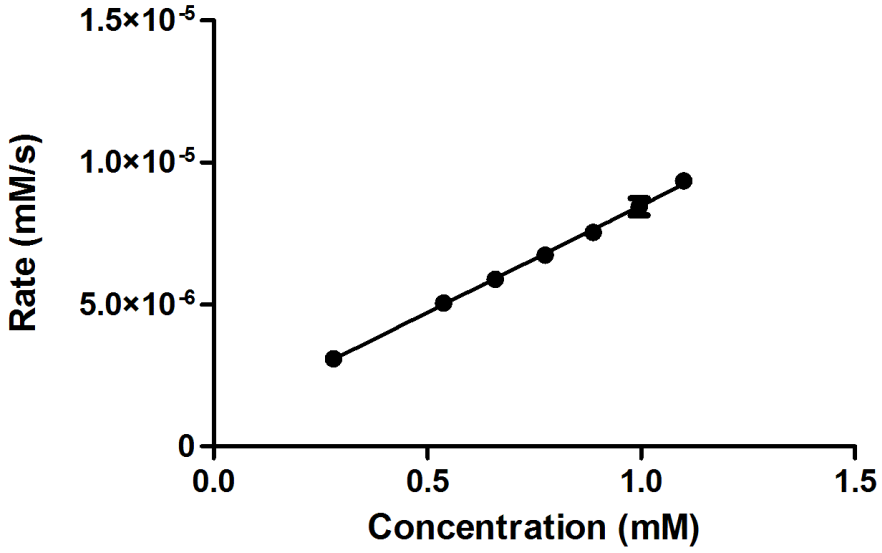

Figure 5.15 Hydrolysis kinetics of *p*-nitrophenyl acetate.

Table 5.1 Kinetics of hydrolysis of *p*-nitrophenyl acetate.

Catalyst Used	**K_m (mM)**	**k_{cat} (s^{-1})**	**V_{max}**
PA1	2.436±0.7223	0.002783±0.0006000	4.175×10^{-5}
PA1+Zn^{II}	2.032±0.6621	0.003412±0.0007744	3.412×10^{-5}
PA2	1.587± 0.7853	0.001737±0.0005487	2.605×10^{-5}
PA2+Zn^{II}	1.625± 0.5558	0.002807±0.0006179	2.807×10^{-5}

Glass coverslips were covered with PA1, PA2, PA1+Zn^{II}, PA2+Zn^{II}, Zn^{II} and only buffer to observe the formation and characterize calcium phosphate crystals formed on the surface of coverslips on day 1 and day 3 as written at experimental part. Calcium phosphate crystals were characterized with SNOM+Raman spectrometer, SEM, EDS and XRD.

In Raman spectra of calcium phosphate crystals generated with enzyme mimetic nanostructures were taken to further characterize calcium phosphate crystals. In Figure 5.16 and 5.18, optical and confocal Raman image of calcium phosphate crystals generated with PA1 and Zn^{II}, and PA2 and Zn^{II} covered on glass coverslips on day 3, respectively. Confocal Raman images demonstrated the Raman intensities at 2950 cm^{-1}. Also, Figure 5.17 and 5.19 show average Raman spectra of surfaces. For the calcium phosphate crystal prepared with PA1 and Zn^{II}, at 402, 437, 476 and 490 cm^{-1}, doubly degenerate bending mode of the PO_4 group (O-P-O bond) was present. At 969 cm^{-1}, there was totally

symmetric stretching mode of the tetrahedral PO_4 group (P-O bond). Vibrations at 1034, 1064 and 1080 cm^{-1} indicated triply degenerate asymmetric stretching mode of the PO_4 group (P-O bond). At Figure5.19, vibrations at 403, 444, and 484 cm^{-1} figured out doubly degenerate bending mode of the PO_4 group (O-P-O bond). Also, vibrations at 1035 and 1076 cm^{-1} indicated triply degenerate asymmetric stretching mode of the PO_4 group (P-O bond). The lack of Raman vibration corresponding to –OH group indicated that the resulting calcium phosphate crystal was β-tricalcium phosphate (TCP).[77]

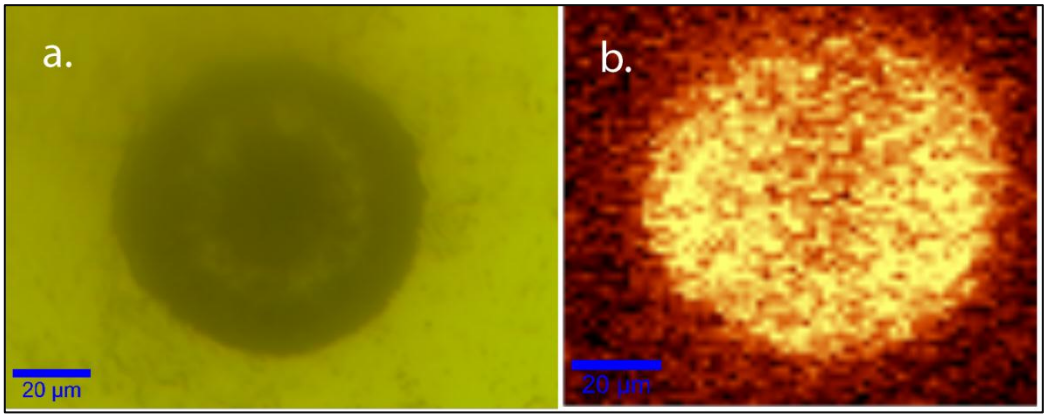

Figure 5.16 a. Optical (20X) and b. Confocal Raman image of calcium phosphate crystal prepared with surfaces covered with PA1 and Zn^{II}.

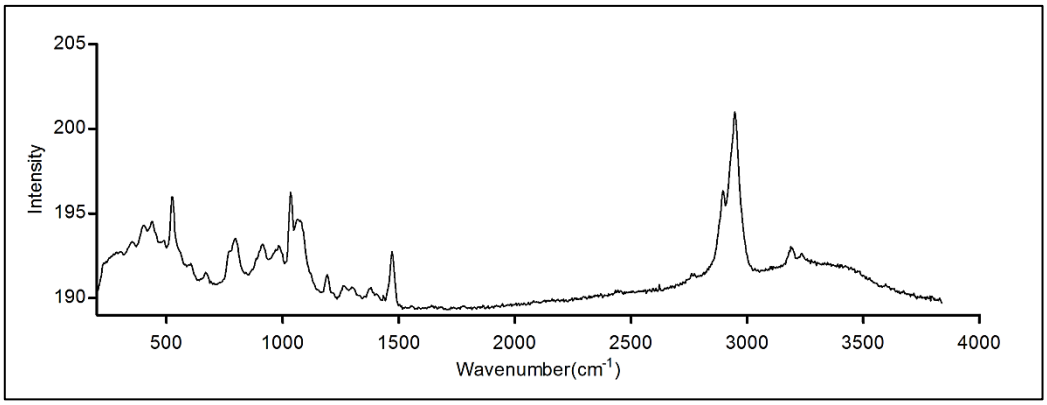

Figure 5.17 Average Raman spectrum of calcium phosphate crystals formed on the 150x150 μm^2 surface of PA1+Zn^{II}.

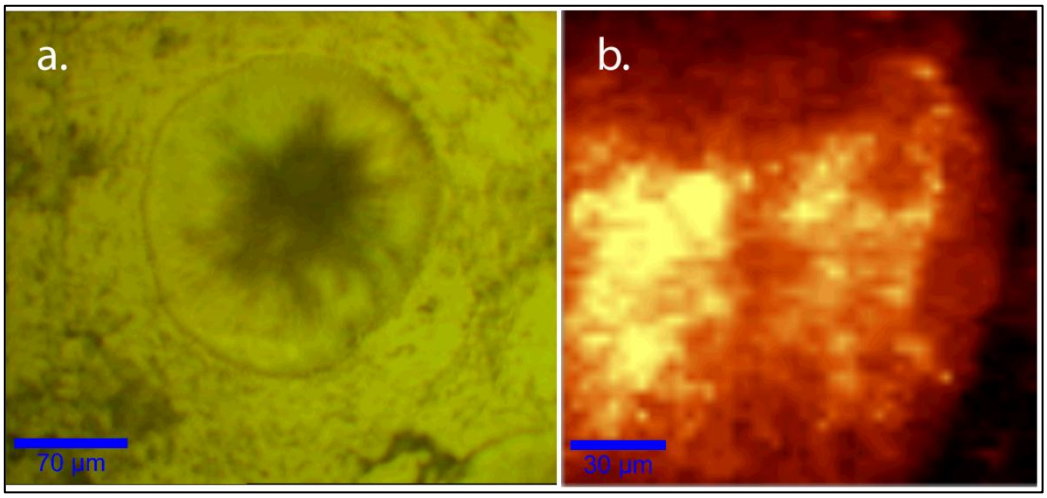

Figure 5.18 a. Optical (20X) and b. Confocal Raman image of calcium phosphate crystal prepared with surfaces covered with PA2 and Zn^{II}.

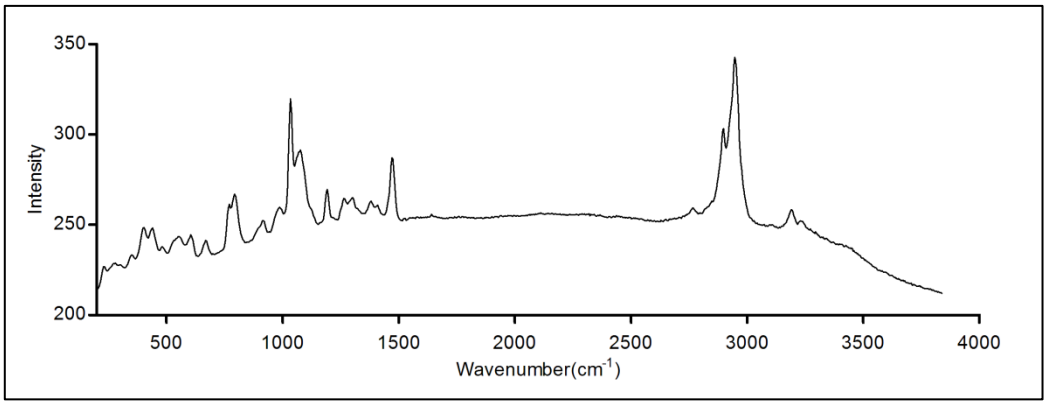

Figure 5.19 Average Raman spectrum of calcium phosphate crystals formed on the 150x150 μm^2 surface of PA2+Zn^{II}.

The calcium phosphate crystals formed on the surface of glass coverslips were imaged with SEM. According to SEM images, calcium phosphate crystals at day 3 had bigger in diameter than the ones at day 1 in both HC and LC surfaces.(Figures 5.20, 5.23, 5.25, and 5.27) However, there was no calcium phosphate crystal on surfaces covered with Zn^{II} and buffer.(Figure 5.29) Also, elemental content of crystals was monitored with EDS. According to EDS results, Ca/P ratio of crystals was 0.7.(Figures 5.21, 5.24, 5.26 and 5.28) Also, elemental mapping of calcium phosphate crystals was taken to show that Ca, P, O densities on the surface.(Figure 5.22) The Ca/P ratio indicated that the resulting crystals were dicalcium phosphate dehydrate.[78]

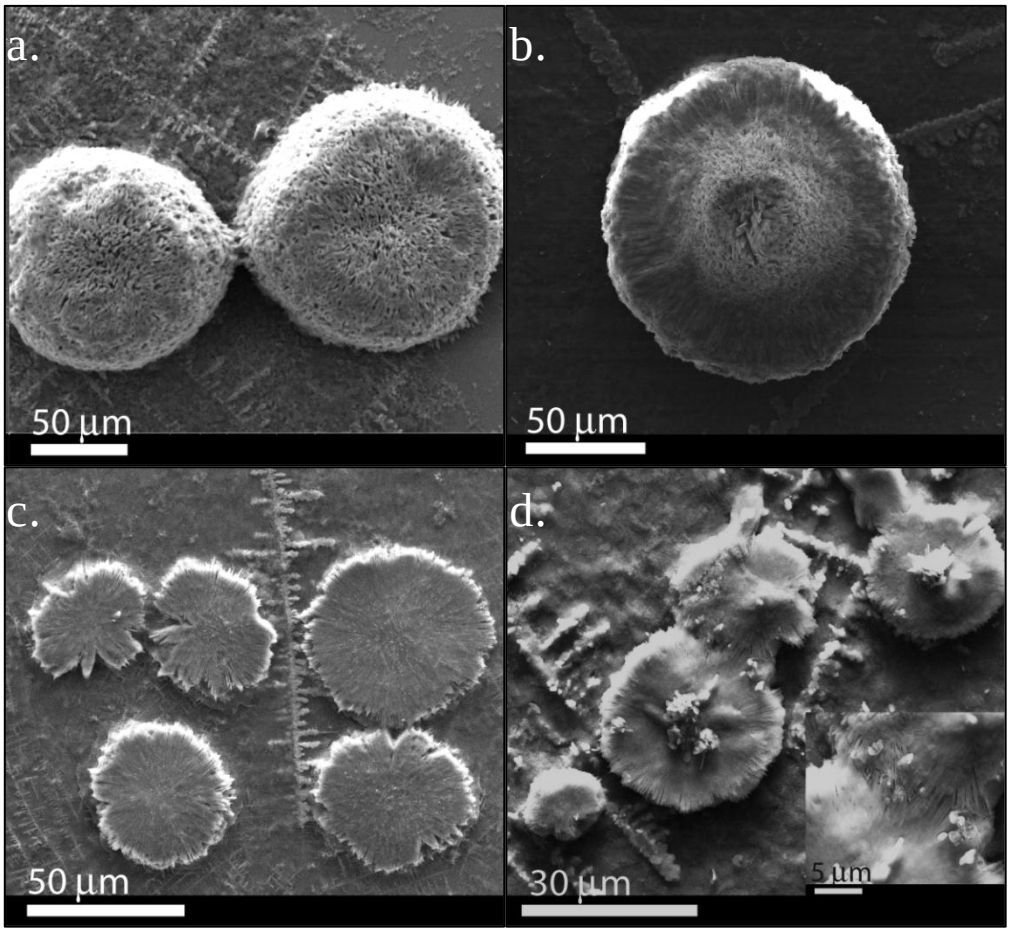

Figure 5.20 CaP crystals formed on HC surfaces covered with a. PA1, b. PA1+Zn^{II}, c.PA2 and d.PA2+Zn^{II} at day 1.

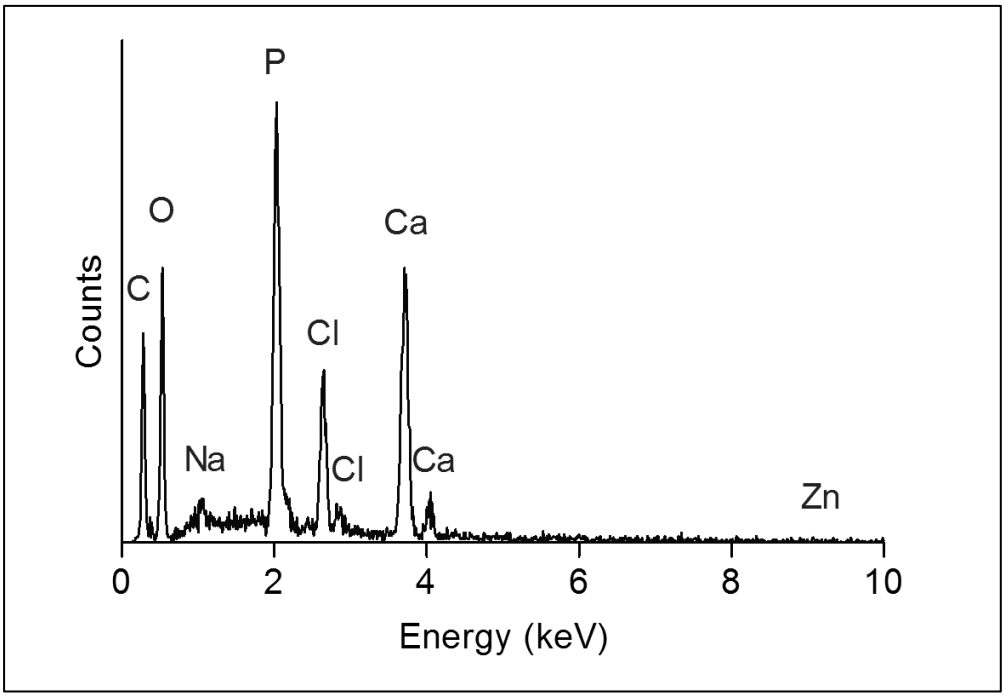

Figure 5.21 EDS spectrum of CaP crystal on HC surface covered with PA1.

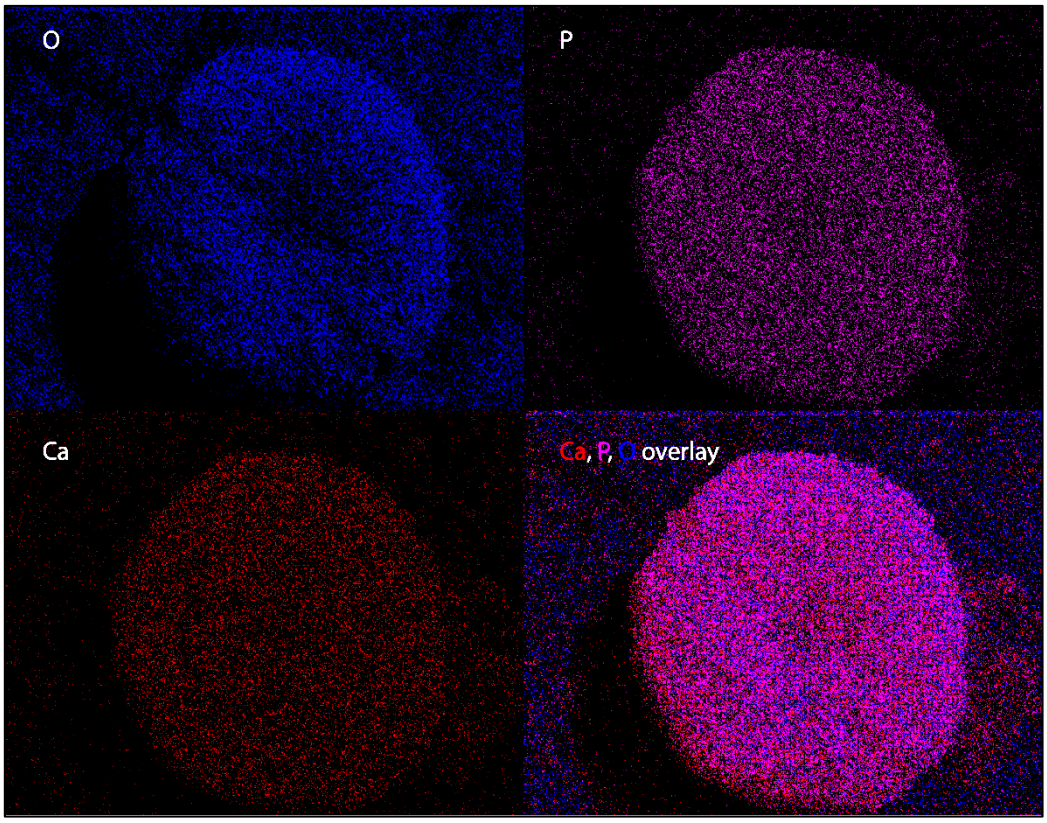

Figure 5.22 Elemental mapping of calcium phosphate crystals on HC surface covered with PA1.

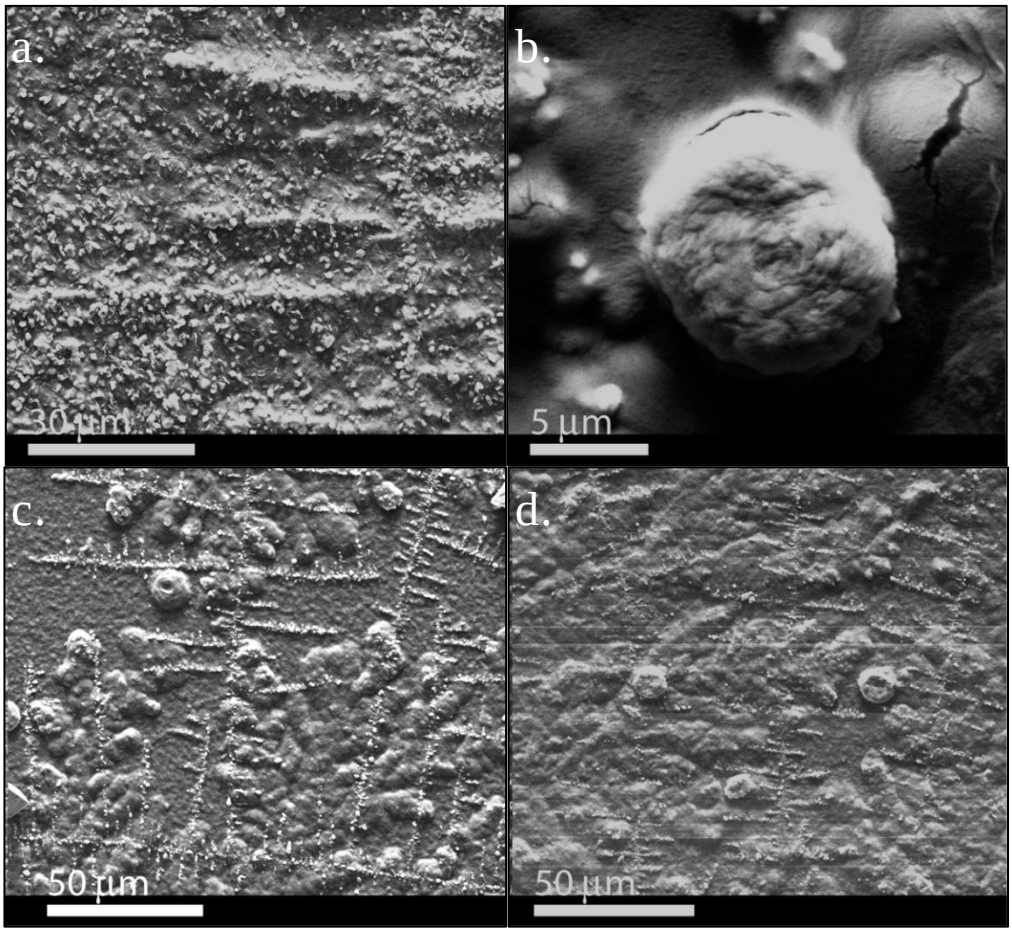

Figure 5.23 CaP crystals formed on LC surfaces covered with a. PA1, b. PA1+Zn^{II}, c. PA2 and d. PA2+Zn^{II} at day 1.

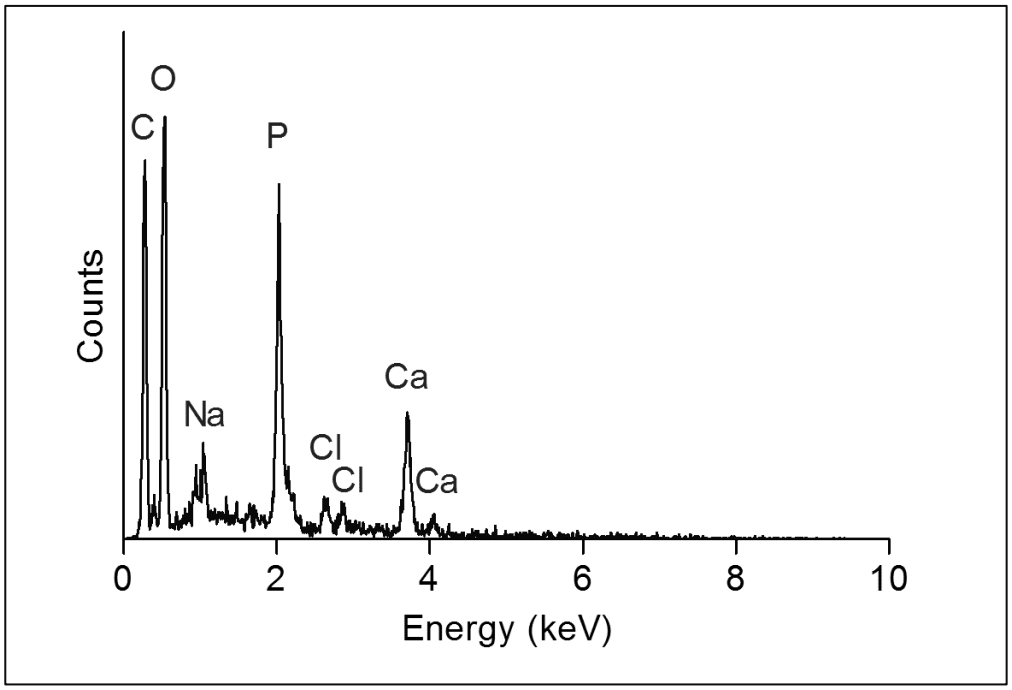

Figure 5.24 EDS spectrum of CaP crystal formed on LC surface covered with PA1.

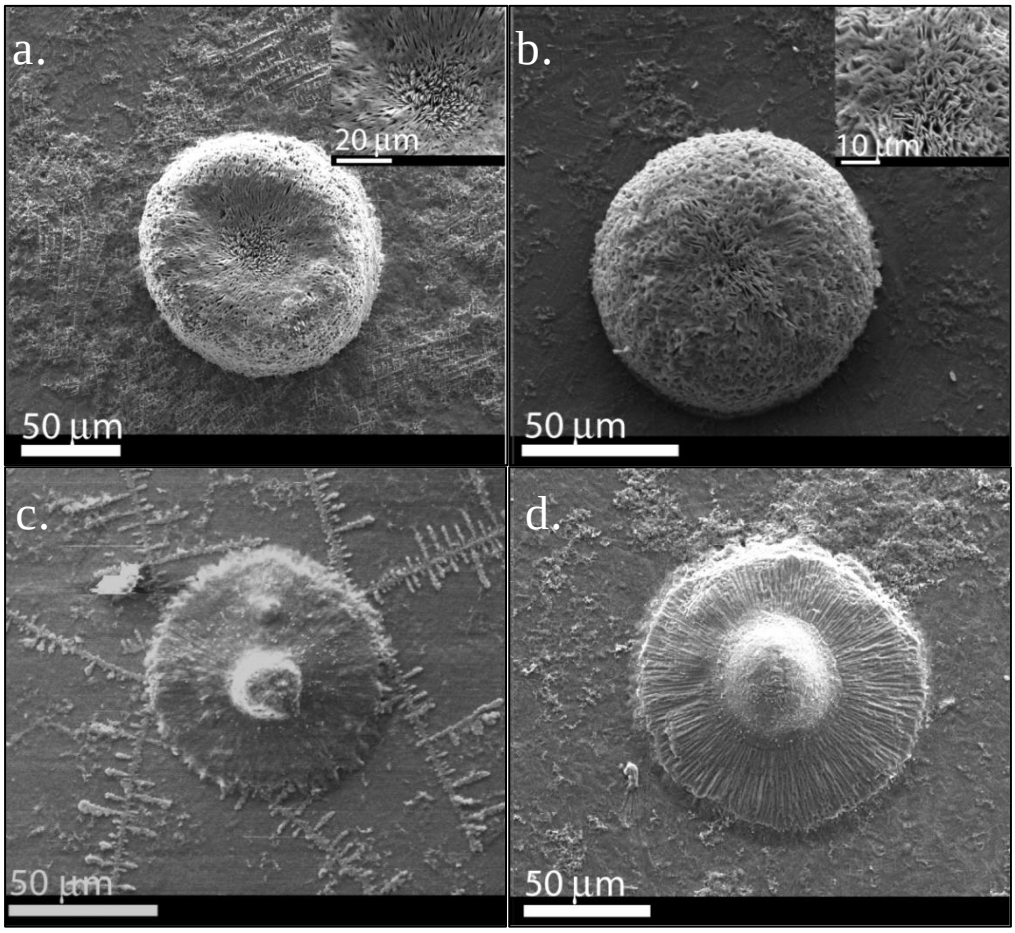

Figure 5.25 Cap crystals formed on HC surfaces covered with a. PA1 b. PA1+Zn^{II}, c. PA2, and d. PA2+Zn at day 3.

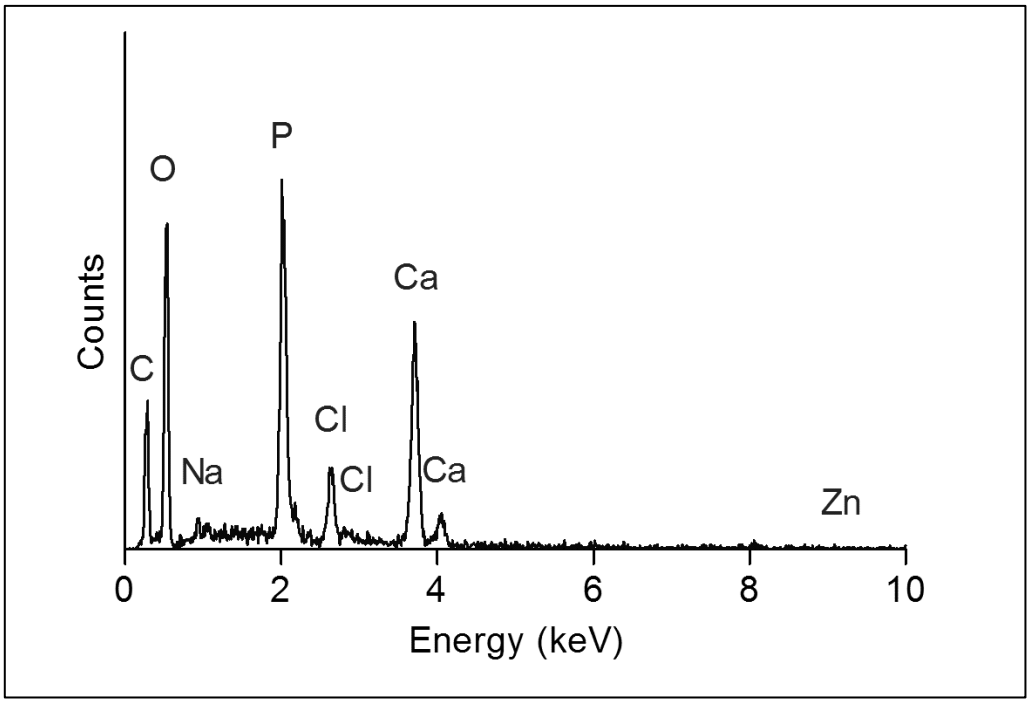

Figure 5.26 EDS spectrum of CaP crystal formed on HC surface covered with PA1.

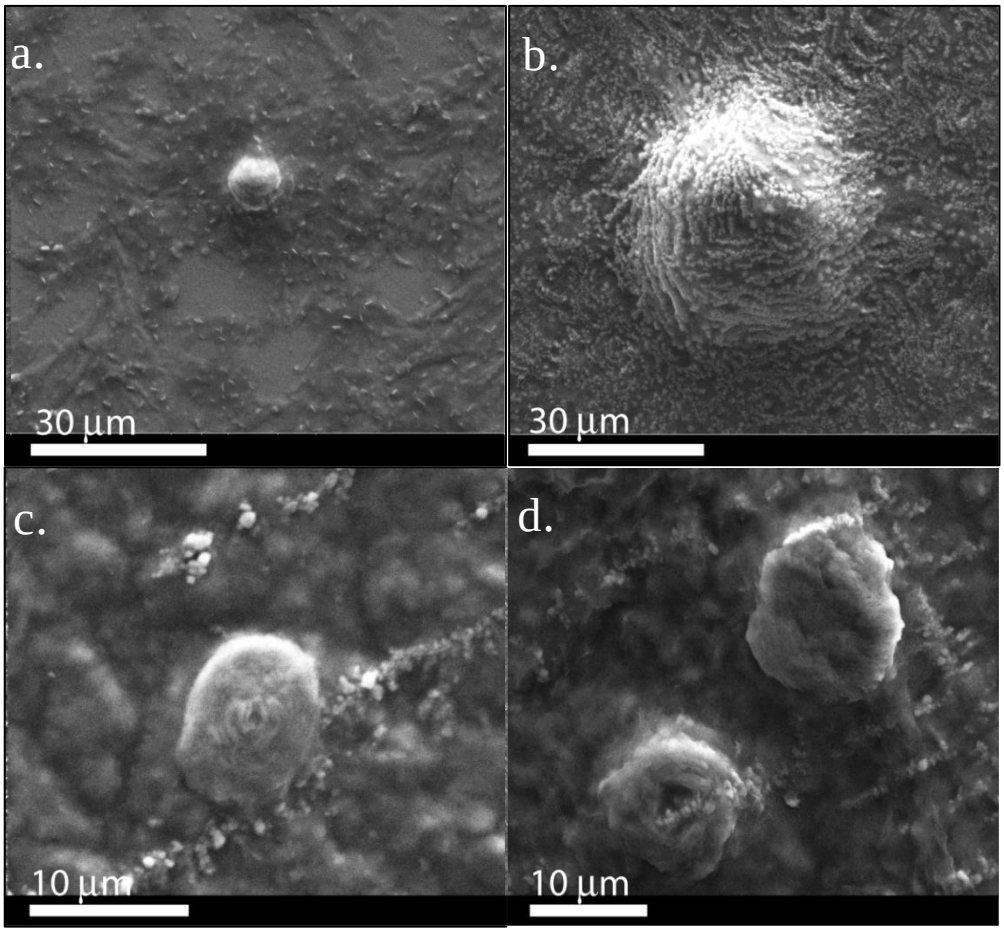

Figure 5.27 CaP crystals formed on LC surfaces covered with a. PA1, b. PA1+Zn^{II}, c. PA2, and d. PA2+Zn^{II} at day 3.

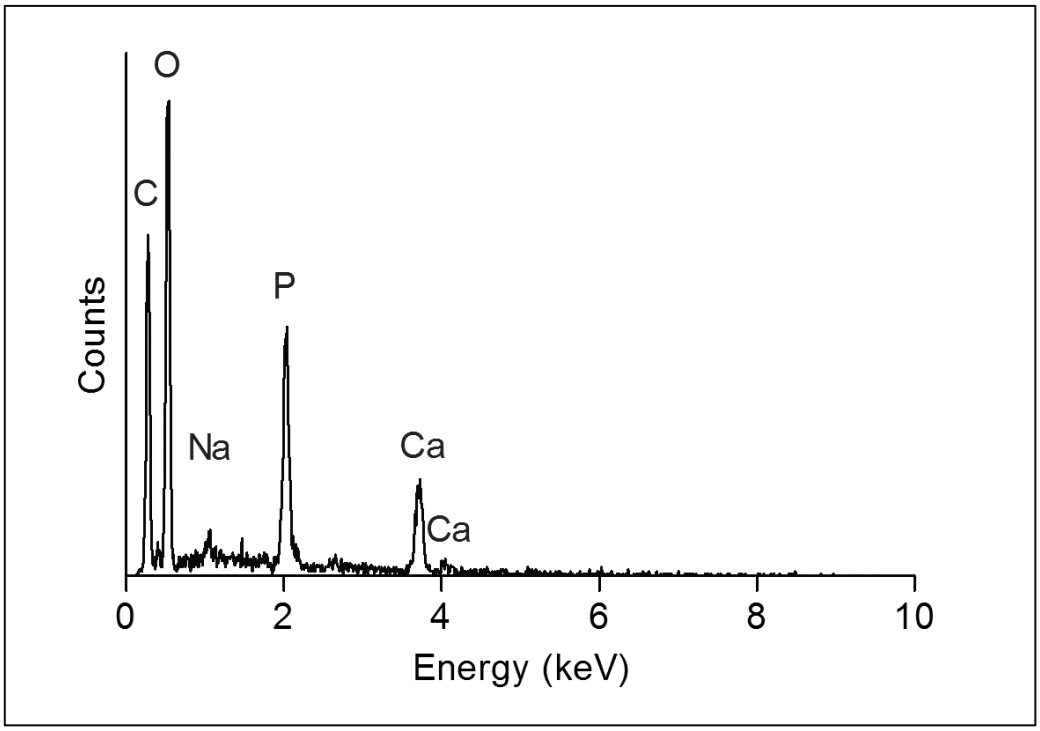

Figure 5.28 EDS spectrum of CaP crystal formed on LC surface covered with PA1.

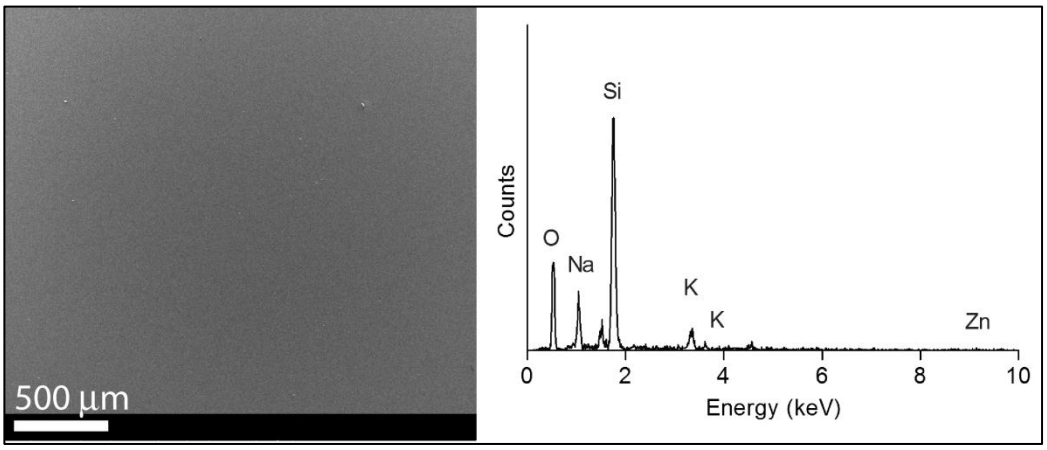

Figure 5.29 HC surface covered with Zn^{II} at day 3.

X-ray diffraction patterns revealed that precipitated calcium phosphate solids were highly crystalline. The dominated planes were (111) and (211) at all of the crystals formed on surfaces.(Figures 5.30-5.37)

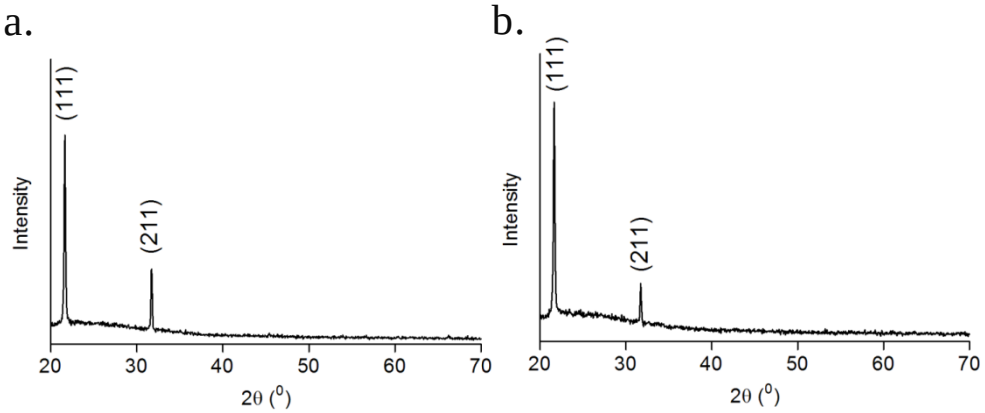

Figure 5.30 XRD pattern of HC surfaces covered with a. PA1 and b. PA1+Zn^{II} at day 1.

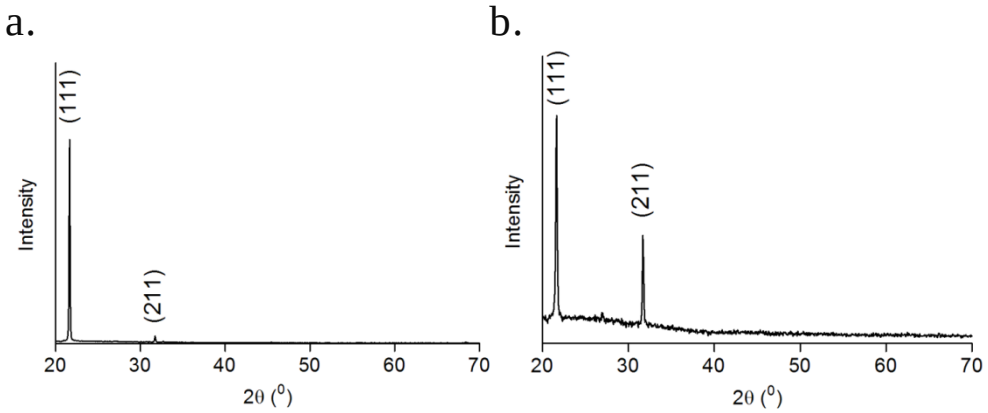

Figure 5.31 XRD pattern of HC surfaces covered with a. PA2 and b.PA2+Zn^{II} at day 1.

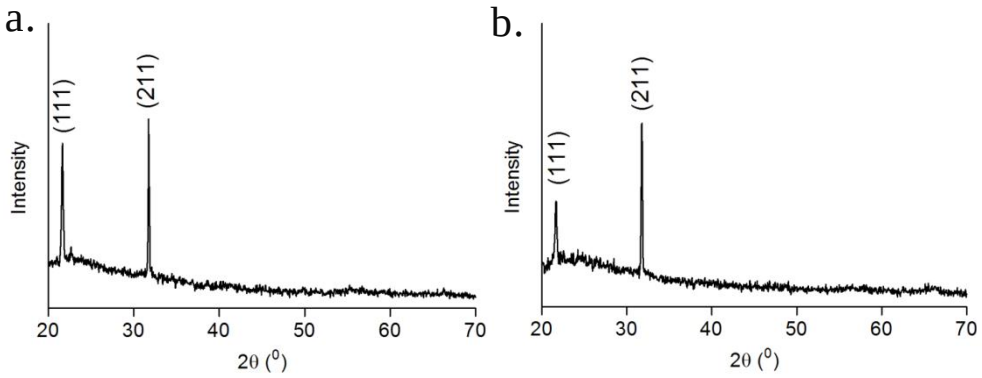

Figure 5.32 XRD pattern of LC surfaces covered with a. PA1 and b. PA1+Zn^{II} at day 1.

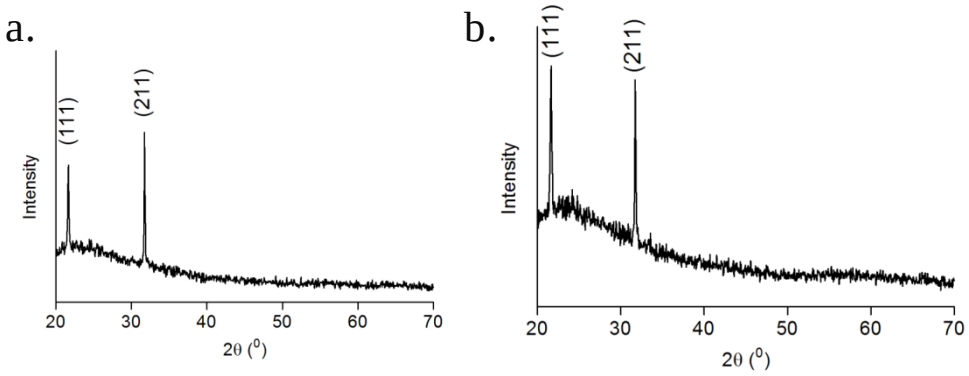

Figure 5.33 XRD pattern of LC surfaces covered with a. PA2 and b. PA2+Zn^{II} at day 1.

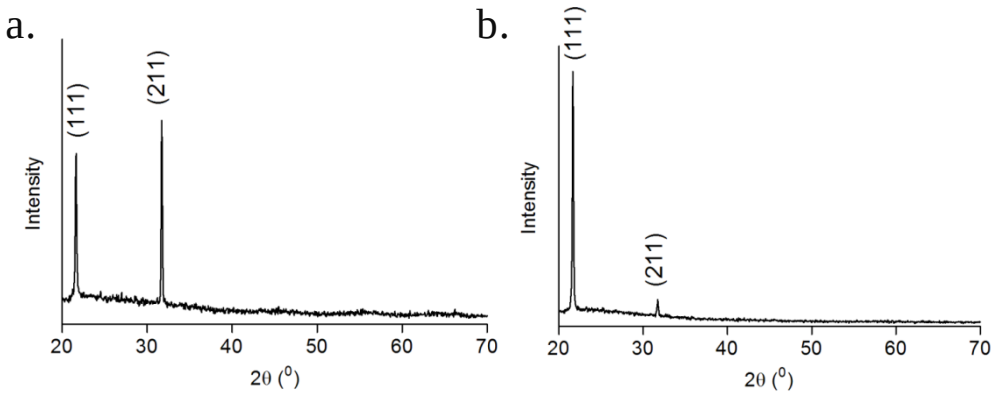

Figure 5.34 XRD pattern of HC surfaces covered with a. PA1 and b. PA1+Zn^{II} at day 3.

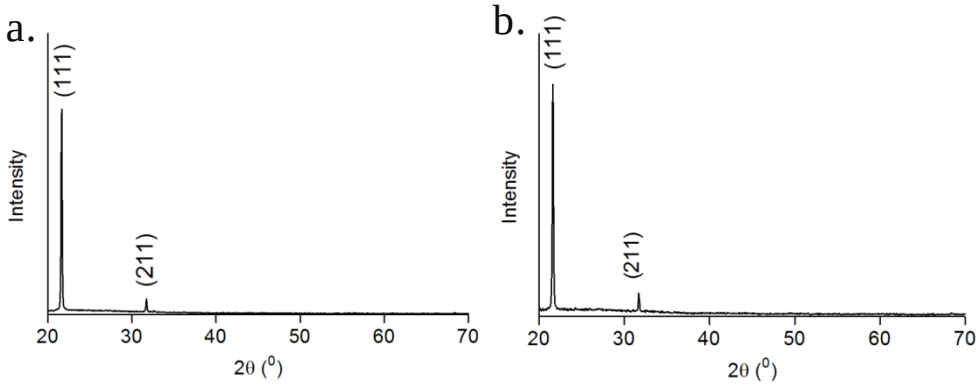

Figure 5.35 XRD pattern of HC surfaces covered with a. PA2 and b. PA2+Zn^{II} at day 3.

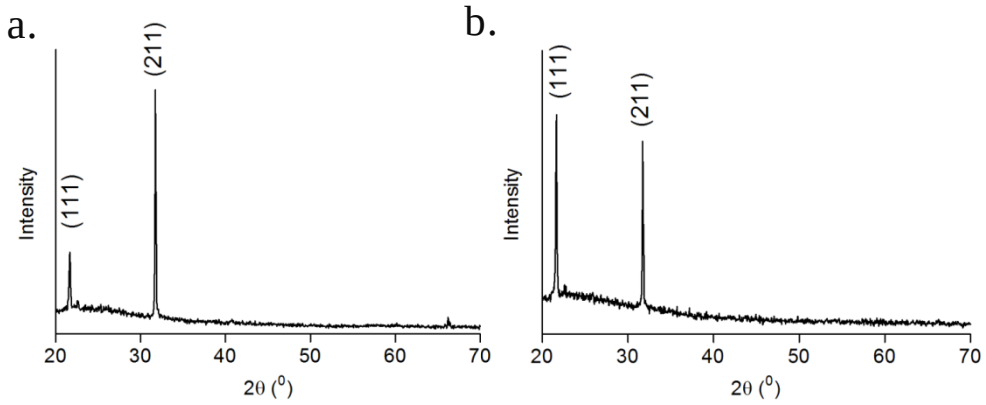

Figure 5.36 XRD pattern of LC surfaces covered with a. PA1 and b. PA1+Zn^{II} at day 3.

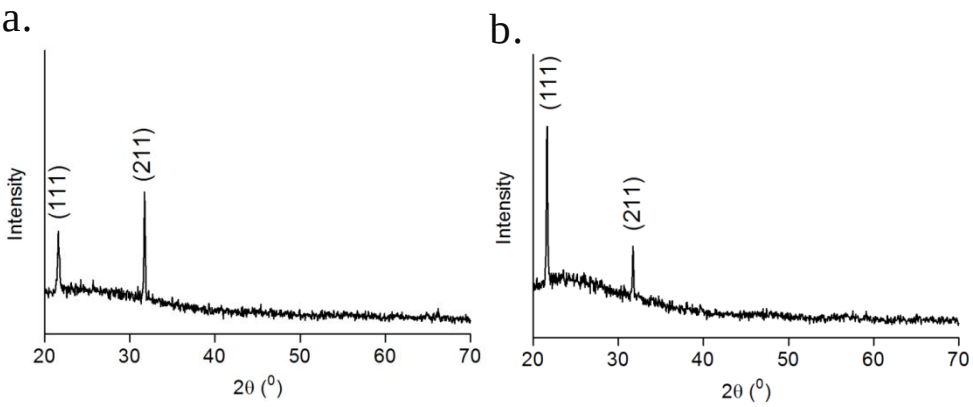

Figure 5.37 XRD pattern of LC surfaces covered with a. PA2 and b. PA2+Zn^{II} at day 3.

5.4 Conclusion

Design of metalloenzyme mimetic nanostructures is a highly attractive topic for scientists studying biomimetic systems. Developing *de novo* metalloenzyme design strategies can reveal hidden aspects of metalloenzymes besides giving clues about designing novel complex

structures like metalloenzymes. Properties of metal ions participating in metalloenzymes are crucial in terms of geometry and flexibility of coordination center and catalytic activity of metalloenzyme. Thus, in this study zinc ion was chosen because of its properties in catalysis to mimic a zinc-containing metalloenzyme, alkaline phosphatase.

In summary, two different enzyme mimetic, self-assembling nanostructures were designed, characterized and compared with each other in terms of catalytic activities in the hydrolysis of *p*-nitrophenyl acetate. Moreover, the structures were used to obtain an inorganic phosphate ion source and form calcium phosphate crystals which were important in bone tissue. The resulting calcium phosphate crystals were also characterized with SEM, EDS, XRD and Raman spectroscopy. The catalytically active self-assembling nanostructures can be used for regeneration of bone tissue by mimicking alkaline phosphatase activity. Also, activity of the bioinspired enzyme mimetic nanostructures can be increased with using different coordination sites or metal ions in further studies.

Chapter 6

Conclusion

6. Conclusion

Nature has always been an inspiration source for scientists working on several different research areas such as optics, electronics, catalysis and tissue engineering etc. and led them to design bioinspired materials. In the design of bioinspired materials, structure-function relation in natural materials should be described clearly. This step constitutes the first part of bioinspired material design. Secondly, physical/chemical background in natural materials should be stated with experimental and theoretical evidences. Finally, engineering sources and economy should be considered in the design of bioinspired materials.

In nature, inorganic and organic contents are in balance to obtain the desired function in materials. Mussel byssi, mollusk shell, bone or cartilage tissue can be given as example for composite materials consisting of organic and inorganic materials within to function properly.

In this thesis, materials were designed with taken advantage of nature's sources for inspiration. First application was to synthesize 1-D peptide Pd nanostructures. Second one was to functionalize electrospun nanofibers with a biomimetic heavy metal binding peptide sequence. Finally, an enzyme mimetic self-assembling nanostructure was designed and used to synthesize calcium phosphate crystals.

Organic template directed inorganic material synthesis method is widely used in the literature with polymer, dendrimers or protein

templates etc. I this thesis, we used self-assembling peptide amphiphile nanofibers as template for direction of palladium nanoparticles. The resulting structure was characterized with TEM, TGA and XRD after characterization of peptide amphiphile molecule. Then, peptide directed palladium nanostructures were used in Suzuki coupling reactions as catalyst. The nanostructures were catalytically active even at room temperature and in environmentally friendly solvent, water.

Xenobiotic heavy metal ions have been removed with several methods such as ion exchange, chemical precipitation, adsorption, membrane filtration and electrochemical techniques so far. In this thesis, we designed a biomimetic peptide sequence which can interact noncovalently to insoluble electrospun cyclodextrin nanofibers through adamantane-cyclodextrin inclusion complex and bind heavy metal ions such as Cd^{II}, Ni^{II}, and Cr^{VI}. After characterization of interaction between metal ions and peptide with UV and ITC analyses, interaction between peptide and β-cyclodextrin molecule was studied with ITC analysis. Then, electrospun cyclodextrin nanofibers were functionalized with this peptide sequence. The functionalization was characterized quantitatively or qualitatively with XPS, FTIR, TGA, Raman spectroscopy, and elemental analysis. Moreover, functional cyclodextrin nanofibers were incubated in metal ion solutions to remove metal ions from water by binding them covalently. The metal ion removal capacity of functional cyclodextrin nanofibers was quantitatively analyzed with the decrease in amount of metal ions in water with ICP-MS. Finally, the resulting metal

ion bound functional nanofibers were characterized with XPS, SEM and Raman spectroscopy. The designed noncovalently functionalized system can be applied with different functional groups for different purposes. Also, peptide sequence can be altered for higher heavy metal ion binding capacity with increasing the number of Glu-Cys repeating unit.

Metalloenzyme mimetic structures are common in nature as their superior activities within enzyme structures. Therefore, it is widely studied by scientists working on bioinspired systems. Here, an alkaline phosphatase mimetic peptide based self-assembling Zn^{II}-peptide amphiphile nanostructure was designed. To emphasize importance of metal coordination center in enzymes, two structurally different peptide amphiphile were designed, branched and linear peptide amphiphiles. After characterization of peptide amphiphiles with LC-MS, CD and TEM, interaction between zinc ion and peptide molecules were studied with CD and ITC. Then, catalytic activities of peptide molecules with and without zinc ion were analyzed in hydrolysis of *p*-nitrophenyl acetate. Addition of zinc ion to self-assembling peptide amphiphile nanostructures increased the rate of hydrolysis of *p*-nitrophenyl acetate. Moreover, peptide amphiphiles with and without zinc ion exhibited enzymatic behavior. Then, these nanostructures were used to obtain inorganic phosphate ion source to form biologically important calcium phosphate crystals on surface. The calcium phosphate crystals were characterized with SEM, EDS, XRD and Raman spectroscopy. These

self-assembling alkaline phosphatase mimetic nanostructures can be used in bone tissue regeneration in the future.

Chapter 7

References

[1] Aizenberg, J. and P. Fratzl, "Biological and Biomimetic Materials", *Advanced Materials*, 21(4),p.,387-388, 2009.

[2] Boesel, L.F., C. Greiner, E. Arzt, and A. del Campo, "Gecko-Inspired Surfaces: A Path to Strong and Reversible Dry Adhesives", *Advanced Materials*, 22(19),p.,2125-2137, 2010.

[3] Drotlef, D.-M., L. Stepien, M. Kappl, W.J.P. Barnes, H.-J. Butt, and A. del Campo, "Insights into the Adhesive Mechanisms of Tree Frogs using Artificial Mimics", *Advanced Functional Materials*,p.,n/a-n/a, 2012.

[4] Ceylan, H., S. Kocabey, A.B. Tekinay, and M.O. Guler, "Surface-adhesive and osteogenic self-assembled peptide nanofibers for bioinspired functionalization of titanium surfaces", *Soft Matter*, 8(14),p.,3929-3937, 2012.

[5] Zastrow, M.L., A.F.A. Peacock, J.A. Stuckey, and V.L. Pecoraro, "Hydrolytic catalysis and structural stabilization in a designed metalloprotein", *Nature Chemistry*, 4(2),p.,118-123, 2012.

[6] Espinosa, H.D., A.L. Juster, F.J. Latourte, O.Y. Loh, D. Gregoire, and P.D. Zavattieri, "Tablet-level origin of toughening in abalone shells and translation to synthetic composite materials", *Nat Commun*, 2,p.,173, 2011.

[7] Phipps, M.C., W.C. Clem, J.M. Grunda, G.A. Clines, and S.L. Bellis, "Increasing the pore sizes of bone-mimetic electrospun scaffolds comprised of polycaprolactone, collagen I and hydroxyapatite to enhance cell infiltration", *Biomaterials*, 33(2),p.,524-534, 2012.

[8] Meng, Z., Q. Wang, X. Qu, C. Zhang, J. Li, J. Liu, and Z. Yang, "Papillae mimetic hairy composite spheres towards lotus leaf effect coatings", *Polymer*, 52(3),p.,597-601, 2011.

[9] Fu, F. and Q. Wang, "Removal of heavy metal ions from wastewaters: a review", *J Environ Manage*, 92(3),p.,407-18, 2011.

[10] Vanassche, F. and H. Clijsters, "Effects of Metals on Enzyme-Activity in Plants", *Plant Cell and Environment*, 13(3),p.,195-206, 1990.

[11] Hankamer, B., J. Barber, and E.J. Boekema, "Structure and membrane organization of photosystem II in green plants", *Annual Review of Plant Physiology and Plant Molecular Biology*, 48,p.,641-671, 1997.

[12] Kerscher, S., S. Dröse, V. Zickermann, and U. Brandt, "The Three Families of Respiratory NADH Dehydrogenases

Bioenergetics", G. Schäfer and H. Penefsky, Editors, Springer Berlin / Heidelberg. p. 185-222, 2008.

[13] Postgate, J., "Nitrogen Fixation": Cambridge University Press.1998.

[14] Zhao, X., F. Pan, H. Xu, M. Yaseen, H. Shan, C.A. Hauser, S. Zhang, and J.R. Lu, "Molecular self-assembly and applications of designer peptide amphiphiles", *Chem Soc Rev*, 39(9),p.,3480-98, 2010.

[15] Philp, D. and J.F. Stoddart, "Self-Assembly in Natural and Unnatural Systems", *Angewandte Chemie International Edition in English*, 35(11),p.,1154-1196, 1996.

[16] Whitesides, G.M. and B. Grzybowski, "Self-assembly at all scales", *Science*, 295(5564),p.,2418-21, 2002.

[17] Watson, J.D., "The double helix : a personal account of the discovery of the structure of DNA". New York: Atheneum.1980.

[18] Anfinsen, C.B., "Principles that govern the folding of protein chains", *Science*, 181(4096),p.,223-30, 1973.

[19] Wright, J.D., "Molecular Crystals": Cambridge University Press.1994.

[20] Cui, H., M.J. Webber, and S.I. Stupp, "Self-assembly of peptide amphiphiles: from molecules to nanostructures to biomaterials", *Biopolymers*, 94(1),p.,1-18, 2010.

[21] Cui, H., T. Muraoka, A.G. Cheetham, and S.I. Stupp, "Self-Assembly of Giant Peptide Nanobelts", *Nano Letters*, 9(3),p.,945-951, 2009.

[22] Aida, T., E.W. Meijer, and S.I. Stupp, "Functional Supramolecular Polymers", *Science*, 335(6070),p.,813-817, 2012.

[23] Paramonov, S.E., H.-W. Jun, and J.D. Hartgerink, "Self-Assembly of Peptide−Amphiphile Nanofibers: The Roles of Hydrogen Bonding and Amphiphilic Packing", *J Am Chem Soc*, 128(22),p.,7291-7298, 2006.

[24] Ulijn, R.V. and A.M. Smith, "Designing peptide based nanomaterials", *Chem Soc Rev*, 37(4),p.,664-675, 2008.

[25] Hartgerink, J.D., E. Beniash, and S.I. Stupp, "Self-Assembly and Mineralization of Peptide-Amphiphile Nanofibers", *Science*, 294(5547),p.,1684-1688, 2001.

[26] Zasloff, M., "Antimicrobial peptides of multicellular organisms", *Nature*, 415(6870),p.,389-95, 2002.

[27] Guler, M.O., L. Hsu, S. Soukasene, D.A. Harrington, J.F. Hulvat, and S.I. Stupp, "Presentation of RGDS Epitopes on Self-Assembled Nanofibers

of Branched Peptide Amphiphiles", *Biomacromolecules*, 7(6),p.,1855-1863, 2006.

[28] Matson, J.B. and S.I. Stupp, "Self-assembling peptide scaffolds for regenerative medicine", *Chemical Communications*, 48(1),p.,26-33, 2012.

[29] Rajangam, K., H.A. Behanna, M.J. Hui, X. Han, J.F. Hulvat, J.W. Lomasney, and S.I. Stupp, "Heparin Binding Nanostructures to Promote Growth of Blood Vessels", *Nano Letters*, 6(9),p.,2086-2090, 2006.

[30] Palladino, P., V. Castelletto, A. Dehsorkhi, D. Stetsenko, and I.W. Hamley, "Conformation and Self-Association of Peptide Amphiphiles Based on the KTTKS Collagen Sequence", *Langmuir*, 28(33),p.,12209-12215, 2012.

[31] Seow, W.Y. and Y.-Y. Yang, "A Class of Cationic Triblock Amphiphilic Oligopeptides as Efficient Gene-Delivery Vectors", *Advanced Materials*, 21(1),p.,86-90, 2009.

[32] Khalily, M.A., O. Ustahuseyin, R. Garifullin, R. Genc, and M.O. Guler, "A supramolecular peptide nanofiber templated Pd nanocatalyst for efficient Suzuki coupling reactions under aqueous conditions", *Chem Commun (Camb)*, 48(92),p.,11358-60, 2012.

[33] Newcomb, C.J., R. Bitton, Y.S. Velichko, M.L. Snead, and S.I. Stupp, "The role of nanoscale architecture in supramolecular templating of biomimetic hydroxyapatite mineralization", *Small*, 8(14),p.,2195-202, 2194, 2012.

[34] Johnson, B.F.G., "Nanoparticles in catalysis", *Topics in Catalysis*, 24(1-4),p.,147-159, 2003.

[35] LaMer, V.K. and R.H. Dinegar, "Theory, Production and Mechanism of Formation of Monodispersed Hydrosols", *J Am Chem Soc*, 72(11),p.,4847-4854, 1950.

[36] Xia, Y., Y. Xiong, B. Lim, and S.E. Skrabalak, "Shape-controlled synthesis of metal nanocrystals: simple chemistry meets complex physics?", *Angew Chem Int Ed Engl*, 48(1),p.,60-103, 2009.

[37] Tagata, T. and M. Nishida, "Palladium charcoal-catalyzed Suzuki-Miyaura coupling to obtain arylpyridines and arylquinolines", *J Org Chem*, 68(24),p.,9412-5, 2003.

[38] Yamada, Y.M., S.M. Sarkar, and Y. Uozumi, "Self-assembled poly(imidazole-palladium): highly active, reusable catalyst at parts per million to parts per billion levels", *J Am Chem Soc*, 134(6),p.,3190-8, 2012.

[39] Astruc, D., "Palladium catalysis using dendrimers: molecular catalysts versus nanoparticles", *Tetrahedron-Asymmetry*, 21(9-10),p.,1041-1054, 2010.

[40] Yuan, B., Y. Pan, Y. Li, B. Yin, and H. Jiang, "A highly active heterogeneous palladium catalyst for the Suzuki-Miyaura and Ullmann coupling reactions of aryl chlorides in aqueous media", *Angew Chem Int Ed Engl*, 49(24),p.,4054-8, 2010.

[41] Crudden, C.M., M. Sateesh, and R. Lewis, "Mercaptopropyl-modified mesoporous silica: a remarkable support for the preparation of a reusable, heterogeneous palladium catalyst for coupling reactions", *J Am Chem Soc*, 127(28),p.,10045-50, 2005.

[42] Dujardin, E., C. Peet, G. Stubbs, J.N. Culver, and S. Mann, "Organization of metallic nanoparticles using tobacco mosaic virus templates", *Nano Letters*, 3(3),p.,413-417, 2003.

[43] Murugadoss, A., R. Pasricha, and A. Chattopadhyay, "Ascorbic acid as a mediator and template for assembling metallic nanoparticles", *Journal of Colloid and Interface Science*, 311(1),p.,303-310, 2007.

[44] Baker, C.O., B. Shedd, R.J. Tseng, A.A. Martinez-Morales, C.S. Ozkan, M. Ozkan, Y. Yang, and R.B. Kanert, "Size Control of Gold Nanoparticles Grown on Polyaniline Nanofibers for Bistable Memory Devices", *Acs Nano*, 5(5),p.,3469-3474, 2011.

[45] Ryoo, H.I., J.S. Lee, C.B. Park, and D.P. Kim, "A microfluidic system incorporated with peptide/Pd nanowires for heterogeneous catalytic reactions", *Lab on a Chip*, 11(3),p.,378-380, 2011.

[46] Pacardo, D.B., J.M. Slocik, K.C. Kirk, R.R. Naik, and M.R. Knecht, "Interrogating the catalytic mechanism of nanoparticle mediated Stille coupling reactions employing bio-inspired Pd nanocatalysts", *Nanoscale*, 3(5),p.,2194-2201, 2011.

[47] Bhandari, R. and M.R. Knecht, "Effects of the Material Structure on the Catalytic Activity of Peptide-Templated Pd Nanomaterials", *Acs Catalysis*, 1(2),p.,89-98, 2011.

[48] Ulijn, R.V. and A.M. Smith, "Designing peptide based nanomaterials", *Chemical Society Reviews*, 37(4),p.,664-675, 2008.

[49] Acar, H., R. Garifullin, and M.O. Guler, "Self-Assembled Template-Directed Synthesis of One-Dimensional Silica and Titania Nanostructures", *Langmuir*, 27(3),p.,1079-1084, 2011.

[50] Tsiveriotis, P. and N. Hadjiliadis, "Studies on the interaction of histidyl containing peptides with palladium(II) and platinum(II) complex ions", *Coordination Chemistry Reviews*, 192,p.,171-184, 1999.

[51] Xia, Y., Y. Xiong, L. Byungkwon, and S.E. Skrabalak, "Shape-Controlled Synthesis of Metal Nanocrystals:Simple Chemistry Meets Complex Physics?", *angewandte Chemie International Edition*, 48,p.,60-103, 2009.

[52] Cornils, B. and W.A. Herrmann, "Aqueous-phase organometallic catalysis: concepts and applications": Wiley-VCH.1998.

[53] Marziale, A.N., D. Jantke, S.H. Faul, T. Reiner, E. Herdtweck, and J. Eppinger, "An efficient protocol for the palladium-catalysed Suzuki-Miyaura cross-coupling", *Green Chemistry*, 13(1),p.,169-177, 2011.

[54] Bernsmann, H., M. van den Berg, R. Hoen, A.J. Minnaard, G. Mehler, M.T. Reetz, J.G. De Vries, and B.L. Feringa, "PipPhos and MorfPhos: Privileged monodentate phosphoramidite ligands for rhodium-catalyzed asymmetric hydrogenation", *Journal of Organic Chemistry*, 70(3),p.,943-951, 2005.

[55] Brudvig, G.W., W.F. Beck, and J.C. Paula, "Mechanism of Photosynthetic Water Oxidation", *Annual Review of Biophysics and Biophysical Chemistry*, 18(1),p.,25-46, 1989.

[56] Wikström, M., "The Respiratory Enzyme as An Electrochemical Energy Transducer", in *Bioinorganic Electrochemistry*, O. Hammerich and J. Ulstrup, Editors, Springer Netherlands. p. 25-35, 2008.

[57] Lea, P.J., "Enzymes of primary metabolism": Academic Press.1990.

[58] Costa, M., Y. Yan, D. Zhao, and K. Salnikow, "Molecular mechanisms of nickel carcinogenesis: gene silencing by nickel delivery to the nucleus and gene activation/inactivation by nickel-induced cell signaling", *Journal of Environmental Monitoring*, 5(2),p.,222-223, 2003.

[59] Hammond, A.L., "Mercury in the environment: natural and human factors", *Journal Name: Science (Washington, D.C.); (United States); Journal Volume: 171*,p.,Medium: X; Size: Pages: 788-789, 1971.

[60] Lu, S.C., "Regulation of hepatic glutathione synthesis: current concepts and controversies", *FASEB J*, 13(10),p.,1169-83, 1999.

[61] Coyle, P., J.C. Philcox, L.C. Carey, and A.M. Rofe, "Metallothionein: the multipurpose protein", *Cell Mol Life Sci*, 59(4),p.,627-47, 2002.

[62] Meldrum, N.U. and M. Dixon, "The properties of pure glutathione", *Biochem J*, 24(2),p.,472-96, 1930.

[63] Rauser, W.E., "Phytochelatins", *Annu Rev Biochem*, 59,p.,61-86, 1990.

[64] Vatamaniuk, O.K., S. Mari, Y.P. Lu, and P.A. Rea, "Mechanism of heavy metal ion activation of phytochelatin (PC) synthase - Blocked thiols are sufficient for PC synthase-catalyzed transpeptidation of glutathione and related thiol peptides", *Journal of Biological Chemistry*, 275(40),p.,31451-31459, 2000.

[65] Satofuka, H., T. Fukui, M. Takagi, H. Atomi, and T. Imanaka, "Metal-binding properties of phytochelatin-related peptides", *Journal of Inorganic Biochemistry*, 86(2-3),p.,595-602, 2001.

[66] Satofuka, H., T. Fukui, M. Takagi, H. Atomi, and T. Imanaka, "Metal-binding properties of phytochelatin-related peptides", *J Inorg Biochem*, 86(2-3),p.,595-602, 2001.

[67] Eftink, M.R., M.L. Andy, K. Bystrom, H.D. Perlmutter, and D.S. Kristol, "Cyclodextrin Inclusion Complexes - Studies of the Variation in the Size of Alicyclic Guests", *Journal of the American Chemical Society*, 111(17),p.,6765-6772, 1989.

[68] Matzapetakis, M., D. Ghosh, T.C. Weng, J.E. Penner-Hahn, and V.L. Pecoraro, "Peptidic models for the binding of Pb(II), Bi(III) and Cd(II) to mononuclear thiolate binding sites", *J Biol Inorg Chem*, 11(7),p.,876-90, 2006.

[69] Potocki, S., M. Rowinska-Zyrek, D. Valensin, K. Krzywoszynska, D. Witkowska, M. Luczkowski, and H. Kozlowski, "Metal binding ability of cysteine-rich peptide domain of ZIP13 Zn2+ ions transporter", *Inorg Chem*, 50(13),p.,6135-45, 2011.

[70] Van Assche, F. and H. Clijsters, "Effects of metals on enzyme activity in plants", *Plant, Cell & Environment*, 13(3),p.,195-206, 1990.

[71] Lu, Y., N. Yeung, N. Sieracki, and N.M. Marshall, "Design of functional metalloproteins", *Nature*, 460(7257),p.,855-62, 2009.

[72] Ulmer D, D. and L. Vallee B, "Structure and Function of Metalloenzymes", in *Bioinorganic Chemistry*, AMERICAN CHEMICAL SOCIETY. p. 187-218, 1971.

[73] Martin, R.B., "Practical hardness scales for metal ion complexes", *Inorganica Chimica Acta*, 339(0),p.,27-33, 2002.

[74] Holm, R.H., P. Kennepohl, and E.I. Solomon, "Structural and Functional Aspects of Metal Sites in Biology", *Chemical Reviews*, 96(7),p.,2239-2314, 1996.

[75] Schwartz, Z., J. Sela, V. Ramirez, D. Amir, and B.D. Boyan, "Changes in extracellular matrix vesicles during healing of rat tibial bone: a morphometric and biochemical study", *Bone*, 10(1),p.,53-60, 1989.

[76] Hench, L.L. and J. Wilson, "Surface-active biomaterials", *Science*, 226(4675),p.,630-6, 1984.

[77] de Aza, P.N., F. Guitián, C. Santos, S. de Aza, R. Cuscó, and L. Artús, "Vibrational Properties of Calcium Phosphate Compounds. 2. Comparison between Hydroxyapatite and β-Tricalcium Phosphate", *Chemistry of Materials*, 9(4),p.,916-922, 1997.

[78] Koutsopoulos, S., "Synthesis and characterization of hydroxyapatite crystals: A review study on the analytical methods", *Journal of Biomedical Materials Research*, 62(4),p.,600-612, 2002.